Feasibility of CO$_2$ capture in a mini-mill plant

A case study from the iron and steel industry

José Maria Azevedo Rego Morais Pires

Thesis to obtain the Master of Science Degree in

Chemical Engineering

Supervisors: Prof. Dr. Henrique Aníbal Santos de Matos, IST-UL
                Prof. Ing. Laura Annamaria Pellegrini, Politecnico di Milano

Examination Committee

Chairperson: Prof. Dr. Maria Cristina de Carvalho Silva Fernandes
Supervisor: Prof. Dr. Henrique Aníbal Santos de Matos
Member of the Committee: Prof. Dr. Ana Catarina Gouveia Braz

February 2023

To my beloved *mamma* and *papà*.

Acknowledgments

Resumo

Atualmente, é amplamente reconhecida a responsabilidade dos gases com efeito de estufa (GEE), como o dióxido de carbono (CO_2), no aquecimento global. Em termos de CO_2 emitido, os setores da energia e industrial são dos mais poluentes, destacando-se, no setor industrial, a indústria do aço. A presente dissertação investigou, por simulação em Aspen Plus® V11, a performance de um sistema de captura de CO_2 por absorção química com monoetanolamina (MEA), aplicado ao processo descontínuo de produção de aço pela fornalha de arco elétrico (EAF). Com efeito, o modelo rigoroso desenvolvido permitiu identificar, através de um estudo paramétrico, as melhores condições operatórias para este sistema, atendendo às suas necessidades processuais de utilidades e matérias-primas, que, em parte, são representativas da sua performance. Em particular, foram observados os efeitos da carga do solvente pobre em CO_2, α_{LEAN}, da altura de enchimento no absorvedor, H_{abs}, da pressão operatória do *stripper*, P_{stp}, e da altura de enchimento no *stripper*, H_{stp}, em indicadores de performance (KPI), *p.ex.*, os requisitos térmicos no re-ebulidor (TER), para inferir as melhores condições operatórias. Priorizou-se a minimização dos TER em detrimento dos restantes KPIs, tendo-se identificado o caso ótimo como sendo aquele em que α_{LEAN} = 0.19, H_{abs} = 32 m, H_{stp} = 10 m e P_{stp} = 2 bara, culminando em reduções de 36% nos TER, quando comparado com o cenário base. Obtidos os parâmetros ótimos para o processo em estado estacionário, concebeu-se e simulou-se um modo flexível de operação, por forma a atender à natureza *batch* da EAF. Por fim, estudou-se a viabilidade económica do processo sugerido. Confrontaram-se os custos de remoção de CO_2 de dois cenários (91$/t CO_2 *vs.* 110$/t CO_2) com o imposto de carbono em vigor em Portugal e o preço dos títulos de emissão de GEE, pelo que se propôs o cenário de utilização de CO_2 para um estudo subsequente mais detalhado. Até onde o autor conseguiu apurar, a simulação de tal sistema acoplado ao processo EAF nunca foi descrita na literatura.

Palavras-chave: captura de CO_2, absorção química, solvente MEA, indústria do aço e do ferro, Aspen Plus®, processo descontínuo

Abstract

Greenhouse gases, as carbon dioxide (CO_2), are one of the main drivers for global warming. Apart from the energy sector, the industrial sector, to which the iron and steel industry belongs, ranks third in the 5 greatest anthropogenic CO_2 emitting sectors. This dissertation assessed the technical and economic performance of a monoethanolamine (MEA)-based post-combustion CO_2 capture system implemented in the electric arc furnace (EAF) steel production pathway, which operates batchwise. In virtue of the developed rate-based Aspen Plus® V11 model, the best operating conditions meeting the process specifications were determined via a parametric study. In particular, it was examined the effect of the lean solvent loading, α_{LEAN}, the absorber packing height, H_{abs}, the stripper operating pressure, P_{stp}, and the stripper packing height, H_{stp}, on user-defined key performance indicators (KPI), such as the reboiler energy requirements (TER). These KPIs quantify the process performance, while simultaneously shed some light on the process requirements, thus enabling to select the best operating parameters. From all KPIs, TER was the one sought to be reduced the greatest. The optimal operating conditions were found to be equal to α_{LEAN} = 0.19, H_{abs} = 32 m, H_{stp} = 10 m and P_{stp} = 2 bara, which resulted in a TER of 3.45 GJ/t of removed CO_2, an energy saving of 36% when compared with the base case scenario. Only after the best case scenario was identified, was a flexible operation mode conceived and analysed to deal with the particularities of the EAF process. Following the process economic evaluation, the CO_2 capture costs for two scenarios (91$/t CO_2 *vs.* 110$/t CO_2) were compared with the current carbon tax in Portugal and the ETS permit cost. As a result, it was suggested that the CO_2 utilisation scenario is to be further analysed as it showed the lowest CO_2 removal cost. To the author's best knowledge, the simulation of such capture system applied to the EAF steelmaking process has never been described before in the literature.

x

Contents

List of Tables

List of Figures

Nomenclature

Roman symbols

p Pressure.

AFCI   Annualized Fixed Capital Investment.

AMP   Aminomethylpropanol.

APEA   Aspen Process Economic Analyser.

BAT   Best Available Technology(ies).

BF   Blast Furnace.

BFG   Blast Furnace Off-gas.

BOF   Basic Oxygen Furnace.

BOFG   Basic Oxygen Furnace Off-gas.

CAPEX   Capital Expenditures.

CCUS   Carbon capture, utilisation and storage.

CEPCI   Chemical Engineering Plant Cost Index.

COG   Coke Oven Gas.

CRF   Capital Recovery Factor.

CW   Cooling Water.

CWC   Cooling Water Consumption.

DEA   Diethanolamine.

DIPA   N,N-diisopropylaminoethanol.

DPC   Direct Production Costs.

DRI   Direct Reduced Iron.

EAF   Electric Arc Furnace.

ETS   European Trading System.

EU   European Union.

FCD   Forced Draft Cooler.

FCI   Fixed Capital Investment.

FDR   Film Discretization Ratio.

G&A   General & Administrative.

GHG   Greenhouse gases.

HBI   Hot Briquetted Iron.

HRC   Hot Rolled Coil.

I&S   Iron and steel industry.

ISM   Integrated Steel Mill.

KPI   Key Performance Indicator.

LPS   Low Pressure Steam.

MDEA   Methyldiethanolamine.

MEA   Monoethanolamine.

NCD   Natural Draft Cooler.

NG   Natural Gas.

OC   Operating Costs.

OPEX   Operating Expenditures.

PCC   Post Combustion Chamber.

PCDD   Polychlorinated dibenzo-p-dioxin.

PCDF   polychlorinated dibenzofuran.

POP   Persistent Stable Organic Pollutants.

R&D   Research and Development.

RCF   Reaction Condition Factor.

SR   Lean Solvent Requirements.

TAC   Total Annualized Costs.

TCI   Total Capital Investment.

TEA   Triethanolamine.

TER   Thermal Energy Requirements.

TGR   Top-gas Recycling.

TRL   Technology Readiness Level.

TRT   Top-pressure Recovery Turbines.

WC   Working Capital.

WCD   Water Cooled Duct.

Chapter 1

Introduction

1.1 Motivation

Climate change has always been a controversial topic, and not infrequently the rightful center of many discussions. Nowadays, recent data has pointed out that the Earth's global temperature has risen $0.08°C$ per decade since 1880, which roughly amounts to an increase of $1.01°C$. In fact, nineteen of the warmest years on the record have occurred since 2000 [1].

Climate change constitutes a pressing challenge at the economic, social and environmental levels, whose long-term effects may threaten the human species' continuity on planet Earth. It is widely accepted that greenhouse gases (GHG), as carbon dioxide (CO_2), are the main responsible for this global warmth, and as such their mitigation within the various fields of activities raises increasingly greater concerns, as the global mean temperature continues to raise uncontrollably.

At the United Nations Climate Change Conference in 2015, through the ratification of the Paris Agreement, the CO_2 atmospheric concentration was established to be mandatorily below 450 ppm by the year of 2100 to guarantee that the global temperature increase remains below $2°C$ [2]. Following the Paris Agreement, the European Union (EU) vouched for reducing greenhouse gas emissions by 80% by 2050, and in 2019, in line with the Paris Agreement, it approved the European Green Deal with the aim of being climate-neutral by 2050 [3]. These truly ambitious energy goals set by the EU were a clear sign of acknowledgement of the urgency in addressing such challenge.

Therefore, economies and, in particular, the industrial sector must undergo all kinds of transformations in order to comply with these goals. In fact, nowhere is this challenge more noticeable than in the industry, which has grown in a consistent and rapid manner over the past few decades. When surveying the CO_2 emissions by sector – see fig. 1.1 –, one sees that the energy sector is the biggest CO_2 emitting sector,

which explains why the vast majority of research work in CO_2 capture has focused on its application to power plants. Apart from the energy sector, the industrial field is among the top-3 of the greatest CO_2 emitting sectors, from which the iron and steel industry stands out. In fact, the industrial sector was responsible for over 12 Gt CO_2 released in 2018, as in fig. 1.1(b).

(a) Electricity and heat generation separated.

(b) Electricity and heat generation allocated to the different sectors.
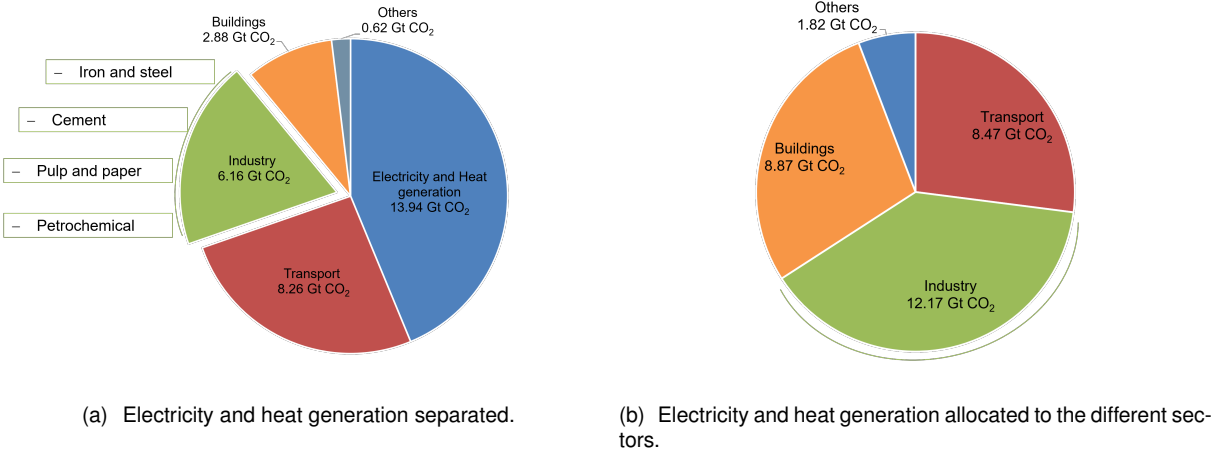
Figure 1.1 – Anthropogenic CO_2 emissions by source (2018). In total, 31 Gt CO_2 were globally released [4].

Among all industries, the cement and iron and steel industries, which make part of the heavy industry group, account for the biggest GHG emitters, as illustrated in the fig. 1.2.
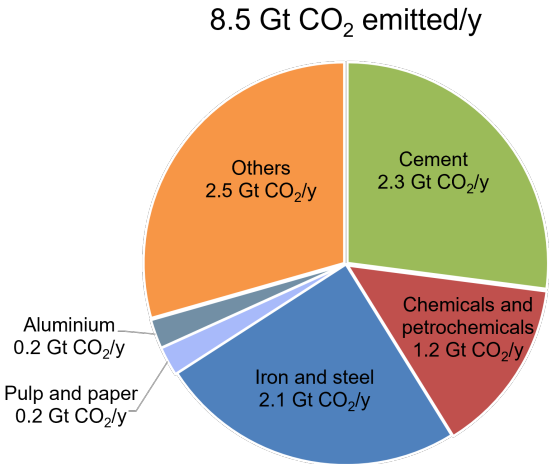
Figure 1.2 – CO_2 emissions by type of industry (2018) [5].

Steel is such an enabling material on many aspects. On the one hand, its combination of properties render it the material of choice for several applications: urban development, transportation, basic sanitation and water facilities, and even renewable energy plants (*e.g.*, wind turbines) all depend on steel [6].

On the other hand, the ever-growing world's population stimulates demand for goods and services, thus burgeoning resource exploitation. Steel, as a core material, and its industry get, of course, vitalized, due to the massive importance of such material. Therefore, the iron and steel industry unsurprisingly

2

thrives, and with it so do economies – making steel an enabling material, for that it creates opportunities for emergent economies, thus driving their development. As a result, countries get industrialized, ultimately resulting in GDP growth, but at the expense of increasing pressure on the long term sustainability of many resources and at the price of large CO_2 emissions into the atmosphere, due to the inherently energy- and carbon-intensive nature of its manufacturing process. The 2018 carbon footprint scenario shows that the iron and steel sector accounts for about 7% of all anthropogenic CO_2 emitted. In addition, with regard to the industrial sector, the iron and steel industry accounts for about 25% of the CO_2 emissions – *see* fig. 1.2. In fact, the production of a single tonne of crude steel emits on average 1.4 tonnes of CO_2 [7]. Tremendous amounts of energy and reducing agents are required to produce steel, both of which come directly from fossil fuels, ultimately ending up in CO_2 emissions.

This clearly motivates the decarbonisation of the iron and steel as it is a vital element to meet climate change mitigation targets. Furthermore, other industrial sectors, as the cement industry, must also be decarbonised as they have their fair share of responsibility in these anthropogenic CO_2 emissions. In particular, the combustion of fuels at cement production plants releases massive amounts of CO_2, as well as the calcination reaction through which *clinker* is produced.

1.2 Topic Overview

1.2.1 The iron and steel industry in numbers

Steel is essentially an iron-carbon alloy with varying amounts of other alloying elements, such as manganese, chromium or nickel. Its mechanical properties depend upon the carbon content, that generally does not surpass the 1%wt [8]. Therefore, the versatility of this class of materials makes it one of the most employed materials in construction, with applications ranging from pipelines to buildings, extending also to the transport industry. Figure 1.3 depicts the share of end uses of the produced steel.

Steel is undoubtedly essential to modern society and has spurred economic growth across the globe. In fact, there is not a single commodity whose importance can surpass that of steel, and the numbers just speak for themselves:

- in 2021, *c.* 1.9 billion tonnes of steel were annually produced worldwide [10];

- recent forecasts predict global steel demand growth rates of 2.5 billion tonnes per *annum* by 2050 [11];

- production rates have been increasing steadily over the years: from 1980 to 2000, it had risen about 19%, whereas from 2000 to 2014 doubled. Despite the smaller time-span, the corresponding production growth rate is bigger. Such trend has been observed due to increased production at emergent countries in an effort to develop their economies [12].

More specifically in Europe, around 0.3 billion tonnes are produced each year with France, Germany and Italy being the largest producers [10]. Since it is responsible for generating 2.5 million jobs within Europe, this heavy industry undoubtedly boosts European industrial sector [10].

1768 Mt steel globally produced
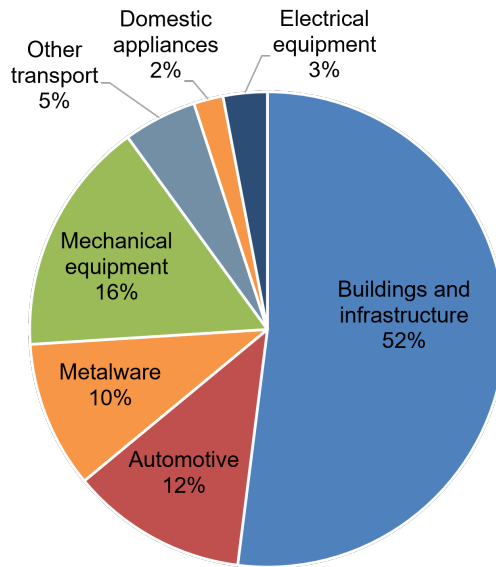
Figure 1.3 – Distribution of the produced steel by its end-uses (2019) [9].

1.2.2 Main steelmaking production processes

As of today, there are several steel production processes. Strictly speaking, steel production can be of two kinds, as shown in fig. 1.4:

- **primary**, meaning that iron is first smelted, and is refined into steel in a later stage;

- **secondary**, where recycled steel (commonly called *scrap*) is used to obtain new steel.
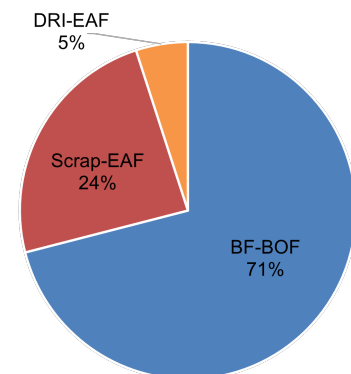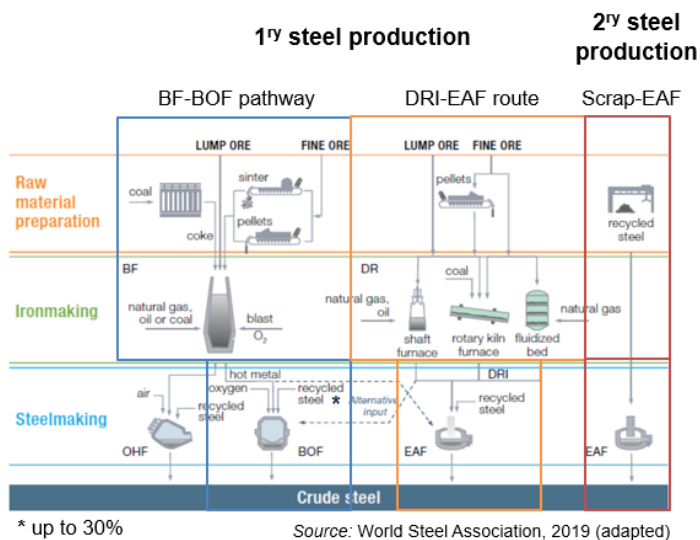
(a) Steel production processes (author's own composition, based on [13]).

(b) Steel production by pathway (2019) [14].

Figure 1.4 – Steel production pathways and their share.

Two dominant steel manufacturing routes can be clearly identified from fig. 1.4(b):
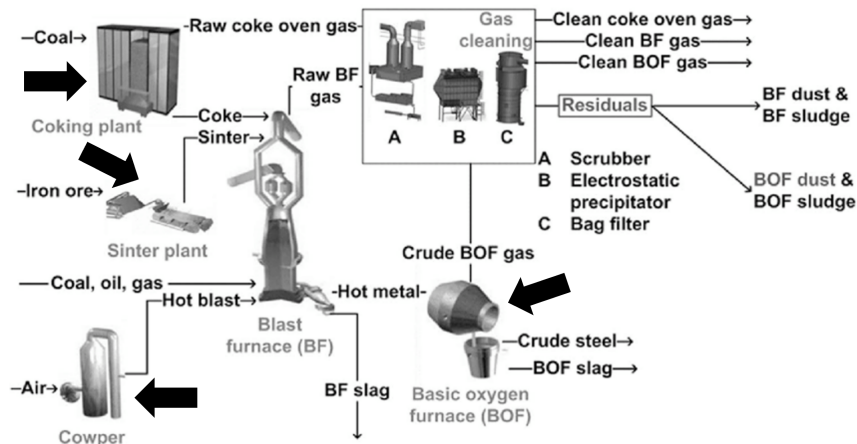
Figure 1.5 – BF-BOF process overview (adapted from [15]). Dark arrows indicate GHG emission points.

- the blast furnace-basic oxygen furnace (BF-BOF) route carried out at the so-called *integrated steel mill* (ISM) plants is the one with greater share. Iron is firstly produced in a blast furnace (BF), being later transformed into crude steel in a basic oxygen furnace or converter (BOF) – look for BF-BOF route in fig. 1.4(a);

- the scrap-electric arc furnace (EAF) pathway is the second largest process, accounting for 24% of the worldwide steel production. In this route, the raw material input comes mainly in the form of scrap, but other materials may be fed to the EAF, depending on scrap availability. Secondary steelmaking plants are commonly called *mini-mills*.

On the other hand, Direct Reduced Iron (DRI)-EAF processes - that correspond to 5% of the worldwide production - may be classified as coal-DRI-EAF (global production share of 1%) or natural gas-DRI-EAF (share of 4%), depending on the reducing agent employed in the furnace. There are also smelting reduction processes, which have evolved into commercial processes, *e.g.* Corex®, Finex®, HIsmelt®, but account for less than 1% of the worldwide steel production.

Let us now go through the main steelmaking production processes.

1.2.2.1 1^{ry} → Blast Furnace-Basic Oxygen Furnace (BF-BOF) pathway

Nowadays, the integrated BF-BOF route is, by far, the most widely used process. This process is schematically depicted in fig. 1.5. At first glance, one can immediately notice that this pathway requires several auxiliary plants to process raw materials, before its admission to the BF. BFs are massive reactors that operate continuously with residence times of about eight hours.

Raw materials When it comes to raw materials, the following are needed to produce crude (or pig) iron:

- iron ore;

- coal;

- limestone (a *flux* agent which facilitates the removal of impurities).

Coal must be pyrolysed into coke in a coke oven (part of the coking plant), while iron ore must be sintered or pelletized in a sinter plant. There are also some auxiliary reductants that are injected throughout BF operation.

All these auxiliary plants generate gaseous effluents with high CO_2 content.

Unveiling the chemistry Coke, limestone and iron ore (in the form of pellets or sinter) are fed to the top of the BF in an alternating configuration, that is, layers of coke interchange with iron ore and limestone. Hot air (commonly called *hot blast*) enriched with oxygen is also injected via tuyeres[1]. Furthermore, pulverised coal (or even natural gas) are also side-fed as reducing adjuvant agents. A reducing agent is required to remove oxygen from the iron oxides, thus forming metallic iron.

As the hot blast enters the BF, it runs into a bed of coke. Air and coke react, forming CO_2 – see rxn (1.1) – that rises into the furnace, and encounters more coke. As a result, carbon monoxide (CO) is formed as coke *gasifies* – see rxn (1.2).

$$C(s) + O_2(g) \longrightarrow CO_2(g) \qquad \text{Combustion of coke} \qquad (1.1)$$

$$C(s) + CO_2(g) \longrightarrow 2\,CO(g) \qquad \text{Coke gasification reaction} \qquad (1.2)$$

While reaction (1.1) is highly exothermic and is, in fact, the primary source of heat for the furnace, reaction (1.2) is endothermic [16]. As such, it lowers the furnace temperature.

The preceding reactions clearly illustrate the two purposes filled by coke: i) as fuel. Its combustion reaction evolves heat; ii) as reducing agent, enabling CO generation which in turn allows iron ore to be reduced.

Freshly produced CO now rises through the furnace until it finally comes into contact with the iron ore. Iron ore is then reduced to metallic iron, according to the rxns (1.3)-(1.5), in the so-called reduction zone. Reduction sequence is comprised of three steps:

$$3\,Fe_2O_3(s) + CO(g) \longrightarrow 2\,Fe_3O_4(s) + CO_2(g) \qquad (1.3)$$

$$Fe_3O_4(s) + CO(g) \longrightarrow 3\,FeO(s) + CO_2(g) \qquad (1.4)$$

$$FeO(s) + CO(g) \longrightarrow Fe(s) + CO_2(g) \qquad (1.5)$$
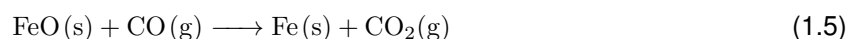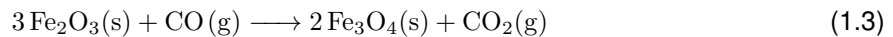
Limestone in the charge gets transformed into calcium oxide and CO_2. Calcium oxide in turn reacts with silicate impurities, forming the so-called *slag*, a molten mass that separates from the crude iron, as it is a low density liquid [16]. Slag formation proceeds according to rxns (1.6) and (1.7). Note that the impurities are represented by SiO_2.

---

[1]A duct through which air is blown into the furnace.

$$CaCO_3(s) \longrightarrow CaO(s) + CO_2(g) \qquad \text{Calcination of limestone} \qquad (1.6)$$

$$CaO(s) + SiO_2(s\,or\,l) \longrightarrow CaSiO_3(s\,or\,l) \qquad\qquad (1.7)$$

BF operation   From the BF, pig iron is withdrawn from its bottom, while a hot gas exits the top of the BF. This hot gas, termed *blast furnace off-gas* (BFG), contains 17-25% in CO_2 and 20-28% in CO [17]. High CO_2 and N_2 contents characterise the BFG, rendering it a low-grade fuel, as both CO_2 and N_2 are non-flammable gases [18]. Even though BFG has a low heating value, it has a great potential for being re-used within the process since enormous amounts of BFG are generated - *circa* 900 m^3/t of produced steel [12]. So, if BFG is to be used as a fuel, it has to be enriched with other gaseous streams that have higher heating values.

In fact, BFG is frequently mixed with the coke oven gases (COG), natural gas (NG) or basic oxygen furnace gas (BOFG) that have higher heating values. BFG is then burned as fuel in i) intake air (blast) heating in the so-called *stoves* (or *cowpers*); ii) coke oven heating. Any excess BFG can be utilised to generate steam and electricity for on-site use or might be sold.

In fact, the BF-BOF is a highly interconnected process [12, 19], as can be seen in fig. 1.6. Nonetheless, there is still room for improvements regarding waste heat recovery, as shall be seen ahead.
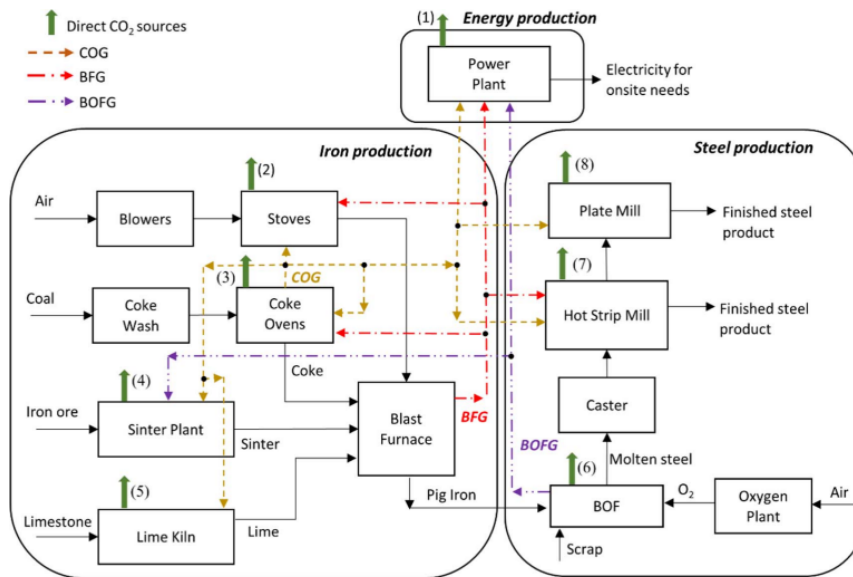
Figure 1.6 – Scheme of BF-BOF process flowsheet [12]. Note the mass and energy integration within the process.

1.2.2.2   1^{ry} $\rightarrow$ **Direct Reduced Iron-Electric Arc Furnace (DRI-EAF) pathway**

DRI process is the current main alternative to the BF. BF-BOF and DRI-EAF processes differ on quite a few aspects, the first of which being how iron is made. In direct reduction processes, iron ore is not melted (as in the BF-BOF process), but instead it is reduced in its solid state using syngas. Syngas – a gas mixture essentially consisting of CO and hydrogen (H_2) – may be generated through either NG or

coal as reducing agent. In terms of equipment, direct reduction processes can be performed on different types of reactors: shaft furnaces (exclusively for NG-DRI-EAF processes), rotary kilns or fluidised bed reactors [17]. However, the fact that no melting or even refining takes place means that all impurities get concentrated in the DRI. There are different commercial processes available, such as Midrex® and Energiron®, the latter developed by Danieli and Tenova [20].

When it comes to natural gas-based DRI-EAF processes (NG-DRI-EAF), natural gas is reformed, hence generating the reducing gas, that contains mostly CO and H_2. While for the coal-based DRI processes, the reducing gas comes from the combustion and gasification of coal and is thus largely composed of carbon monoxide [17]. So, at first glimpse, it would seem that the DRI pathway carbon footprint is smaller than the BF-BOF. However, it largely depends on the reducing agent employed. In actual fact, the coal-DRI-EAF pathway is even more polluting than the standard BF-BOF route [21] - see table 1.1.

1.2.2.3 $2^{ry} \rightarrow$ Scrap-Electric Arc Furnace pathway

In mini-mill plants, the EAF produces raw steel from recycled steel and others, depending on scrap availability, as will be elaborated ahead. Electric power is provided to melt the charged materials. CO_2 emissions arising from a essentially recycled steel-based process are markedly lower than BF-BOF and DRI-EAF processes, as in table 1.1. Furthermore, energy requirements of the scrap-EAF route are about 10% to 15% of those required by primary steel production processes [7].

Table 1.1 – CO_2 emissions from the main steelmaking processes [21]. Note that indirect emissions from electricity generation are accounted.

	Processes	Total emissions (t CO_2/t steel)
1^{ry} production	BF-BOF	2.0
	Coal-DRI-EAF	2.4
	NG-DRI-EAF	1.4
2^{ry} production	Scrap-EAF	0.4

1.2.3 Industrial CO_2 emissions

Within any industrial process, CO_2 emissions can be classified as either direct or indirect, according to its nature.

- **Direct** emissions:

    – those resulting from the combustion of fossil fuels as a means to generate utilities (*i.e.*, steam);

    – process-related emissions, meaning those arising from the process operation itself. In this case, as steel is obtained through the refinement of iron by reducing carbon content, it is expected that the released off-gases will contain carbon in whichever form.

8

- **Indirect** emissions are due to electricity consumed during regular process operation. Electricity has to be somehow generated, and its generation often relies on the use of fossil fuels.

1.2.4 Tackling CO_2 emissions from the iron and steel industry

The I&S industry is one of the largest GHG emitters, due to the intensity of its processes. Primary steelmaking routes are the most polluting of all steel production processes, as illustrated in fig. 1.7.
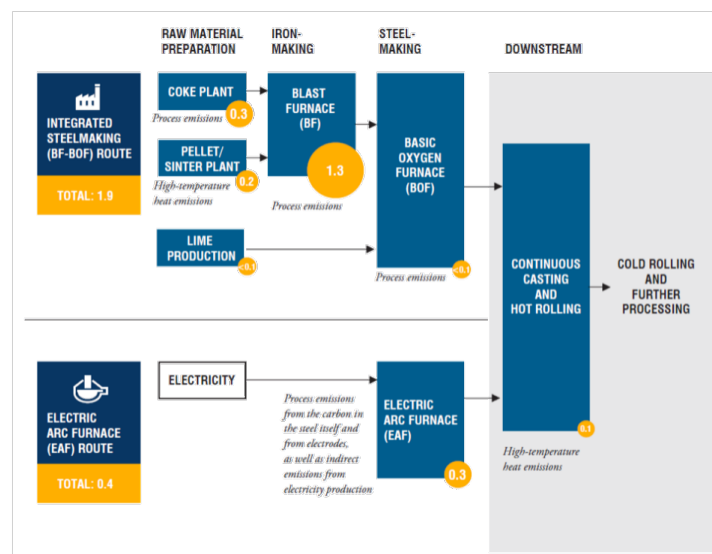
Figure 1.7 – Overview of the CO_2 emissions arising from the main steelmaking processes [7, 22]. Emissions are in tCO_2/t steel produced.

Given the importance of steel for mankind, its production will not slow down at all, with the associated GHG emissions continuing to rise. In any case, climate change issues must be addressed as they will jeopardize the continuity of the human species on Earth. So, reducing CO_2 from steelmaking plants is of utmost importance. At this point, three possible choices can be formulated to reduce CO_2 emissions from steelmaking processes: i) reduce steel demand; ii) increase steel recycling, thus favoring the scrap-EAF pathway; iii) develop new carbon-free, green, sustainable steel manufacturing technologies or innovate the existing production technologies [23].

Of these three options, the first is unfeasible: steel consumption (hence, demand) will steadily grow in the next years given its natural importance as a construction material. So, a paradigm shift in the production route (towards the scrap-EAF route) might be desirable and ultimately fruitful, but:

i) it is highly dependent on the availability of high-quality and low-priced steel scraps. The limitations in the supply of scrap steel prevent the scrap-EAF process from penetrating deeper into the global steelmaking profile, thus hindering its possibility to become a major player in the steel industry [14, 17, 23];

ii) scrap-EAF process is not a fully clean and eco-friendly process. Nonetheless, it is the most environmentally sound of the three main processes and there is still some room for process improvements.

Developing new steelmaking processes or innovating the existing manufacturing technologies implies the conception of ways of dealing with the CO_2 emissions. Whether new process routes are explored, existing process streams are valorized or CO_2 is captured, these polluting emissions are curbed at all times, contributing for a healthier planet Earth.

Therefore, CO_2 emissions from the I&S industry can be substantially reduced if new scrap-EAF plants are commissioned (having in mind that plant sites are dependent on scrap availability) and new steelmaking processes are developed or the existing ones are improved.

Generally speaking, adopting the following measures can lower CO_2 emissions (not ranked by order of importance) [17, 24]:

 i) improving energy efficiency through heat and mass integration;

 ii) resorting to renewable-based systems;

 iii) changing the fuel type;

 iv) changing heat source;

 v) perform CO_2 separation and capture, on which the present thesis focuses.

1.2.4.1 Energy efficiency - valorizing streams, thus recovering energy

Minimising energy consumption and improving energy efficiency are key to abate CO_2 emissions (either direct or indirect). Regarding the energy efficiency measures that lead to reductions in direct CO_2 emissions, some of the best available technologies (BATs), if not already in use, are [17]:

- regarding the BF-BOF process $\rightarrow$ injection of auxiliary reducing agents, such as pulverised coal, leads to coke consumption decrease [17]. As a consequence, not only CO_2 emissions are reduced but also savings are achieved since coke is more expensive than coal. In that event, the coking plant gets under less demand;

- energy recovery from process streams $\rightarrow$ a common practise in all ironmaking processes. For instance, BFG heating value is recovered either when BFG is burnt as fuel in the hot blast stoves combustion or when it is utilised to generate plant utilities -, hence helping to lower direct CO_2 emissions. Another example might be that of direct reduction reactors, where the calorific value of the off-gas is recovered. Either way, produced gases are valorised, as they are utilised as fuels to produce steam or even generate electricity;

- energy recovery from the pressurised gas exiting at the top of the BF, resorting to top pressure recovery turbines (TRT). As BFs operate at high pressure (in order to achieve higher productivity), its (pressurised) exhaust gas can drive a gas turbine, thus generating power.

Even so, there is still scope to increase energy efficiency as it is estimated that 20-50% of the energy input is lost as waste heat [23] which reveals that process heat recovery systems are somewhat

immature. Waste heat recovery systems exploit sensible heat from the various process streams [17], as molten slag heat recovery technologies [23].

As of now, steelmaking plants have implemented several measures that have led to CO_2 substantial reductions over the past 30 years. In fact, energy requirements have decreased from 110 GJ/t of produced steel to 20 GJ/t of produced steel from 1970 to 2012 with many experts claiming that steel plants are operating close to its thermodynamic limit [25]. Even though energy efficiency measures play an undeniable role in decreasing CO_2 emissions, these are not enough *on their own* to offset the growing nonstop annual CO_2 emissions let alone abate *all* CO_2 direct emissions. So, this means that further CO_2 reduction can only be attained resorting to an additional measure from those listed previously, as carbon capture and storage (CCS).

1.2.4.2 CO_2 capture

Carbon capture, utilisation and storage (CCUS) is widely acknowledged as a pivotal climate change mitigation strategy. CCUS systems can be classified as post-combustion, pre-combustion and oxyfuel combustion, depending on where CO_2 is to be captured. This text focuses on post-combustion CCUS, where CO_2 is captured after combustion takes place. Currently, there are many available technologies to perform CO_2 capture [23]:

- chemical or physical absorption (or even a combination of both);

- solid adsorption;

- membranes;

- cryogenics;

- chemical bonding via mineral carbonation.

1.2.4.3 CO_2 mitigation programs

In 2003, the World Steel Association launched *CO_2 Breakthrough Programs* in an effort to decarbonise the I&S industry, and possibly come up with a carbon-free sustainable iron and steel production. Under this program, several other projects have emerged such as ULCOS, POSCO, COURSE50, among others. All these target at the development of breakthrough steel manufacturing technologies that go around the CO_2 emission issue [23]. To that purpose, one or more of the previously listed mitigation measures is followed.

Ultra Low CO_2 Steelmaking (ULCOS) Commissioned by the EU and involving 48 different institutions and companies, the ULCOS project was split up into two phases: ULCOS-I (2004) and ULCOS-II (2010). From this project, four major technological developments involving several steelmaking processes have stemmed [12, 23, 26]:

- Top-gas recycling blast furnace (TGR-BF), including a CCS scheme, as illustrated in fig. 1.8(a): instead of heating the *cowpers* or serving other purposes, BFG is simply recycled to the blast furnace. Exhausted BFG passes through a CO_2 capture scheme and is then fed to the hot stoves. Thus, there is no need of a fresh blast as BFG is recycled. As a consequence, fuel rates could be decreased. However, at the same time, BFG would remain unavailable for usage in downstream processes. ULCOS project has pointed vacuum pressure-swing adsorption (VPSA) as the best separation process to capture CO_2. Note that this technology combines the implementation of both CCS and energy efficiency strategies;

- HIsarna smelter, HIsarna makes part of the smelting reduction processes. In particular, it aims at coke free steelmaking and comprises two process units - the cyclone converter furnace for ore melting and its pre-reduction, followed by a smelting vessel, where final ore reduction takes place. HIsarna process design conceives a nitrogen-free and CO_2 rich off-gas, enabling easier CO_2 capture [17]. So far, a pilot plant has been operating at a nominal capacity of 60 kt pig iron produced/year. Ongoing plans include the construction of a second large-scale pilot plant in India [27];

- ULCORED - Direct iron reduction with natural gas project aims at revamping the DRI-EAF process by selecting natural gas as the reducing agent. Other efforts have also shown the possibility of using biomass to generate a reducing gas [23];

- ULCOWIN - Direct electrolysis of iron ore, iron ore electrolysis produces both metallic and oxygen, with associated zero carbon emissions. ULCOWIN has examined the electrolytic smelting of iron ore at 110°C. Production rates is the major challenge of such technology [23].

(a) Conventional BF process scheme. BFG used as fuel to the hot stoves and fed to a gas turbine, generating electricity.

(b) TGR-BF scheme. BFG is entirely recycled to the stoves. No need of intake air.
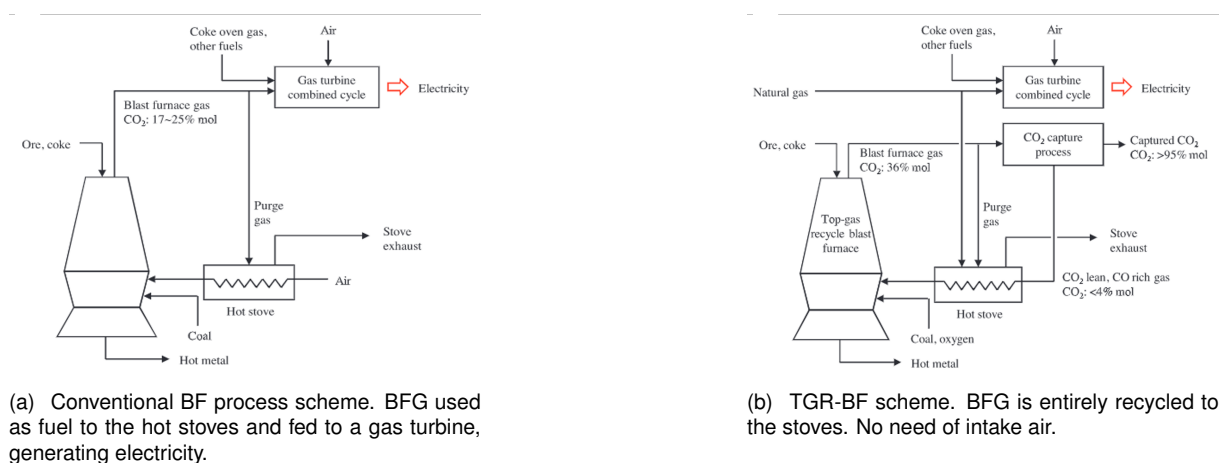
Figure 1.8 – Comparison between the conventional blast furnace and the TGR-BF configuration [28].

COURSE50 program Following the endeavours of the late prime minister of Japan, Abe Shinzo, the CO_2 ultimate reduction in steelmaking process by innovative technology for cool Earth 50 (COURSE50) project was launched, whose outline is depicted in fig. 1.9. Its main concern is reducing CO_2 emissions

from BFs up to 30% through capture, separation and recovery of CO_2 from BFG [23]. COURSE50 relies on the hydrogen reaction with the iron ores as the key factor to mitigate emissions. This program is based on three pillars [23]:

i) in the conventional BF-BOF process, CO_2 is generated after CO reacts with the iron ore, whereas, in this process, hydrogen reaction with the iron ore generates H_2O;

ii) hydrogen concentration in the COG is increased in order to greatly reduce CO_2 process emissions;

iii) CO_2 recovery, separation and capture from BFG are put into practise through chemical absorption, adsorption, low-temperature condensation or membrane separation methods.
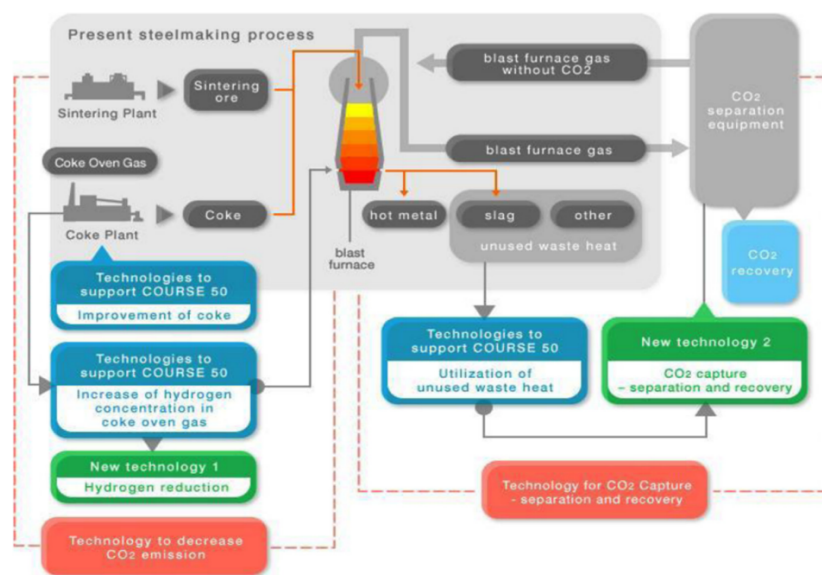
Figure 1.9 – Outline of the COURSE50 program [23].

POSCO - Pohang Iron and Steel Company - project   POSCO is greatly committed to decrease greenhouse gases emissions. To this purpose, POSCO has approached this problem from three points of view that can complement each other: i) development of carbon-lean steelmaking technologies, including its FINEX process (which outside the scope of this text); ii) implementation of CCS strategies in steelmaking processes; iii) hydrogen utilisation in the ironmaking processes [23].

At the moment, four major technological frameworks have been approved:

i) CO_2 capture using ammonia (absorption) and waste process heat (desorption);

ii) CO_2 fixation using marine bio-slag;

iii) H_2 production using byproduct gaseous streams;

iv) sensible heat recovery of sintered iron ore.

Other innovative projects There are still other R&D efforts that have been carried out with some promising results. As an example, HYBRIT, a swedish project which is developing a H_2 based-DRI process that expects to demonstrate the feasibility of this technology at industrial scale as early as 2026.

Moreover, Fan and Friedmann [14] identified more concrete available decarbonisation technologies for this industrial sector:

- hydrogen (preferably green) injection, as H_2 is a powerful reducing agent. Recall how hydrogen is produced as not to generate more indirect emissions.

- solid biomass substitution. Solid biofuels can readily substitute conventional feedstocks if exhibiting key physical properties similar to those of the conventional fuels [14];

- utilisation of zero-carbon electricity;

- CCS retrofit, on which this work will focus.

or even a combination of these.

1.2.4.4 Key challenges to CO_2 abatement in primary steelmaking

Hydrogen usage H_2 may well be utilised in both primary steelmaking processes - BF-BOF and DRI-EAF routes. In the BF-BOF process, it may only partly replace CO (formed from coke or coal), as full H_2 operation is not possible. Blind increases in the H_2 concentration in the furnace will impact the basic reaction chemistry, downgrading the performance of the BF [14]. However, according to Midrex Technologies, DRI processes can fully accommodate NG replacement by H_2 with minimal plant retrofit [17].

CCS retrofit Abating CO_2 emissions from the dominant BF-BOF process via a CCS retrofit is quite demanding. This is mainly due to the complexity of the plant sites:

- emissions are quite dispersed over a large number of point sources as a consequence of the diverse unit operations along the process [14, 17];

- stack gases emitted from distinct points have different compositions [19, 29];

- long-lived assets (*e.g.*, 25 years) pose as a barrier to the implementation of new technology [6, 14, 30].

So, the aforementioned factors make difficult to enforce a CCS strategy. On the other hand, CCS retrofits have high technical maturity and relatively low implementation cost [14].

When it comes to a typical DRI plant, other questions may rise. As most CO_2 exits the furnace, post-combustion capture is only required there, thus making DRI plants more simple to retrofit than ISMs [14].

1.2.4.5 Key challenges to CO$_2$ abatement in secondary steelmaking

Currently, there is extensive research devoted to abating emissions from primary steelmaking processes [12], since secondary steelmaking emits less CO$_2$ than primary steelmaking processes, as was seen in fig. 1.7. What is more, as the scrap-EAF pathway has a quite simpler process framework than that of the primary steelmaking processes, scrap-EAF CO$_2$ emissions are lower. So, it may come as no surprise that the key challenges to decarbonise secondary steelmaking plants are different. In fact, when comparing the conventional BF-BOF process with the scrap-EAF route, one quickly notices that mini-mills do not have auxiliary plants like integrated steel mills have. Therefore, there will not be multiple emission points. So, if a CCS retrofit is aimed at, then this point makes it more simple to capture, and thus mitigate these emissions.

Even so, other challenges come up, for example:

i) <u>indirect emissions</u>:

- **how is provided electricity generated?** Zero-carbon electricity ensures that CO$_2$ indirect emissions are tackled [14, 17].

ii) <u>direct emissions</u>:

- unavoidable emissions from the carbon-based electrodes;

- **use of auxiliary equipment** in the EAF that employ fuels as well as O$_2$: it generates direct CO$_2$ emissions, but reduces total emitted CO$_2$. These newly-generated emissions are unavoidable, but can be captured using, for example, a chemical absorption scheme, which is further explained under chapter 2.

1.3 Objectives and Deliverables

As a conceptual study, the present work focuses on modeling a CO$_2$ capture plant via a chemical absorption scheme applied to the scrap-EAF route, which to our best knowledge has never described before in the literature. The goals of this dissertation are essentially:

- to develop a rate-based model of an industrial-scale CO$_2$ capture plant;

- to gain a better understanding of the CO$_2$ capture process applied to mini-mills, in light of the urgency of mitigating climate change;

- to propose a flexible operation mode for such capture facility, considering the idiosyncrasies of a mini-mill plant. This will expectably incentive the implementation of this solution at the industrial scale;

- to assess the economic feasibility of such project.

1.4   Thesis Outline

This thesis is divided in five chapters, as follows:

- **the first** of which lays the groundwork for the chemical absorption strategy be applied in the scrap-EAF pathway: that is, chapter 1 introduces the iron and steel industry in figures as well as the main steelmaking routes. The factors that drive for the implementation of carbon capture in a mini-mill, motivating it, are developed;

- **in chapter 2**, a state-of-the-art review of the electric arc furnace is provided as well as a theoretical overview of the absorption/desorption unit operations. At the end of this chapter, the MEA-CO_2 chemical system under study is addressed, along with some notes on modelling;

- **in chapter 3**, the developed model in *Aspen Plus$^®$ V11* is extensively described as well as the methodology used;

- **in the fourth chapter**, the obtained results are presented along with a thorough discussion. The effect of a specific set of operating parameters on the performance of an amine-based chemical absorption CO_2 capture process applied to a mini-mill is analysed. Afterwards, the actual conditions in terms of fumes flow rates variability are introduced, thus culminating in the so-called flexible mode of operation. Lastly, an economic evaluation of the process is carried out;

- the **final chapter 5** summarizes the key findings and makes some final considerations. Moreover, potential future work which can be developed from this work is also presented.

Chapter 2

Background

A brief (at least, the author hopes so) theoretical overview is provided in this chapter. Firstly, the secondary steelmaking process is reviewed. Secondly, some notes on generic gas absorption processes are outlined. At the end of this chapter, the focus then turns to the chemical system under study – the MEA-CO_2 one – with topics on modelling being covered. Special attention is also given to the different types of models, as this is fundamentally a modelling study.

2.1 Electric Arc Furnace - state-of-the-art

Like every other chemical plant, a *mini-mill plant* is made of several building blocks: the reactors are undoubtedly one of the most important. In fact, the core of a mill-mill lies on the electric arc furnace (EAF), that massive reactor from which raw steel is withdrawn.

At first sight, electric arc steelmaking looks more environmental-friendly than the conventional blast furnace-basic oxygen furnace (BF-BOF) route. In actual fact, despite that the EAF pathway emits considerably less greenhouse gases (GHG) compared to the BF-BOF pathway, there are still GHG emissions arising from the aforementioned route, not to mention other equally preoccupying emissions (in terms of particulate matter).

2.1.1 Secondary steelmaking process overview

In the fig. 2.1, a simple scheme outlines the typical steelmaking process. The process starts at the EAF, from which raw steel is obtained, and includes a separation system to deal with the EAF off-gas emissions. The produced raw steel is then submitted to further downstream processing.

The gas cleaning system comprises a post-combustion chamber, a baghouse filter, some canopy hoods, and fans. After the EAF off-gas is treated, it is released into the atmosphere through a stack.

17
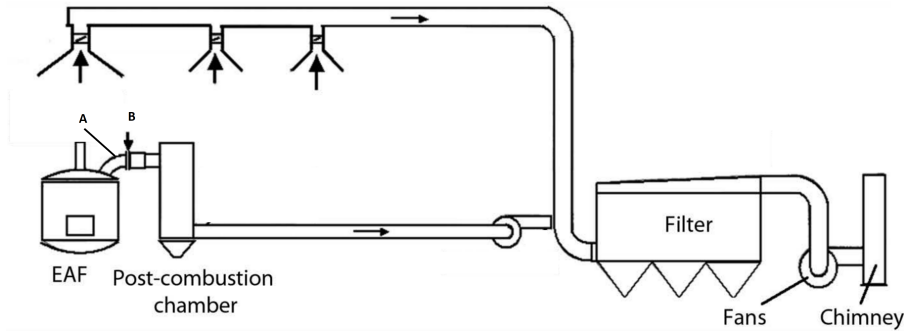
Figure 2.1 – EAF process overview (adapted from [31]). A - the fourth hole (refer to page 24 for details); B - air gap.

2.1.2 Overview of the conventional EAF operation

Electric-based steelmaking relies on the EAF that operates discontinuously through electrical energy supply. Broadly speaking, an EAF is a covered (roofed) vessel set up with water-cooled walls, equipped with either one or three electrodes, some mechanical equipment and other electrical parts [31, 32].
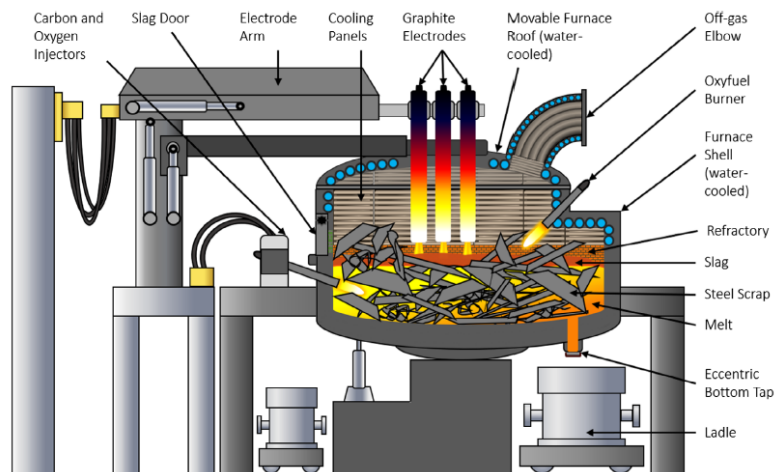
Figure 2.2 – Section view of an EAF [32].

An operating cycle can be identified on the grounds of the EAF batchwise nature. Each cycle has a definite service time of approximately one hour, even though newer (and more powerful) EAFs can show reductions in the service time of about 30% [33]. Generally speaking, every EAF operating cycle goes through the following phases:

 i) charging;

 ii) melting;

 iii) refining (additions and decarburisation);

 iv) slagging;

 v) tapping, in which liquid raw steel – the final product – is withdrawn from the furnace.

18

The time it takes to complete one cycle (that is, going from one tapping to another) is the cycle or service time, usually acknowledged as tap-to-tap time [33].

2.1.2.1 Production phases of an EAF batch (service time $\approx$ 1 hour)

Charging   Scrap (*i.e.*, recycled) steel is the main input into the EAF. Along with scrap steel, it is possible to feed other types of materials, such as pig (crude) iron, direct reduced iron (DRI) or hot briquetted iron (HBI) in several proportions. Therefore, all things considered, the share of scrap in a single EAF charge can be quite variable, ranging from 60% to 100% depending on whether the aforementioned substitute materials are also loaded or not [33]. In effect, the quality of which can influence the EAF electricity consumption rates. Moreover, the choice of which materials are to be inputted into an EAF is subject to the local availability [17].

In addition, there are other materials that are fed as well to the furnace, and generally go by the name of *fluxes* [33]:

- limestone - a slagging agent, meaning that allows to remove impurities from the steel, such as phosphorous;

- iron alloy, used to tune the crude steel chemical composition as per request;

- carbon (as graphite), serving the purpose of:

  - increasing the amount of carbon in the furnace – yet, steel *per se* is characterised by poor carbon content. If oxygen (O_2) is then somehow injected in the EAF, it reacts with the existing carbon, oxidising it to carbon monoxide, while evolving a tremendous amount of chemical energy as this reaction is highly exothermic. So, what if more carbon is fed? More energy will be evolved. Therefore, feeding carbon (and injecting O_2) enables the possibility of exploiting chemical reactions as a means to provide energy to the furnace, thus decreasing electric power requirements (which are largely attributable to the melting phase). Further details are provided under section 2.1.2.2.

    * provided that CO is formed, dissolved hydrogen and nitrogen gas concentrations in the liquid steel pool are cut down.

Melting   During this phase, electrical energy is supplied to melt the charged materials. Electrical energy, which is supplied via the graphite-based electrode(s) positioned in the furnace, is transformed in heat via radiation. The number of electrodes (either one or three) depends on the furnace type. In fact, as it was just unveiled, chemical energy can also be provisioned (besides electrical) to assist the melting process which requires huge amounts of electrical energy – please see section 2.1.2.2. After melting takes place, a liquid metal pool remains in the furnace vessel, readily prepared for the refining phase that leads to the production of raw steel.

Refining   At this stage, there are several elements that must be removed from the liquid steel pool in order to achieve the raw steel composition standards. Therefore, this phase aims at removing carbon, phosphorus, and sulphur through several oxidation reactions. These operations refer to decarbonisation (or decarburisation), dephosphorization, and desulphurization, respectively. Manganese, aluminium and silicon are also removed (as its reaction with O_2 forms insoluble oxides) along with the abovementioned elements.

Slagging   During the refining phase, several impurities were oxidized forming insoluble compounds that come to the surface of the liquid metal pool. This by-product, commonly called *slag*, is then easily removed by physical separation (*e.g.*, decantation) during the course of this phase.

Tapping   Once the required steel chemical composition and temperature is achieved, the liquid steel is unloaded from the furnace. In fact, this is just crude steel, as it is further processed at downstream unit operations. After tapping, the EAF is set up for the next batch, meaning that: i) the vessel roof is lifted as well as the electrodes and ii) the refractory lining is thoroughly examined to check for potential damages.

2.1.2.2   Auxiliary equipment

I) Providing chemical energy - motivation   In the hypothetical case that electrical energy is to be the sole energy input to the EAF, then electric power requirements are expected to be quite considerable. However, had chemical energy been provided (through O_2 and carbon supply), then these requirements would have been lowered, as it was just seen under section 2.1.2.1. Even if decreasing the electric power requirements alone would not suffice as a motive to supply chemical energy to the furnace, then the fact that electrical energy on its own is not the most efficient strategy to melt the charged materials clearly prompts its use. In fact, melting does not occur in an uniform manner inside the furnace, and as a result hot spots do originate [33]. This markedly motivates the use of oxyfuel burners[1] and O_2 lances in order to render the melting stage more homogeneous, as these devices are arranged around the furnace with its flames directed at the cold spots. Therefore, not only are electrical power requirements (mainly due to the melting phase energy demands) decreased but also melting occurs in a more efficient way when chemical energy is supplied to the furnace.

II) Oxyfuel burners and O_2 lances   These equipment are used to deliver chemical energy simultaneously with the electrical energy supplied by the electrodes. What is more chemical energy is not only provided by the oxyfuel combustion reactions, but also comes from the oxidation of carbon to carbon monoxide, as previously mentioned.

So, resorting to either oxyfuel burners or O_2 lances in EAFs reduces the required electricity consumption while, at the same time, intensifies its operation. This ultimately results in considerable productivity gains. However, these outcomes come at the expense of increased GHG emissions, that is, a portion

---

[1]devices that burn either natural gas and O_2 or a mixture of air and O_2 [17, 33].

of the consumed electricity gets substituted with O_2 and fuels, thus generating more CO_2 as a consequence of the combustion reactions. Nevertheless, plant data shows that total CO_2 emissions are effectively lowered via the savings in the consumed electricity (responsible for CO_2 indirect emissions) [17]. So, all things considered, there are several advantages in employing such equipment that can be plainly summarised as below [33]:

- the first of which is simply the reasoning that called for the need of inputting chemical energy in the furnace: cuts in electricity consumption rates and hot spots avoidance (thus, rendering melting more homogeneous);

- the latter result is a direct consequence of the enhanced heat transfer by radiation and convection enabled by this type of equipment;

All this ultimately leads to decreasing melting times, which in turn means increased productivity (*i.e.*, intensified operation).

- decreased electrode consumption (less wearing with time).

So far, it has just been seen the equipment which allows O_2 to be admitted to the furnace, thus making way for chemical energy to be supplied. Moreover, the preceding discussion casted light on some of the clear advantages to bringing chemical energy into the furnace. Nonetheless, there are still a few left that will be covered now. To such end, let us now quickly review the phases during each batch where O_2 is employed, while running through the rationale behind its utilisation.

i) during <u>melting phase</u>: carbon is fed purposely along with lime and iron alloy as adjuvant agents. As oxygen is provided, carbon reacts with it forming carbon monoxide, while liberating a great amount of energy that can cover approximately 30%-40% of the EAF energy requirements [33]. Savings in the inputted electrical power follow.

ii) during <u>refining phase</u>, through direct injection in the liquid steel pool [33], resulting in:

    (a) removal of the carbon contained in the melted metal bath by reaction with oxygen – *decarbonisation* – as the materials fed to the furnace have different provenience (meaning different carbon contents), carbon must be removed to a greater or lesser extent depending on the desired raw steel composition [33]. More energy is expected to be evolved from this oxidation reaction;

    (b) removal of undesirable elements, for instance silicon and manganese. Such elements react with the injected O_2, forming several oxides that float at the surface, coating it – *slag* – due to their reduced solubility in the molten steel pool. In addition, since oxygen reacts exothermically with these elements, additional energy is evolved as these reactions proceed, which is thereafter provided to the process [33].

iii) <u>throughout an EAF operation cycle</u>, CO evolves from the steel bath. As it evolves, O_2 in great excess may be injected in the EAF free board[2], allowing *local CO post-combustion* to take place, hence

---

[2]the upper region of the EAF vessel.

forming CO_2 and providing more supplementary energy to the furnace. This phenomenon is to be subject of further discussion. It should be noted that it may be the case that O_2 is not injected in the free board. If so, then other measures must be taken as CO emissions are not swiftly abated therein.

So far, the EAF has been the focus of our discussion as it lies at the heart of a mini-mill plant. However, the process flowsheet includes also a separation system, which is dedicated, in this case, to manage the EAF off-gases that are generated concomitantly with the liquid steel.

2.1.3 Emissions and current practices to handle EAF off-gases

During each operation cycle, huge amounts of energy are inputted to the EAF, generating generating a high-temperature off-gas that is discharged from the furnace upon batch completion. This must undergo a cleaning treatment prior to its release into the atmosphere due to the presence of polluting and hazardous species.

Emissions Strictly speaking, the EAF off-gas consists mainly of carbon monoxide (CO), carbon dioxide, nitrogen (N_2) and O_2 [31] – nevertheless, hydrogen (H_2) and water vapor (H_2O) may also be present as well as other organic compounds (*e.g.*, dioxins, furans) and different-sized solid particles (dusts, powders) - see table 2.1.

There are two types of emissions arising from an EAF operation: primary and secondary. The former stem from the EAF regular operation (melting phase and metal bath refining) and are responsible for about 90% of total gas emissions from an EAF, whereas the latter get mainly released following furnace charging operations (as the EAF roof must be lifted and moved away from the furnace to do so) and liquid steel tapping, accounting for the remaining 10% of the total gas emissions [31].

Table 2.1 – Average composition of the EAF off-gas **immediately** after exiting the fourth hole [33].

	CO	CO_2	H_2	H_2O	N_2
Mole fraction (%)	20-50%	10-30%	0-40%	10-20%	20-50%

Regarding carbon monoxide, it is produced as carbon contained in the charge (and some carbon from the graphite-made electrodes) is oxidised to CO. Then, as it evolves from the steel bath, it can be combusted through *local CO post-combustion*, forming carbon dioxide and generating more energy; if O_2 is not provided, then CO emissions are to be tackled in the off-gas handling system. In either way, CO polluting emissions into the atmosphere are curbed.

Besides being formed through CO post-combustion, CO_2 can also be formed in some other ways: i) upon reduction of the iron oxides present in the slag and ii) after carbonates decompose into CO_2.

In virtue of i) the own nature of a batchwise process and ii) the heterogeneity of the charged materials in terms of characteristics, both the flow rates and the compositions of the EAF fumes fluctuate between cycles [33]. In addition, stream compositions vary greatly with the location in the process. That is,

if one analyses the fumes composition at different points along the process, for instance, at the EAF outlet or after the air gap (dilution) or even after the post-combustion chamber, soon finds out different compositions.

CO post-combustion   So far, it has been seen that CO post-combustion can be used as a strategy to curb polluting CO emissions. In particular, it has only been addressed the *local CO post-combustion* as that performed in the EAF free board. In that case, while CO evolves from the liquid steel pool, O_2 is injected, forming thereafter CO_2.

However, there is also the so-called *water cooled duct* (WCD) *CO post-combustion*. Consider that the local CO post-combustion is not completed or not even performed (if O_2 is not provided). In that case, and considering the CO polluting nature, it could only be fully combusted if WCD post-combustion takes place.

The EAF off-gas is, in fact, a solid-gas mixture, which exits the furnace through an elbow-shaped duct that connects the fourth hole (located at the roof) to the water-cooled duct. In between these two ducts, atmospheric air enters to the conduit through a gap (see fig. 2.3) in order to complete the CO and H_2 combustion reactions as per reactions (2.1) and (2.2). Thus, compliance with strict regulations on CO emissions is guaranteed.

$$CO\,(g) + O_2(g) \longrightarrow CO_2(g) \tag{2.1}$$

$$H_2(g) + O_2(g) \longrightarrow H_2O\,(g) \tag{2.2}$$

At the same time, this stream is diluted in view of the admitted large air flow rates. Even though more CO_2 is formed, the overall CO_2 mole fraction in the exhaust gas plummets to around 11%. This figure reveals itself to be highly important as it will define how "big" must the capture plant be.
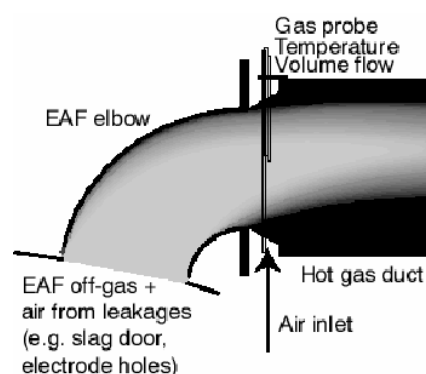
Figure 2.3 – Illustration of EAF elbow duct after which WCD post combustion occurs [34].

Environmental protection systems   The EAF off-gas must be subject to thorough downstream cleaning as it contains great amounts of particulate matter and may contain products of incomplete combustion, such as CO. Either way, environmental concerns come into play. A typical scheme of the purification section is illustrated in fig. 2.4.
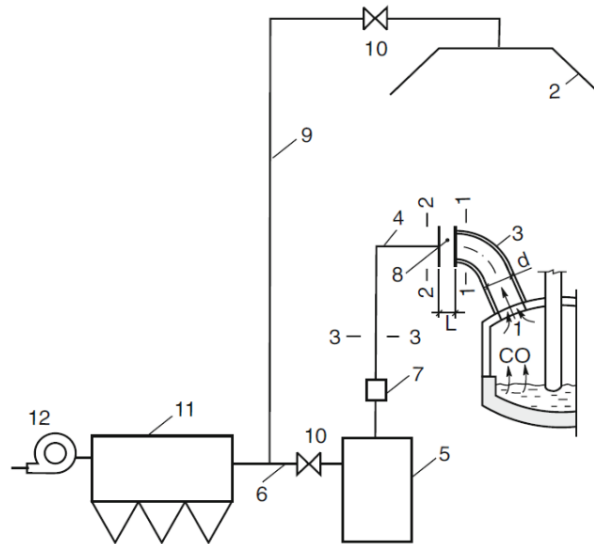
Figure 2.4 – Evacuation and purification system of the EAF off-gas [35]. 1 - opening in the furnace roof; 2 - canopy hood; 3 - roof elbow duct; 4 - stationary gas duct; 5 - drop out box; 6 - gas duct; 7 - water quenching tower; 8 - air gap; 9 - gas duct; 10 - off-gas flow rate control valve; 11 - baghouse filter; 12 - fan/exhauster.

The EAF off-gas exits the furnace with an average temperature greater than 800°C (with peaks reaching 1600°C [33]) through the elbow conduit located at the fourth hole[3]. As soon as atmospheric air is admitted to the duct, WCD post-combustion takes place, while, at the same time, the mixture temperature drops thanks to the air intake.

However, there are some flaws within this purification system that allow fumes to escape through doors, joints or the electrode openings, thereby bypassing the direct evacuation system [35, 36]. Besides, as the furnace has some mobile components (*e.g.*, doors) and operates batchwise (meaning that the roof must be opened), the EAF cannot be tightly sealed off. For this reason, EAF systems usually make use of a canopy hood to extract the secondary emissions. In either way, these fume leaks are due to changes in pressure.

The air gap design is of paramount importance as it determines the amount of intake air [31, 36]. On the one hand, a too small air flow rate might mean oxygen deficiency, leading to an incomplete combustion of CO and H_2. On the other hand, a too high air flow rate will generate high total gas flow rates, meaning that more powerful fans are needed to evacuate the exhaust gas as well as larger ducts [33].

A more detailed view on the EAF off-gas treatment system, located right after the EAF, is shown on fig. 2.5. After the air gap, the exhaust gas passes through the first of a series of WCDs designed to lower the temperature of this solid-gas mixture, as shown in fig. 2.5. Enormous potentials to recover this heat have already been identified [31]. In particular, WCD1 is built with high thermal resistance materials that can sustain these high temperatures. Thereafter, the former mixture is directed to a settling chamber equipped with a burner where not only the aforementioned combustion reactions are completed but also coarse solid particles are allowed to settle. Other authors refer to this settling chamber as post-

---

[3]Usually, at an EAF roof, there are four different holes, three of which are conceived for the electrodes, and through the remaining one - hence, the "fourth hole" - fumes exit. In some furnaces, there may be a fifth hole through which adjuvant agents are added.

combustion chamber (PCC) or drop out box.
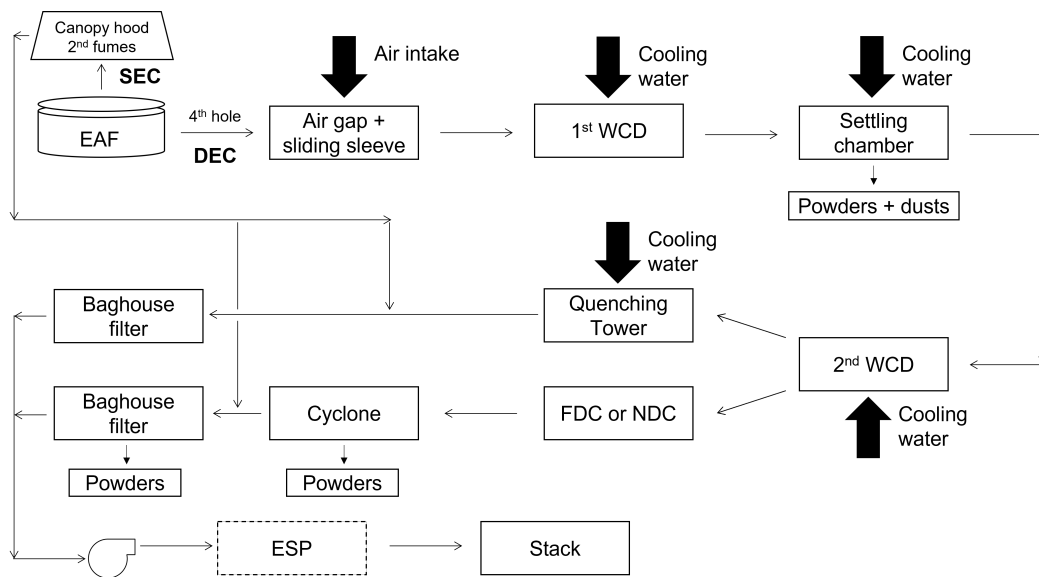
Figure 2.5 – Schematic of the EAF exhaust gas system (author's own elaboration, based on [33]). DEC: Direct Evacuation Circuit (for primary fumes); SEC: Secondary Evacuation Circuit (for secondary fumes); ESP: Electrostatic precipitator (optional).

What is more, the PCC aims at reducing largely the amount of emitted *dioxins* and *furans*, two groups of heterocyclic organic compounds whose long-lasting environmental effects are well documented, and whose toxicity varies widely. Here, dioxins and furans refer to chlorinated tricyclic organic compounds. Having this in mind, the structure of dioxins involves two benzene rings fused to a 1,4-dioxin – a non-aromatic compound whose basic "skeleton" is made up of two oxygen and four carbons. On the other hand, furans consist of two benzene rings connected to a furan – a five-membered aromatic ring with only one oxygen atom and the remaining of carbon atoms [37]. Among all types of dioxins and furans, polychlorinated dibenzo-*p*-dioxins (PCDDs) – a derivative of dibenzo-*p*-dioxin – and polychlorinated dibenzofurans (PCDFs) – a derivative of dibenzofuran – are the ones most commonly found at off-gases emitted from secondary steelmaking industrial facilities, whose chemical structures are shown in fig. 2.6. Both these compounds are persistent stable organic pollutants (POPs), which are frequently emitted as by-products of combustion processes [38]. During an operative cycle, PCDDs and PCDFs are formed, but are destructed due to the high temperatures inside the furnace. However, as fumes are extracted and subsequently cooled, PCDDs and PCDFs are allowed to re-form taking advantage of the also present powders that act as catalysts [33]. This phenomenon, which is referred to as *de novo synthesis* – from the latin, "from scratch" –, reaches its maximum productivity at 300-500°C, despite taking place at temperatures ranging from 280°C to 600°C [33, 37].

The amount of formed PCDDs and PCDFs by *de novo* is dependent on the time the mixture steadily remains at temperatures between 280°C and 600°C. That is, the more time exhaust gases endure at the reaction favorable temperature range the more PCDD/Fs form. So, if emissions of the aforementioned compounds are to be reduced, then post-combustion must take place in the more efficient way as possible. Inasmuch as fumes remain at relatively high temperatures (*i.e.*, slow cooling) for sufficient time

25
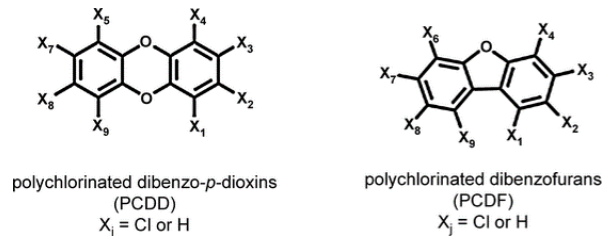
Figure 2.6 – Chemical structures for dioxin-like compounds [39].

and turbulent flow is provided, post-combustion is considered efficient, and so emissions of PCDD/Fs can be reduced.

Therefore, once consumed all CO and H_2, these fumes pass through another water-cooled duct (WCD2) to further reduce their temperature until 600-800°C. After the WCD2, there comes a conduit made of COR-TER® steel, designed to endure any thermal stress, through which the exhaust gas flows at temperatures lower than 550-600°C. Now, as the temperature range for PCDD/Fs re-forming is approached, these reactions must be stopped by all means if *de novo* synthesis is to be avoided. Rapid cooling – *quenching* – is now required with that end in view. So, the exhaust gas is redirected to either a quenching tower or a draft cooler. At any rate, fumes are rapidly cooled to temperatures around 200°C [33]:

i) if a quenching tower is made available:

- hot gas stream enters at the bottom of the tower, flowing countercurrently to liquid water droplets that are sprayed from the top of the tower. As water is at a lower temperature than that of the hot gas, water droplets vaporise, while the gas cools.

- quenching towers are usually 10-15 m long and 3.2-6 m wide.

ii) if, on the contrary, a draft cooler – a process-air shell-and-tube or plate heat exchanger – is available:

- draft coolers can be of two kinds, depending on the type of convection: natural (NDC) or forced (FDC). The choice between the two falls almost exclusively on economic considerations rather than engineering ones. For this reason, NDC are frequently preferred:

  - in a NDC, heat transfer is chiefly determined by the inlet air temperature and available surface area.

  - in a FDC, fans have to be installed to blow air into the heat exchanger, thus increasing heat transfer [40].

In the event NDCs or FDCs are employed a cyclone comes right after. This equipment aims at separating solid particles, and above all at preventing fine solid particles from igniting. Recall that cyclone efficiency is determined by gas velocity. As EAF exhaust gases have velocities around 40-60 m/s, high degree of separation at the cyclone is attained. However, high gas speeds imply high gas pressure drops, as fluid head losses are proportional to the velocity squared. Moreover, cyclone performance gets undermined as gas flow rates are not constant (*i.e.*, intermittent) through time as a consequence of the own EAF working behavior.

26

At last, primary and secondary emissions are always mixed before being conducted to the baghouse filter, regardless of the type of cooling equipment employed. The baghouse filter captures fine solid particles, thus releasing a clean gas from the solids point of view. It is worth noting that the inlet gas temperature should be relatively low (*e.g.*, $< 150°C$), but still higher than the gas dew point. It is highly unadvised to have condensation on the filter bags, as it slows down gas flow, thus increasing fluid head losses.

Upon its release from the filter, the exhaust gas is discharged into the atmosphere through the evacuation system (fan + stack). Usually, electrostatic precipitators are not employed, given their capital costs.

Let us now go through the secondary evacuation circuit. It mainly consists in a canopy hood that extracts gradually fumes as they evolve – during charging or slagging phases. Currently, there are other alternatives to the standard canopy hood that are more efficient [31], as practically all emissions are exhausted:

- *dog house* in which the EAF and its surroundings are covered by some metallic panels that encapsulate them.

- *elephant house*, where the EAF and auxiliary equipment are encapsulated in a closed chamber.

In this regard, the current best available technologies (BAT) are:

- fumes extraction at the fourth hole + canopy hood;

- fumes extraction at the fourth hole + dog house;

- fumes extraction at the fourth hole + plant complete encapsulation (*i.e.*, elephant house).

as shown in fig. 2.7.
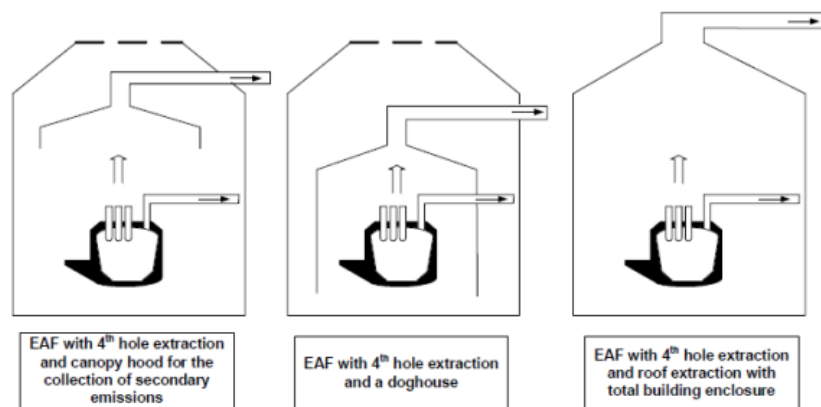
Figure 2.7 – BATs for fume extraction [33].

2.1.4 Heat recovery systems

Large amounts of heat are lost along side with the high-temperature fumes that are exhausted from the EAF. In fact, not only is the off-gas heat wasted but also the off-gas post-treatment system requires

a lot of energy to guarantee gases are properly treated and cleaned before being discharged into the atmosphere [35]. This clearly motivates an energy optimization of the whole process.

Exhaust gases coming from the EAF have a great potential to preheat the incoming scrap, given their huge heat content. In fact, if the hot gases are put in contact with the scrap steel, then this heat content can be exploited, thus optimising the process from an energy point of view. What is more, melting energy requirements can be reduced as scrap enters the furnace already heated. For this reason, scrap preheating has been a common practise in secondary steelmaking plants for about 30 years [33].

Applying heat recovery to the EAF process - the conventional EAF + heat recovery process
Traditional preheating takes place in the charging buckets, as depicted in fig. 2.8. Some of the hot exhaust gas is directed into a chamber where the bucket is placed, thereby heating the scrap.
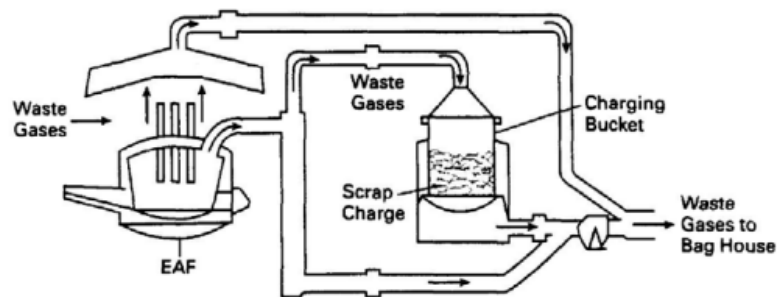
Figure 2.8 – Scheme of the conventional EAF + heat recovery (preheating) [33].

This system has some inconveniences: mainly its high operating costs and the generation of a new emission source point [33].

An upgrade to the conventional EAF + heat recovery process - the Consteel® process Tenova has developed the Consteel® process, currently being leader in this technology. The major differences to the conventional EAF process regard the way scrap is fed and its preheating. In the Consteel® process, scrap is continuously fed to the EAF through some belt conveyors placed in a closed tunnel, as illustrated in fig. 2.9. In the meantime, exiting fumes from the furnace flow countercurrently to the scrap, thus preheating it to temperatures around 300-400°C [33]. Similarly to the conventional EAF process, air is inherently admitted along with the moving scrap in this preheating section, and so CO is automatically oxidized to CO_2. As this reaction is exothermic, more energy is allowed to be recovered [41].

What is more, as the EAF operates in a semi-batch mode (continuous feeding), this means a liquid metal bath is kept constantly (as opposed to the conventional EAF where solid scrap is charged and only then melts in the first stage), *see* fig. 2.10. So, entering scrap gets melted by immersion in the liquid metal pool. This means the electric arc is more stable as the electrodes are not working on solid scrap [41].

Besides, continuous charging means that the EAF roof is closed at all times. So, gas exhaustion is always performed from the direct (primary) evacuation circuit, and not by the secondary circuit (canopies).
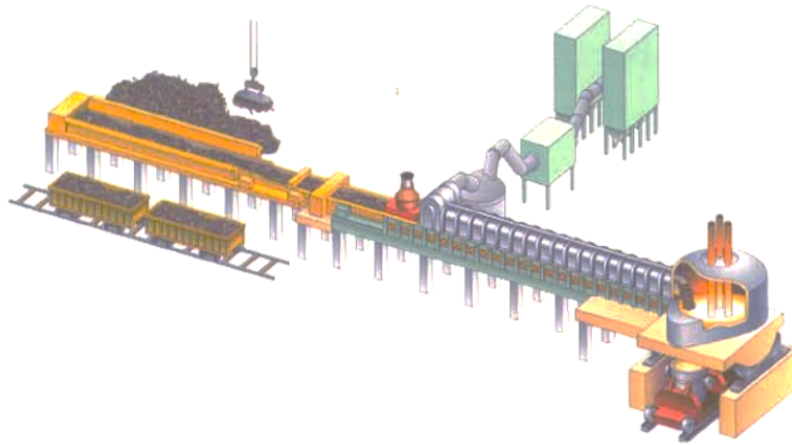
Figure 2.9 – Illustration of the Consteel® process [42]. Please compare with fig. 2.1.

Top-charge EAF   Consteel® EAF
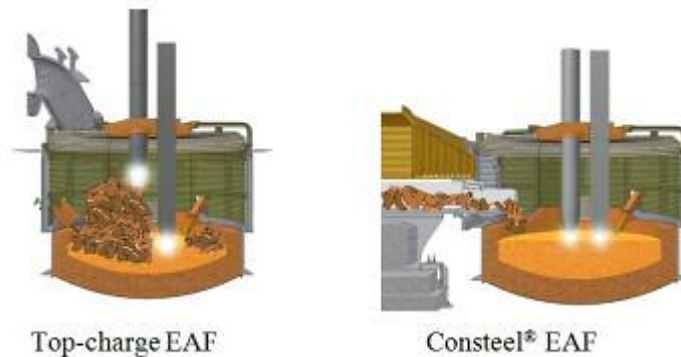
Figure 2.10 – Comparison between the conventional EAF (top-charge feeding) and the Consteel® EAF (continuous feeding) [43].

Therefore, there are smaller chances of unwanted gas leaks that somehow are able to bypass the canopies [41].

Consteel® technology has provided an efficient method of dealing with dusts: as the preheating tunnel has a greater cross section area than the normal EAF off-gas duct, then fumes travel at smaller velocities. As a result, coarse particles are allowed to settle at the belt conveyor, being then transported into the furnace [42].

2.1.5 Final considerations

So far, the EAF off-gas was cleaned (*i.e.*, particulate matter was all virtually removed) and there are almost no traces of CO. After the off-gas treatment process, this gaseous effluent is discharged as it is into the atmosphere – that is, with a considerable amount of CO_2, for which nothing was made about throughout all the purification and cleaning process. This is, in fact, the major point source of *direct* CO_2 emissions in a mini-mill [17]. Thus, in an effort to abate CO_2 and decarbonise this sector of the iron and steel industry, some strategy must be pursued to capture these direct point emissions and deliver a truly clean gas from a carbon point of view.

To this purpose, a carbon capture technology may be considered for implementation, which is, in

fact, the concept this thesis tries to prove as well as its feasibility. From all carbon capture technologies, amine-based chemical absorption technologies may present a reasonable solution to capture these emissions from the EAF exhaust gas, since they have been considered highly-mature, hence ready for deployment in commercial service, which is equivalent to a technology readiness level (TRL) 9 [44]. This scale quantifies the maturity of a given technology for commercial distribution.

However, an additional problem arises and may apparently pose as a challenge to the implementation of such technology in the EAF process: recall that the EAF operates in a discontinuous manner, but a typical capture plant (absorption + desorption) operates continuously. In chapter 4, a thorough discussion regarding a possible solution to overcome this problem is provided.

Furthermore, one must also take into consideration that *indirect* CO_2 emissions also arise from the production of other process inputs to the EAF (*e.g.*, lime) and from the consumed electricity that had to be somehow generated, with the point being whether this electricity was produced from renewable sources or not [17].

2.2 Absorption and stripping

2.2.1 Introduction

Gas absorption has long been used as a means to separate gas mixtures in the Chemical and Petrochemical industrial sector. In such separation process, a gas and a liquid (the so-called solvent[4]) stream are kept in direct intimate contact, and provided that a driving force exists, mass transfer between the two phases is enabled. That is, owing to a gradient in chemical potential, one or more gaseous components diffuse into the liquid phase. One may designate the liquid phase (solvent) as the mass-separating agent, responsible for unleashing the separation by phase affinity [45]. Under certain conditions, it is reasonable to approximate that a chemical potential gradient gives way to a concentration gradient.

Generally speaking, gas absorption aims at [46, 47]:

- purification through the selective removal of one (or more) impurities, contaminants or pollutants (referred as solutes or absorbates) and

- recovery of valuable chemicals existing in those gas streams.

2.2.2 Gas absorption (or the art of removing solutes from gas streams)

Gas absorption typologies It is widely acknowledged that gas absorption processes can be classified into two major categories: physisorption and chemisorption, according to the intrinsic nature of interaction between the absorbent and the solute [45, 48]. In table 2.2, a few examples of industrial applications are summarized.

---

[4]The absorbent will be contained in the solvent.

Table 2.2 – Reaction types on a classical reactive absorption process.

Physical	Reactive	
	Irreversible	**Reversible**
CO_2 with H_2O	SO_3 with water (producing H_2SO_4)	CO_2 with amines, *e.g.* MEA

- **physical absorption**, where gaseous components to be absorbed dissolve in an non-reactive liquid solvent. Regarding mass transfer, diffusional mass transfer takes place at the gas-liquid interface and convective mass transport within the *bulk* phases. This type of absorption hinges largely on gas solubility [49]. Phenomenologically speaking, *Henry's law* describes mathematically the gas-liquid equilibrium of mixtures with low solute partial pressures, relating the partial pressure of the component i in the gas to the corresponding concentration of the dissolved component i in the solvent.

$$p_i = Hx_i \qquad H, \text{ Henry coefficient in } [P] \text{ unit} \qquad (2.3)$$

A word of caution is in order regarding the wide variety of Henry coefficients, but such discussion is beyond the scope of the present work. Physical absorption is also contingent upon working conditions as temperature and pressure. Different components absorb differently in the same solvent as a result of its differences in solubility in the solvent [45]. Therefore, selectivity and consequently separation are achieved.

- **chemical or reactive absorption** (chemisorption), where physical dissolution takes place in a first moment, followed by chemical reactions. Therefore, chemical absorption can be conceived as physical absorption supported by chemical reactions [45]. Reaction stoichiometry, reactant concentration and mass transfer rates all influence reactive absorption [49]. In particular, reaction stoichiometry establishes the solvent loading, which is an important property of a given solvent, as will be seen. Reactions themselves can be roughly classified as:

  i) **reversible**, where reactants (in this case, solvent and free solute molecules) and products (that is, solute bounded to absorbent) can be easily interchanged by shifting the reaction from the point of equilibrium. An example could be the reaction of CO_2 with an amine-based, like monoethanolamine (MEA), as shown below. This facilitates solute recovery, and, at the same time, solvent regeneration, thus allowing to recycle the solvent to the absorber. In this class of reactions, the major question to be answered is "*how far* does the reaction go?". The equilibrium state dictates how much product can be formed. At a given temperature and pressure, an equilibrium conversion exists (that cannot be exceeded), and constrains the extent of reaction [40, 50].

$$CO_2 + 2\,MEA \rightleftharpoons MEACOO^- + MEAH^+$$

At this point, one may think "but *how long* does it take to approach equilibrium?". In theory, a reversible reaction proceeds to equilibrium, regardless of the time it takes to reach it. It may happen that it takes a few seconds or a couple of hours for that the answer to this question simply lies on reaction kinetics. To put in another way, whereas thermodynamics imposes a limitation on the extent of reaction, reaction kinetics reveals how quickly would this limit be attained, provided that sufficient time for equilibrium to be reached is allowed. Either way, under no circumstances can the reaction proceed beyond the equilibrium state, no matter how fast it might go [51], which is why reversible reactions are said to be *equilibrium-controlled*. Even so, real systems may not necessarily achieve the equilibrium conversion, and these thermodynamic limit values are only maximum attainable ones for a given set of conditions. For this reason, kinetics may also have a role to play.

ii) **irreversible**, in which equilibrium is either severely shifted towards the reactants (in which case no reaction happens at all) or the products side. That is, equilibrium itself does not determine the ultimate reaction outcome, but rather the exhaustion of the limiting reagent [52]. If a reaction of this class is carried out in an ideal reactor, there will not be any thermodynamic limitation on the possible achievable conversion, meaning that the rate of exhaustion of the limiting reagent will dictate conversion. As such, these reactions may well be called *kinetically* or *rate-controlled* reactions. As far as chemical absorption is concerned, if the solute reacts irreversibly with the solvent, it will not be feasible to regenerate the solvent thereafter, as it would imply high energy requirements to do so. An example could be the reaction between SO_3 and water:

$$SO_3 + H_2O \longrightarrow H_2SO_4$$
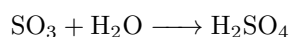
In reality, irreversible reactions are not generally employed unless a valuable chemical can be produced upon the absorption reaction and/or the solvent being employed is relatively inexpensive.

In one way or another it is desirable to have fast absorption reactions (*i.e.*, high reaction rates), as the contact time between the gas-liquid phases is finite. In fact, as the phase interaction is established along the column height, then the height of the absorption column will determine how long will the two phases contact each other [45].

2.2.2.1 Reactive absorption

According to Cussler [53], the choice of a particular liquid absorbent is determined by the percent removal rate and the contaminant(s) concentration(s) in the feed gas. In fact, should the feed gas have a high partial pressure (concentration) of an impurity, say H_2S, then physical absorption is to be preferred; whereas if the feedstock has low impurity concentration, then separation must be carried out by chemical absorption. It is quite easy to understand the latter statement: the absorbed molar flow of a component i increases with the reaction's occurrence. As reactants are continuously depleted, a steady driving force builds up, hence enhancing mass transfer. So it comes as no surprise that chemical solvents are employed when the concentration of the target component in the feed gas is quite low [45]. This

clearly proves that the integration of the phenomena of physical absorption and chemical reaction is much prolific.

In the vast majority of the chemical absorption processes, the reaction (either irreversible or reversible) takes place in the liquid place. Even so, there are other reported cases where the reaction occurs in both phases or just at the gas-liquid interface (in which case it must necessarily be an instantaneous reaction).

Effect of the working pressure and temperature on gas absorption   When it comes to just dissolving gases in liquids, it is generally accepted that high pressures and low temperatures favour gas solubility in liquids [40, 45]. This is the case of physical absorption. However, recall that reactive absorption involves coupling the occurrence of physical absorption with chemical reactions. Reaction rates are temperature-dependent in such a way that higher temperature enable faster reactions (as per Arrhenius's equation). So, a clear trade-off exists between kinetics and gas solubility as both are strongly influenced by temperature. Furthermore, pressure influences chemical reactions (think of Le Chatêlier's principle), with pressure being in turn dependent on the reaction stoichiometry. The effect of pressure is more profoundly noted in gas-phase reactions. All in all, for a given reactive absorption operation, there is an operating pressure and temperature window under which desired performance is accomplished [45].

The absorbent in reactive absorption processes   It is a common practise in the treatment of gases containing CO_2 and/or H_2S to use aqueous solution of alkanolamines, carbonates or ammonia [49]. In this work, only absorption with alkanolamines is considered and a short summary about the basic chemistry between amine aqueous solutions and CO_2 will follow.

   Amine structure   Alkanolamines are organic compounds consisting of both amino groups and hydroxyl, as in fig. 2.11. According to their structure, alkanolamines can be divided into three categories: i) primary amines; ii) secondary amines and iii) tertiary amines, depending on the number of substituents. There are also sterically hindered amines, as aminomethyl propanol (AMP). For instance, primary amines have a central nitrogen atom to which a substituent is bonded and two other hydrogen atoms. The most common acknowledged alkanolamines [49] are monoethanolamine (MEA) - a primary amine -, diethanolamine (DEA) - a secondary amine -, triethanolamine (TEA) - a tertiary amine -, *N,N*-diisopropylaminoethanol (DIPA) - a secondary amine -, methyldiethanolamine (MDEA) - a tertiary amine.

   The amino group provides alkalinity to the aqueous solutions, which is required for the absorption of acid gases, like CO_2. On the other hand, hydroxyl groups increase i) the solubility of these compounds in water owing to the establishment of hydrogen bonds, meaning more intermolecular forces and ii) reduce the vapor pressure of such solutions. Also, stronger intermolecular forces mean that volatility is decreased (as molecules cannot escape as readily from the liquid surface), and therefore surface tension is also increased [49, 54].

Figure 2.11 – Chemical structures of some of the most common alkanolamines.

Amine solutions - general characteristics and trends   When screening potential solvents to be used in gas treatment operations, several properties have to be considered [49]:

- heat of reaction;

- heat of vaporisation;

- reaction rate (with solute);

- corrosivity, which largely influences the choice of equipment, increasing capital costs;

- loading, which describes the solvent absorptive capacity based on the one mole solvent. That is, how many moles of acidic gases can a single mole of solvent accommodate? Later on, this property will be further analysed.

In table 2.3 it is roughly shown how do these properties vary with the amine type.

Table 2.3 – Some general qualitative trends on the main alkanolamines properties (based on [49]).

Alkanolamines		
Primary MEA	Secondary DEA	Tertiary TEA, MDEA
High	$\xleftarrow{\text{heat of reaction}}$	Low
High	$\xleftarrow{\text{heat of vaporisation}}$	Low
High	$\xleftarrow{\text{reaction rate}}$	Low
High	$\xleftarrow{\text{corrosivity}}$	Low
Low	$\xrightarrow{\text{loading}}$	High

Heat (enthalpies) of reaction and vaporisation show the same behavior and decrease from primary to tertiary amines, that is, as the number of substituents in the alkanolamine increases. The reason for such behavior will be analysed under the paragraph *reaction mechanisms*. As will be seen, these quantities are related with the required energy for solvent regeneration.

High reaction rates are desirable during chemical absorption. In fact, primary alkanolamines show higher reaction rates than tertiary alkanolamines. As a consequence, if tertiary alkanolamines are used as solvent, higher solvent flow rates are necessary to achieve the same separation.

On the other hand, corrosivity is another aspect to take into consideration when selecting a solvent as it directly affects the equipment material (and might potentially limit the options to choose from). If reactants and the reaction products are highly corrosive, additional costs are introduced (increasing the capital costs) as corrosion resistance materials are more expensive.

Reaction mechanisms   Different types of amines react differently. So, let us now briefly address the involved reactions for each type of alkanolamine. Regardless of the amine type, the following reactions take place in all aqueous solutions:

$$H_2O \longleftrightarrow H^+ + OH^- \qquad \textit{Water ionisation} \qquad (2.4)$$

$$CO_2 + H_2O \longleftrightarrow H_2CO_3 \longleftrightarrow HCO_3^- + H^+ \qquad \textit{CO}_2 \textit{ equilibria} \qquad (2.5)$$

$$CO_2 + OH^- \longleftrightarrow HCO_3^- \qquad (2.6)$$

$$HCO_3^- \longleftrightarrow CO_3^{2-} + H^+ \qquad (2.7)$$
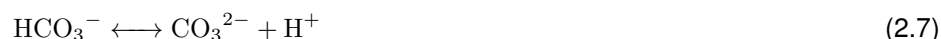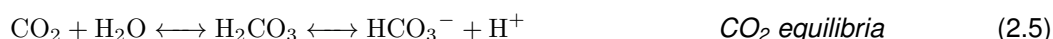
When amines are present, the following additional reactions proceed, depending on the type of amine.

Primary (RNH$_2$) and secondary (R$_2$NH) amines

Primary and secondary amines are believed to react via the so-called zwitterion mechanism, as a zwitterion intermediate is formed that later leads to the formation of the carbamate ($RNHCOO^-$) species [55]. An example for a primary amine, as MEA, is given. Here, MEA is represented as RNH_2.

$$1) \quad RNH_2 + CO_2 \longleftrightarrow RNH_2{}^+COO^- \qquad \textit{Carbamic acid (a zwitterion) formation} \quad (2.8)$$

$$2) \quad RNH_2{}^+COO^- + RNH_2 \longleftrightarrow \underset{\text{carbamate}}{RNHCOO^-} + RNH_3{}^+ \qquad \textit{Carbamate formation} \quad (2.9)$$

which translates into the global reaction

$$CO_2 + 2\,RNH_2 \longleftrightarrow \underset{\text{carbamate}}{RNHCOO^-} + RNH_3{}^+ \qquad (2.10)$$

As stable carbamates are formed, primary and secondary alkanolamines, like MEA and DEA, react quite fast with CO_2. Conversely, this means higher solvent regeneration costs as stable carbamates will require more energy to break into CO_2 [55].

Tertiary (R$_3$N) amines

35

This type of amines, in turn, reacts without forming any carbamate. Reaction proceeds via a bicarbonate mechanism.

$$1) \quad CO_2 + H_2O \longleftrightarrow HCO_3^- + H^+ \qquad \textit{Bicarbonate formation} \qquad (2.11)$$

$$2) \quad R_3N + H^+ \longleftrightarrow R_3NH^+ \qquad \textit{Amine protonation} \qquad (2.12)$$

which translates into the global reaction

$$R_3N + CO_2 + H_2O \longleftrightarrow R_3NH^+ + HCO_3^- \qquad (2.13)$$

Tertiary alkanolamines, like TEA, have low CO_2 reactivity mainly due to the bicarbonate formation by CO_2 hydrolysis. However, it should be noted that all amines can undergo protonation.

Remark (on loading). As it was seen previously, loading is markedly one of the most important characteristics of a solvent. A given reaction equation shows the proportions by which reagents react with each other, giving products. Besides, the reaction equation foreshadows (by means of the reaction stoichiometry) the amount of CO_2 that can be absorbed per mole of amine, assuming that the reaction proceeds to completion.

Primary and secondary amines react with CO_2 in the same way, forming carbamates - as rxn (2.10). Looking at the reaction stoichiometry, 1 mole of CO_2 reacts with 2 moles of amine, which means a mole of amine can absorb at most 0.5 mol CO_2. On the other hand, tertiary amines react via another mechanism - as rxn (2.13) - by which a loading of 1 mol CO_2/mol amine can be theoretically achieved, as one amine molecule reacts with a single CO_2 molecule. As a consequence, if primary amines are chosen as the absorbent, then higher primary amine concentrations in the solvent are needed to achieve comparable results to those obtained if tertiary amines are employed. This is, in fact, twice the loading of primary and secondary amines. Note that these are the maximum achievable loadings for the current state-of-the-art amine-based solvents [56]. However, greater loadings can be achieved if physical absorption also takes place (which can happen at high CO_2 partial pressures).

2.2.3 Gas desorption (or the art of stripping solutes from a solvent)

In order to minimize solvent waste generation, the solvent can be recycled to the absorber after the solute is stripped. In reality, this mass transfer process is simply the reverse of absorption. In a chemical absorption plant, the desorption unit operation is the cost-determining phase, considering the energy costs. These come down to the desired degree of regeneration of the solvent (purity) at the desorber outlet. Generally speaking, there are four methods to perform desorption [45, 48]:

- increase the temperature in the desorber and reboil the solvent, generating in the meantime a stripping vapor;

- stripping with an inert gas stream or steam;

- reduce the system pressure to let the target component desorb; in other words, flash the solvent to lower the partial pressure of the dissolved components;

- precipitate the reaction products.

A combination of the above-mentioned methods is frequently employed: for instance, desorption by pressure reduction finds wide application in physical absorption processes since its energy requirements are low [48]. Furthermore, if the absorption unit operates at high pressures, reduced-pressure desorption is favored as the process shifts from high to low pressures. After the fluid depressurization at the desorber inlet, an inert gas stream can strip the target component. This option is a combination of two strategies, and is more economic than thermal regeneration which would require the solvent to be reboiled. The choice for stripping with an inert gas over stripping with thermal regeneration is clear when the solvent has a low boiling point such that a slight temperature increase would mean high solvent losses [45].

Nonetheless, for chemical absorption processes, the combination of techniques is, frequently, solvent flashing, followed by solvent vaporisation at the reboiler (thermal regeneration). Utilities (steam) are required at the reboiler, and its operating pressure and temperature must be carefully defined. In the case of MEA-based processes for CO_2 capture, temperature at the reboiler is chosen so not to degrade MEA (or vaporize it, given the environmental concerns). Therefore, at the reboiler, ideally only water vaporizes, thus generating a stripping vapor that is, essentially, steam [57].

In chemical absorption processes, strippers frequently operate at high temperatures and above-ambient pressures. High temperatures ensure low affinity between CO_2 and the solvent, as: i) temperature changes shift chemical equilibria; and ii) gas solubility decreases with temperature increases. In fact, as mentioned previously, the extent to which CO_2 absorbs chemically to the absorbent is solely controlled by the chemical equilibrium position [58]. Mass transfer can influence the reaction, but it cannot be responsible by the degree of affinity between the absorbent and solute. Changing the temperature shifts the equilibrium position, and thus changes the affinity between the absorbent and CO_2 [58]. Furthermore, desorption reactions are endothermic, so heat must be put into the vessel. These temperatures and pressures are maintained by the reboiler operation where solvent is continuously reboiled.

Remark (on the operating pressure)**.** Strictly speaking, the operating pressure of a given equipment is chosen by the designer and is established thanks to the operation of i) auxiliary equipment like a reboiler; or ii) proper pressure changing devices (*e.g.*, pumps, fans). Also note that the pressure and temperature at which an equipment operates may also be ascribable to the fluid thermophysical properties (including the number of phases, *e.g.*, saturated liquid) that are admitted to that equipment.

Setting (and maintaining) this above-ambient pressure is guaranteed by the reboiler operation, when the stripping vapor is generated. On the other hand, the rich solution exiting the absorber is pumped to an above-ambient pressure while on its way to the stripper. As it enters the vessel, the rich solution is flashed (thus favoring desorption), since the vessel operates at another different pressure. Inside the

stripper two phases coexist, vapor and liquid; thus, its operating pressure will be mainly due to the partial pressures of CO_2 and H_2O [59]. This water partial pressure is, in fact, made of two contributions: that arising from the H_2O vaporised from the rich solution and another from the stripping steam that flows countercurrently to the liquid rich solution. Upon stripping steam generation at the reboiler, it condenses along the column as heat transfer takes place from the steam to the rich solvent; this means that the evolved latent heat is channelled into the solvent regeneration. As steam condenses along the column, its partial pressure decreases, and so it must be compensated by the CO_2 partial pressure. This effect pushes and helps to maintain a steady driving force for CO_2 mass transfer. Besides, at the same time, released CO_2 must be continuously diluted (hence calling for more stripping steam), so that its partial pressure does not reach the equilibrium one, as mass transfer would have ceased as soon as the CO_2 partial pressure reached the CO_2 partial pressure value at equilibrium conditions.

So by now it should be clear that there are several phenomena contributing to the overall reboiler energy requirements: i) the latent heat required to produce stripping vapor (essentially steam); ii) the sensible heat required to bring the incoming rich solution temperature to the stripper operating temperature; iii) heat required to drive desorption reactions. In fact, the thermal energy requirements (TER) at the reboiler are the overall result of these phenomena, and a deeper insight into the stripper performance is obtained when the TER are dissected into these components, as in eq. (2.14):

$$q_{\text{reboiler}} = q_{\text{reaction}} + q_{\text{stripping vapor}} + q_{\text{sensible}} \Leftrightarrow$$
$$\Leftrightarrow q_{\text{reboiler}} = \dot{n}_{CO_2} \Delta H_{\text{des},CO_2} + \dot{n}_{H_2O} \Delta H_{\text{vap},H_2O} + \dot{m}_{\text{solv}} \bar{c}_p (T_{in} - T_{out}) \tag{2.14}$$

where q_{reboiler} (kW) is the reboiler heat duty, q_{reaction} (kW) is the heat of reaction for CO_2 desorption, $q_{\text{stripping vapor}}$ (kW) is the heat required to generate the stripping vapor (steam) and q_{sensible} (kW) is the sensible heat contribution. Note that all this thermal energy is largely provided by the reboiler, or better by the steam supplied to the reboiler. $\dot{n}_{CO_2}$ is the molar flow rate of regenerated CO_2 at the stripper (mol/s) and $\Delta H_{\text{des},CO_2}$, the heat of desorption (kJ/mol). $\dot{n}_{H_2O}$ is the molar flow rate of steam leaving the stripping column (mol/s) and ΔH_{vap}, the (latent) heat of vaporisation of water (kJ/mol). At last, $\dot{m}_{\text{solv}}$ is the solvent mass flow rate (kg/s), $\bar{c}_p$, the solvent specific heat capacity (kJ/kg K) and $(T_{in} - T_{out})$ the solvent temperature difference between the stripper inlet and outlet (K) [60].

A typical scheme of an absorption unit coupled with stripping for solvent regeneration is shown in fig. 2.12. As it unfeasible to feed fresh solvent every time the absorption operation is ran, CO_2-loaded solvent must be regenerated after the absorption step. Gas absorption is carried out in vertical columns, where the solvent - fed at the top of the column - and the gas mixture to be treated - that enters from the bottom - contact each other in a countercurrent pattern. As the solvent flows downwards in the column, it washes out the absorbate from the gas, and gets progressively enriched in the solute. Therefore, at the outlet of the absorber, the once *lean solvent* (relative to the absorbate) is now a *rich solvent*, which is then subjected to the CO_2 stripping step (regeneration).

The regenerated solvent - lean solvent - flows through the *lean-rich heat exchanger* where it loses
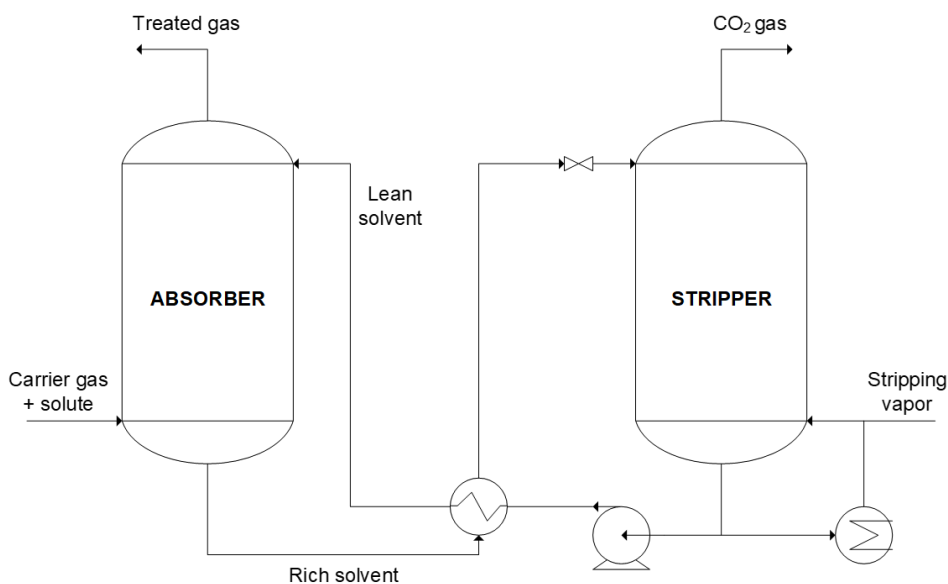
Figure 2.12 – Scheme of an absorption-stripping unit operation.

some thermal energy to the rich solvent that flows towards the stripper. After the lean-rich heat exchanger, the lean solvent is cooled down to an adequate temperature, and is re-admitted to the absorption column. Despite not shown in fig. 2.12, there is usually a fresh amine solution make-up to compensate for solvent losses either due to solvent evaporation or irreversible chemical reactions that subtract the amount of available solvent for the separation [48]. What is more amine make-up guarantees flowsheet convergence when these type of processes are simulated, which clearly prompts amine solution replenishment - see chapter 3.

Please note that a detailed explanation on how to design an absorption + desorption unit will not be provided as it is outside of the scope of the present work.

2.2.4 Modelling

More often than not absorption-based operations are modelled in the industry, as considerable less experimental effort is required. To correctly design absorption columns (or scale-up existing ones), rigorous and reliable models are needed [45]. That is to say detailed models are only obtained if there is a profound understanding of heat and mass transfer that translates into an adequate description of such phenomena in the model.

Modeling an absorption column (or whichever vapor-liquid separation operation) involves dividing it into vertical segments, that may be called stages. To be more specific, the column height is discretized into a certain number of parts - the so-called stages [61]. Note that here a stage can be a single tray or a collection of those or might even be a segment of a packed section, depending on the vapor-liquid separation equipment [46]. The mathematical description of each stage n is based on the *MESH* – mass, equilibrium, summation and enthalpy – equations which are solved during the simulation. Inside the absorber, liquid and vapor phases contact one another: as concentration differences between phases exist, then mass transfer should occur until equilibrium with respect to mass transfer is reached.

However, for a given stage n, equilibrium might be achieved or not. So, depending on the assumptions made, there are several approaches to <u>model mass transfer</u> [45]:

- the simplest - an equilibrium-stage model, which assumes that exiting streams attain equilibrium;

- the *in-between* - a *HTU-NTU* model, mass transport kinetics are considered;

- the hardest - a rate-based model which involves axial discretization and builds up on the latter approach.

2.2.4.1 Equilibrium-stage models

The theoretical tray (plate) is the core concept upon which the theoretical foundations of distillation were based. Also the McCabe-Thiele plots are contingent upon this same idea. In fig. 2.13, a theoretical stage is illustrated, which is one such that the following assumptions are satisfied: i) streams exiting the plate are at equilibrium; ii) there is complete mixing of the liquid in the plate; and iii) liquid droplets do not entrain the gas stream leaving to the next plate.

$$L', \ X_{i,n-1} \qquad \qquad G', \ Y_{i,n}$$

Stage n

Global MB:
$$L'X_{i,n-1} + G'Y_{i,n+1} = G'Y_{i,n} + L'X_{i,n}$$

$$L', \ X_{i,n} \qquad \qquad G', \ Y_{i,n+1}$$
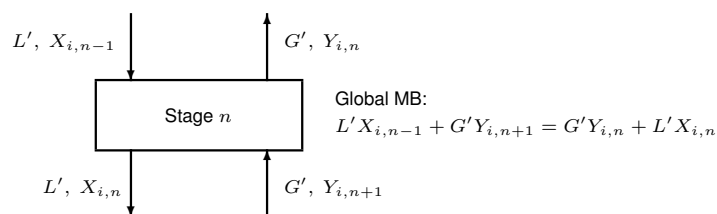
Figure 2.13 – Schematic of a single equilibrium stage. L' and G' correspond to solute-free mole flow rates and X_i, Y_i mole ratios for component i.

If equilibrium is assumed to be achieved, then no mass transfer rates are to be calculated [47], since thermodynamics has determined the maximum possible extent of the mass transfer of a component i, so that equilibrium is attained. So, when solving the *MESH* set of equations, mass balances will depend on the information given by the equilibrium equations, which state the equilibrium compositions for that stage.

In fact, these assumptions are rarely fulfilled, especially exiting vapor-phase mole fractions are not related to exiting liquid-phase mole fractions by thermodynamic *K*-values [46]. As a consequence, actual mass transfer is lower than that predicted by these equilibrium models. So, more conceptually complex models are needed, in which nonidealties of the equilibrium are be accounted. That is to say mass transfer rates now have to be calculated. Nonetheless, equilibrium considerations provide valuable insight, when, for instance, making a first estimate of the minimum amount of solvent required to perform a given separation task.

On the other hand, individual stages cannot be physically distinguished within packed columns (as opposed to tray columns). For this reason, the concept of the height equivalent to a single theoretical stage (HETP) arose. If the number of theoretical stages (determined by McCabe-Thiele graphical procedure or by stage-by-stage methods) that ensure the product specifications is known as well as the packing HETP, then the required packing height is straightforwardly determined.

2.2.4.2 *HTU-NTU* models

HTU-NTU analysis takes into consideration that mass transfer might be limited and so equilibrium is not reached. Further details are outside of the scope of the present work, but the reader can find them thoroughly explained in [46, 47].

2.2.4.3 Rate-based models

Nowadays, these non-equilibrium transport models are the most rigorous models available as the traditional approach for solving such problems clearly does not hold for all cases. Rate-based models account for interfacial mass transfer between the liquid and vapor phases, the reaction kinetics and the electrolytic interactions [62]. Rate-based models utilize once more *MESH* equations, applied at every single segment in which the column height was divided. In this approach, mass and energy balances are now written for each phase (like in the *HTU-NTU* analysis) in a segment rather than performing mass and energy balances around each segment, as illustrated in fig. 2.14. In other words, the spatial domain of a rate-based segment is divided in four zones: the gas bulk, the gas film, the liquid film and the liquid bulk.

Figure 2.14 – Schematic of a single non-equilibrium stage for a rate-based method [63]. The subscripts i and j refer to the components and the stages, respectively. F, L and V refer to the feed, liquid and vapor molar flow rates. N refers to the molar transfer rates, H to the enthalpies and T to temperatures. x and y refer to liquid and vapor mole fractions, respectively. q the heat transfer rate and Q the heat input to a given stage j.

Remark (on the difference between stages and segments). At this point, it should be noted again that a stage can be a single tray or a collection of those or might even be a segment of a packed section [46]. When dealing with rate-based models to simulate packed columns, *stages* should be referred to as *segments*.

By changing the perspective on how control volumes are defined (from a control volume enclosing a whole segment to a control volume enclosing each of the phases coexisting in a segment), mass balances are now written in such a way that interfacial mass and heat transfer is accounted in the balances

through the dedicated mass/heat transfer rates. In particular, mass transfer rates are calculated upon selecting an adequate mass transfer theory to serve that purpose, as the Lewis-Whitman's two-film theory. Lewis and Whitman envisioned vapor-liquid equilibrium at the interface between two phases and that temperature and concentration gradients (the heat and mass transport drivers, respectively) are confined in two thin film layers that surround the vapor-liquid interface. Regarding transport at the films, multicomponent diffusion in the films is described by the Maxwell-Stefan equations [49]. Mass transfer resistance is assumed to lie in these films, while bulk phases are considered ideally mixed (as if they were CSTRs) [62, 64]. If the bulk phase of every segment behaves like a CSTR, then the collection of bulk phases in all segments will mean that the bulk phase (as a whole) behaves like a plug-flow reactor.

Reaction in rate-based models   Reactions can be implemented in the reactive absorption processes models by simple introducing reaction source terms in the mass balances stated for each phase. Furthermore, a reaction source term must be included in the mass transport equation (describing mass transfer over the film). Chemical reaction interferes with mass transfer processes.

The MEA-CO_2 system   For a given segment at a particular column height, typical partial pressure and concentration profiles that describe the CO_2 absorption in a MEA-based solvent are depicted in fig. 2.15, thus illustrating mass transfer. In accordance with the two-film theory, CO_2 molecules are transported from the bulk gas (convective mass transfer) to the interfacial surface; then CO_2 molecules are transported across the interface to the liquid phase (CO_2 dissolution), and at last CO_2 is transferred to the bulk conditions of the liquid phase.
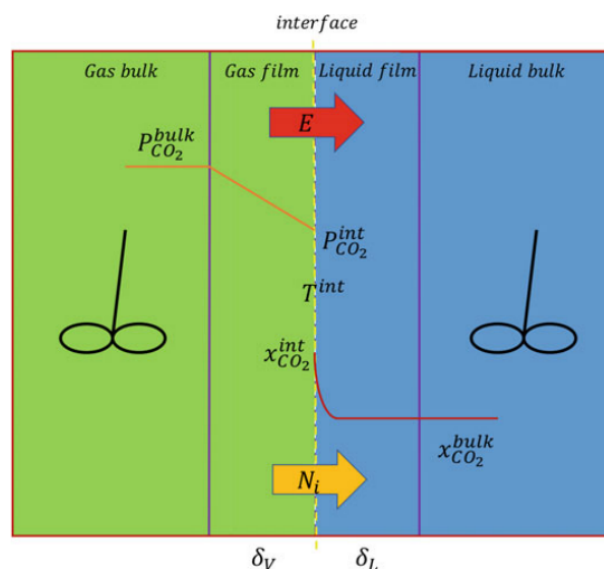
Figure 2.15 – Two-film theory representation of a single segment in which CO_2 absorbs in a MEA-based solvent. [61].

Due to a small gas film resistance, CO_2 partial pressure does not decrease sharply [65]. At the interface, equilibrium is assumed. As soon as CO_2 dissolves in the liquid phase, it reacts with the absorbent (contained in the solvent solution fed to the absorber). These reactions can be limited either by

equilibrium considerations or chemical reaction kinetics. In any case, this topic was thoroughly detailed in section 2.2.2.

CO_2 reacts mainly in the liquid film, as shown in fig. 2.15, which is why i) the concentration of dissolved CO_2 plummets and ii) at the same time, the concentration of free amine diminishes from the bulk to the liquid film.

Several reaction regimes can be distinguished, as shown in fig. 2.16 for the case of a second-order reaction with reactants A and B, as the MEA-CO_2 reaction [66]. Comparing fig. 2.15 with fig. 2.16 - medium reaction profile - one notes their general similarity.
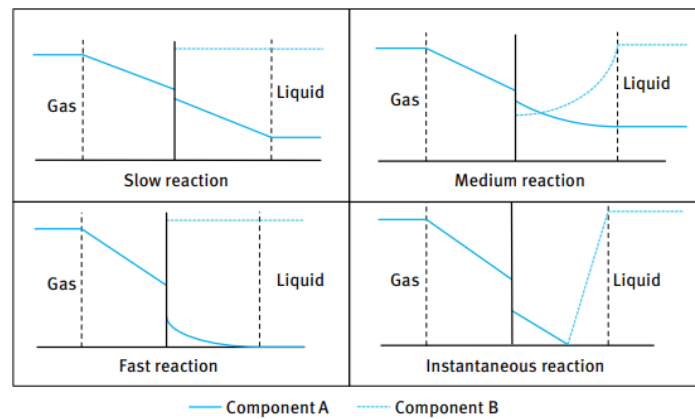
Figure 2.16 – Liquid film second-order reaction regimes and concentration profiles [45].

Let us now note two apparently mutual excluding facts [53], but that actually depend on what is the focus:

i) the first: reaction results in *enhanced* mass transfer. In fact, during the course of a reaction, the local concentration of a reactant reduces, thus increasing its concentration gradient and flux. Therefore, interfacial mass transfer is increased.

ii) the second: mass transfer itself can be responsible for *reduced* reaction rates in such a way that mass transfer limits the transport of reactants to active sites (specially important in catalysis), compromising the extent of a catalytic reaction.

As far as *enhanced* mass transfer enabled by reaction is concerned, *enhancement factors* are calculated, which are defined as

$$\epsilon = \frac{\text{flux with reaction}}{\text{flux without reaction}} \tag{2.15}$$

Calculating these enhancement factors is essentially the same as asking "by what amount has the mass transfer been increased by chemical reaction?".

Furthermore, a dimensionless number - the *Hatta* number - can be defined as

$$Ha = \frac{\text{reaction rate in the film}}{\text{diffusion through the film}} \tag{2.16}$$

43

allowing to classify the absorption process. Based on Ha, reaction can be rate-limited or diffusion-limited (*i.e.*, mass transfer limitations exist). Suppose that diffusion is quite fast compared to the reaction rate, then reaction is rate-limited, and $Ha < 1$. On the other hand, consider the limiting case in which the reaction rate is almost infinite. Reaction is thus instantaneous, which results in $Ha = \infty$ [45].

Film discretization   According to the two-film theory, vapor and liquid films are separated by the gas-liquid interface. These two films can be further divided into segments in rate-based models. This additional discretization allows better concentration profiles to be computed, which in turn enables a more detailed analysis of the degree of mass transfer enhancement due to the chemical reaction [45, 64]. A more detailed discussion is provided under chapter 3.

3

Methodology

A fool with a tool is still a fool.

GRADY BOOCH (1955 –)

A detailed description of the model developed in Aspen Plus® V11 is provided in this chapter. The methodology adopted in this research work is also thoroughly laid out. According to our best knowledge, the simulation of such system applied to a mini-mill has never been reported before in the literature.

3.1   Overview of the followed methodology

The primary goal of the this work was to simulate a MEA-based chemical absorption CO_2 capture plant located just after the cleaning treatment of the EAF off-gas. To that end, an Aspen Plus® rate-based model was built, adapting an example of a model provided by AspenTech [67]. However, recall that under Aspen Plus® only steady-state simulation can be performed, which is not consistent with the EAF intermittent nature of fumes emission. The variability of the fumes flow rates clearly denotes a transient process. So, a first approach to this problem was to assume a constant flow rate of fumes entering the capture plant to be treated – which was the first phase of the followed methodology, leading to the so-called base case simulation.
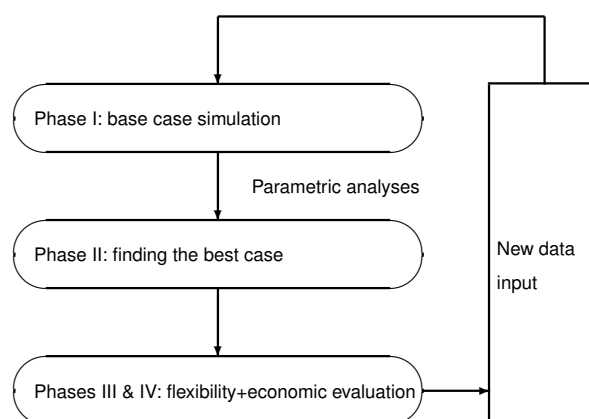
Figure 3.1 – Scheme of the devised methodology.

After the base case simulation, a series of sensitivity analyses were carried out to identify the best case scenario. An outline of the adopted strategy to build this initial simulation is delineated in subsection 3.2.3.

After the best scenario was found, the washing section was optimised and the particularity of the EAF transient nature was taken into consideration in the flexible operation mode analysis. Having reached the desired objectives, an economic evaluation was performed to assess the feasibility of such technological solution. Whenever new data (as new feed compositions) are considered and inputted, the above-mentioned reasoning is repeated. In fig. 3.1, an outline of the followed steps is shown.

3.2 Aspen Plus® model implementation - base case simulation

The remaining of this chapter will be dedicated to detail the implementation of the steady-state base case simulation. As usual, the first step in setting up an Aspen Plus® simulation is to adequately select the chemical system and thermodynamics models, prior to building the flowsheet.

3.2.1 Chemical system and physical properties

The electrolyte Non-Random Two Liquid (e-NRTL) model was adopted for the thermodynamic calculations with the Redlich-Kwong (RK) extension, as suggested by [67] and in accordance with the works of [60, 61, 68]. A chemistry and two reaction models were created, as follows.

Chemistry: MEA model   This model is used as the global electrolyte calculation option and consists of the following instantaneous reactions:

$$MEAH^+ + H_2O \longleftrightarrow MEA + H_3O^+ \qquad \text{\textit{Amine protonation}} \qquad (3.1)$$

$$MEACOO^- + H_2O \longleftrightarrow MEA + HCO_3^- \qquad \text{\textit{Carbamate formation}} \qquad (3.2)$$

$$2\,H_2O \longleftrightarrow H_3O^+ + OH^- \qquad \text{\textit{Water hydrolysis}} \qquad (3.3)$$

$$CO_2 + 2\,H_2O \longleftrightarrow HCO_3^- + H_3O^+ \qquad \text{\textit{Bicarbonate formation}} \qquad (3.4)$$

$$HCO_3^- + H_2O \longleftrightarrow CO_3^{2-} + H_3O^+ \qquad \text{\textit{Carbonate formation}} \qquad (3.5)$$

Since reactions (3.1)-(3.5) are instantaneous, their reaction rates are virtually equal to infinite, thus making reaction kinetics negligible when it comes to deciding the reaction outcome. That is to say that kinetics do not rule what is the final distribution of products. Therefore, chemical equilibrium can only be the sole responsible for the reaction outcome. The equilibrium constants of reactions (3.1)-(3.5) are calculated from standard free Gibbs energy change. Note that saying a reaction is instantaneous does not mean that equilibrium is shifted to one side of the reaction. Instantaneous means that the reaction proceeds so fast that kinetics does not interfere with the reaction outcome, leaving thermodynamics (equilibrium) to command it. Once more, these type of reactions are *equilibrium-controlled*. Equilibrium

may then reveal whether the reaction is shifted towards one side of the reaction (making it a irreversible reaction) or not (a reversible reaction).

Reaction: `MEA-RXN` **and** `MEA-STP` **models**   These two reaction models are used to represent the reactive processes within the absorption and desorption columns. Reactions (3.1), (3.3) and (3.5) also make part of the `MEA-RXN` and `MEA-STP` models, as well as the following finite rate ones:

$$CO_2 + OH^- \longrightarrow HCO_3^- \tag{3.6}$$

$$HCO_3^- \longrightarrow CO_2 + OH^- \tag{3.7}$$

$$MEA + CO_2 + H_2O \longrightarrow MEACOO^- + H_3O^+ \tag{3.8}$$

$$MEACOO^- + H_3O^+ \longrightarrow MEA + CO_2 + H_2O \tag{3.9}$$
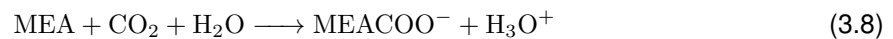
These are *rate-controlled* reactions, meaning kinetics are not instantaneous, and thus have a role to play in terms of the reaction outcome. Power-law kinetics are assumed, and so rate expressions of reactions (3.6)-(3.9) share the following form:

$$r = k \exp\left(-\frac{E}{RT}\right) \prod_{i=1}^{N} (x_i \gamma_i)^{\alpha_i} \tag{3.10}$$

where r is the rate of reaction; k, the pre-exponential factor; T, the absolute temperature (in K); E, the activation energy (in cal/mol); R, the universal gas constant (in cal/(mol K)); x_i, the mole fraction of component i; γ_i, the activity coefficient of component i in the reaction; α_i, the stoichiometric coefficient of component i in the reaction equation and N, the number of components involved in the reaction. The aforementioned parameters were all extracted from [67]. CO_2, O_2 and N_2 were also inputted as Henry components in Aspen Plus®.

3.2.2   Simulation environment: setting up the flowsheet

The final process flowsheet for the baseline case simulation is shown in fig. 3.2. One must note that amine makeup was necessary in the flowsheet to ensure the mass balance closes and to aid convergence. Moreover, the duplicator blocks were found to be of great help to convergence. That is, at some points in the flowsheet setup, duplicator blocks were added as it was observed that otherwise recycle loops would have not converged.
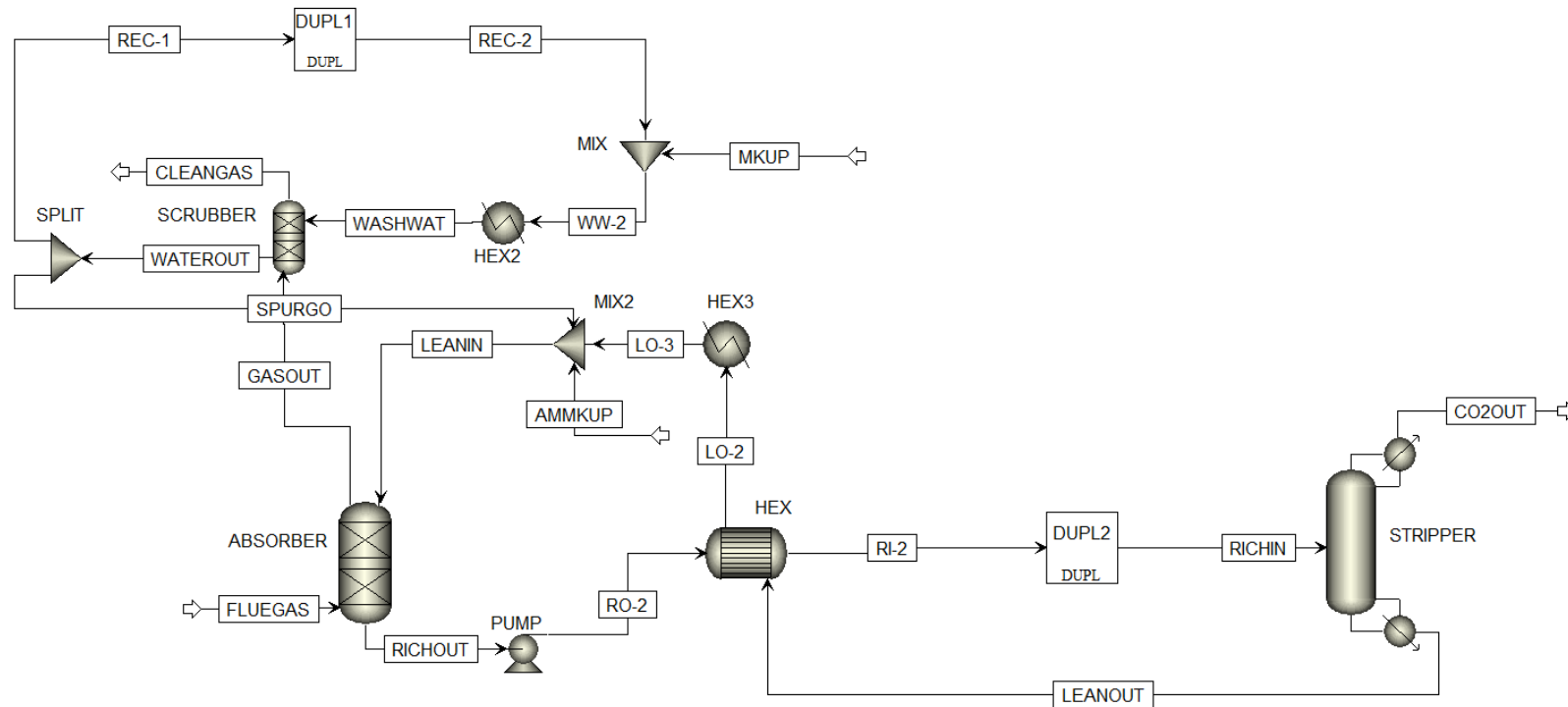
Figure 3.2 – Final process flowsheet regarding the baseline case simulation.

Table 3.1 – Stream labelling.

Stream	Source	Sink	Stream	Source	Sink
FLUEGAS	EAF off-gas evacuation system	ABSORBER	LEANOUT	STRIPPER	HEX
CO2OUT	STRIPPER	Storage	WASHWAT	HEX2	SCRUBBER
GASOUT	ABSORBER	SCRUBBER	WATEROUT	SCRUBBER	SPLIT
CLEANGAS	ABSORBER	Stack	REC-1	SPLIT	MIX
LEANIN	MIX2	ABSORBER	SPURGO	SPLIT	MIX2
RICHOUT	ABSORBER	PUMP	MKUP	Process water network	MIX
RICHIN	HEX	STRIPPER	AMMKUP	Raw material storage	MIX2

3.2.3 Outlining the method adopted for process simulation in Aspen Plus V11

The capture process flowsheet was build step-by-step, unit-by-unit, ensuring convergence of the different blocks as they were added. In fig. 3.3, the different phases of the developed model are shown.

First data input

↓

Design of the absorber + desorber system

↓

Design of the lean-rich heat exchanger

↓

Design of the amine scrubbing unit

↓

Design of the water recycle circuit

↓

Global mass balance closure - amine solution recycle
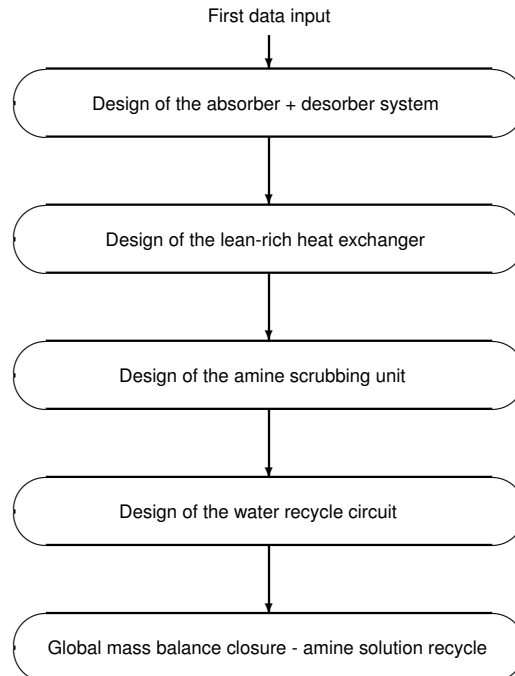
Figure 3.3 – Scheme of the taken steps to build the flowsheet for the base case scenario.

3.2.4 Unit operation blocks - an overview

Recall fig. 2.12, where the flue gas contacts with a MEA aqueous solution at atmospheric pressure and the loaded (with CO_2) amine solution is then regenerated at the desorber. The treated gas (now lean in acidic gases) passes then through the washing section (usually, located in the absorber) in order to avoid MEA emissions into the atmosphere and, at the same time, reduce amine losses in the system. So, the following equipment are involved in such a process:

Absorber A RADFRAC rate-based packed column was used to model the absorber, which operates at atmospheric pressure (1 bar). The packing height totals 32 m, and corresponds to 20 stages. Bear in mind that here stages do not represent equilibrium stages, but rather the number of discretization segments. Mellapak 250Y™ was the selected structured packing, following the works of Gardarsdóttir et al. [69], Sundqvist et al. [70]. Chemical reaction was incorporated in stages 1-20 through the previously defined reaction `MEA-RXN` model.

Stripper A 12.5-m tall (total height) RADFRAC rate-based packed column was selected and discretized to the same degree (20 segments). The desorber operates at 2 bara. Here, chemical reaction was incorporated into the block through the previously defined reaction `MEA-STP` model.

Heat Exchangers From a simulation point of view, two different types of blocks were used: i) an heater; ii) an HeatX. When modeling the lean-rich heat exchanger, the HeatX block was used, while the two remaining coolers were modelled using heater blocks. More details are provided in subsection 3.2.8.

Scrubber Following the works of Li et al. [71], the washing section of the absorption column (here called SCRUBBER) is strictly modelled by a separate column. This strategy allows easier analysis and simulation of a washing section [71]. Differently from the previous cases, it was assumed that equilibrium was achieved in the amine scrubber [28]. The scrubber had 10 equilibrium stages and its packing height was set to 4 m, as this is the typical height of washing sections located in absorbers [69]. Chemical reaction is included from stages 1-10, resorting to the reaction MEA-RXN model. Further details are provided in subsection 3.2.9.

Other equipment Between the absorber and the lean-rich heat exchanger, a pump, whose discharge pressure was set at 2.9 bar, was added for the following reasons:

- provide motion to the fluid as it travels along the process lines, overcoming downstream head losses;

- keep the rich solution stream at a pressure such that its partial vaporisation is avoided when this stream is heated in the lean-rich heat exchanger.

3.2.5 Problem description

Flue gas coming from the EAF after the cleaning treatment is subjected to chemical absorption treatment with a 30%wt MEA aqueous solution to promote CO_2 capture. A gas flow rate of 50 kNm^3/h [33] and flue gas composition were assumed, based on

i) the typical emissions from the EAF (as addressed in chapter 2, page 22);

ii) Wiley et al. [72] work - see table 3.2.

Table 3.2 – Characteristics of the fumes emitted through the EAF fourth hole, as per Wiley et al. [72] work.

Mini-mill plant: EAF off-gas		
Flow rate (Nm^3/h)		21600
Pressure (bar)		1.013
Temperature (°C)		300
	N_2	56
Compositions (%vol)	H_2O	1
	CO_2	40
	O_2	3

3.2.6 Absorber design

3.2.6.1 Starting the absorber simulation - process calculations

Recall that the problem data for the flue gas (considering data from table 3.2) as well as the lean solvent characterisation are known and available, except for the required solvent flow rate for a given degree of separation (*i.e.*, capture rate). This process variable is the first to be determined. Consider a typical absorption column as depicted in fig. 3.4.
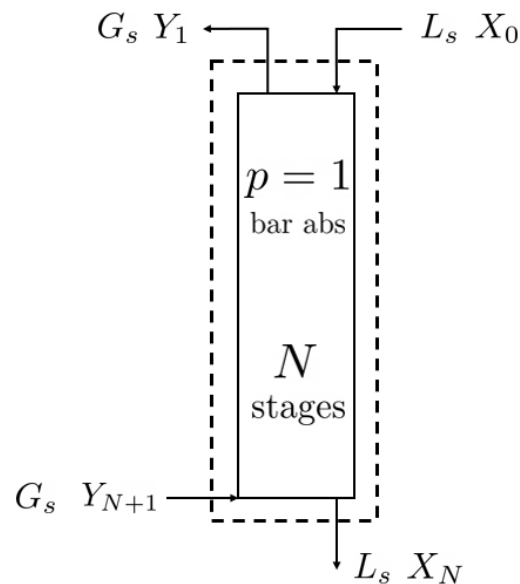
Figure 3.4 – Global mass balance around the absorber. G_s stands for the molar flow rate of solute-free (carrier) gas, L_s is the molar flow rate of solute-free solvent, Y_{N+1} the mole ratio of solute to solute-free gas in the vapor at the bottom of the absorber, Y_1 the mole ratio of solute to solute-free gas in the vapor at the top of the absorber, X_N, the ratio of solute to absorbent (MEA) in the liquid at the bottom of the absorber and, X_0, the ratio of solute to absorbent (MEA) in the liquid at the top of the absorber.

A degree of freedom analysis points out the solvability of this problem:

- # of variables = 6 $\rightarrow$ G_s, L_s, Y_{N+1}, Y_1, X_N, X_0

- # of independent equations = 4 $\rightarrow$ 1 global mass balance + 3 process specifications (G_s, Y_{N+1}, X_0)

- degrees of freedom = 2 $\rightarrow$ set: capture rate and X_N $\rightarrow$ problem exactly specified.

G_s is known (and constant): as so, then setting the capture rate automatically fixes Y_1 (*i.e.*, the CO$_2$ content of the absorber off-gas). The capture rate also determines the amount of CO$_2$ to be transferred to the liquid solvent. Along with the capture rate, X_N may be independently specified as L_s is yet to be determined. For this capture rate, more or less solvent will be needed as long as the outlet concentration specification is satisfied: greater capture rates will need higher solvent flow rates fed to the column to ensure a given X_N. Or perhaps the capture rate is somewhat smaller, which then would mean less

solvent is required to still guarantee X_N. Besides, note that X_N is an intensive property since it is a concentration.

The available problem data is shown in table 3.3. As the previous analysis indicated, the available degrees of freedom for the absorber are exhausted if the designer sets the degree of separation at 90% and fixes X_N equal to 0.49. In this event, the solvent (*i.e.*, MEA + H_2O solution) flow rate is automatically fixed, and L_s may found resorting to a global mass balance to the absorber.

Table 3.3 – Available data for the absorber inlet and outlet streams. Note that several different units were used to report compositions. [1] To be determined. [2] CO_2 loading in the lean solvent was assumed.

			Inlet		Outlet
			Flue gas	Solvent (lean)	Solvent (rich)
Temperature (°C)			48 [68]	40 [19, 69]	–
Pressure (bar)			1.05 [70]	1.00 [68]	–
Molar flow rate (kmol/h)			2.23×10^3	TBD[1]	–
Compositions	Mole fractions [72]	CO_2	0.40	–	–
		H_2O	0.01	–	–
		N_2	0.56	–	–
		O_2	0.03	–	–
	Mass fractions	MEA	–	0.30	–
		H_2O	–	0.70	–
	Mole ratios (mol CO_2/mol MEA)	CO_2	–	0.09 [2]	0.49 [19]

Required solvent flow rate   Consider the simplest scenario possible, assuming that:

- solvent is non-volatile, while the carrier gas is insoluble;

- isothermal operation.

The required solvent molar flow rate to achieve the desired degree of separation is determined with a *global* mole balance around the absorber. Looking at the problem data – table 3.3 –, one quickly realises the variety of units used to report the compositions of the various streams. In particular, solvent composition in CO_2 is known in mol CO_2/mol MEA – a mole ratio –, rather than usual mole fractions. For this reason, dimensional analysis reveals the convenience of using solute-free molar flow rates to ensure unit coherence. Hence, a CO_2 global mole balance around the control volume envelope shown in fig. 3.4 gives:

$$G_s Y_{N+1} + L_s X_0 = G_s Y_1 + L_s X_N \qquad \text{[mol } CO_2\text{/h]} \quad (3.11)$$

where G_s is a CO_2-free gas molar flow rate (*i.e.*, the carrier gas molar flow rate) in mol carrier gas/h, L_s is the MEA molar flow rate in mol MEA/h. X e Y are mole ratios in mol CO_2/mol MEA and mol CO_2/mol carrier gas, respectively.

Rearranging eq. (3.11), L_s - the sole unknown - is determined:

$$L_s = G_s \frac{Y_N + 1 - Y_1}{X_N - X_0} \qquad\qquad \text{[mol MEA/h]} \quad (3.12)$$

Knowing the MEA molar flow rate (which is assumed to be constant), the water mole flow rate at the absorber inlet can be found. The latter may also be assumed as constant, as a rough approximation (in fact, water will certainly evaporate into the gas phase). At last, the amount of CO_2 transferred is determined by the capture rate. So, the total molar flow rate is determined, being used as a first guess to initiate the simulation.

Table 3.4 – First guess for the lean solvent mass flow rate admitted to the absorber.

	MEA	H_2O	CO_2	TOTAL
Mass flow rate (kg/s)	34.1	73.7	2.20	110

Having determined a first rough estimation on the necessary solvent flow rate, the absorber can now be simulated.

Design specification   Then a flowsheet design specification was put in place to rigorously ensure the capture rate. The solvent flow rate was varied until the capture rate of 90% was attained. This way, a more accurate value for the required solvent flow rate was obtained.

3.2.6.2   A performance problem

At this stage, this simulation problem is just a rating one, since only outlet conditions are to be calculated, as if a real column were available and ready for use, implying that no internal design changes could be made. Therefore, the number of stages, the packing type and height and the column diameter are specified accordingly, considering other works from the literature.

Column internals   Regarding the column internals details, the following were imposed, as if a real column were at use.

Number of stages   As this is a packed column, no physical stages can be identified. Liquid will flow downwards along the packing with the gas phase filling the voids. It is widely acknowledged that packed columns are better simulated through rate-based models. In Aspen Plus®, a number of stages, which is in fact the number of segments of discretization, must be inputted. 20 segments were assumed, as per [28, 67].

Absorber packing type and height   For the structured packing, Mellapak 250Y™ was selected [69, 70]. Other works on the simulation of industrial-scale absorbers typically report packing heights of 20 to 35 m [61, 69]. Furthermore, higher absorber packing heights mean phases contact each other for longer time, which results in better absorption performance. For these reasons, it was assumed that the absorber was 32 m high. On a side note, the absorber packing height will be divided into as much

segments of discretization as the number of segments stated under the number of stages specification in Aspen Plus® interface.

Absorber diameter   Even though, the aim is to determine the absorber diameter for which a given separation is attained, the RADFRAC subroutine forces the user to specify at this point a first-guess diameter, even if it is not the most accurate. In other words, a plausible and reasonable first guess must be inputted. For that purpose, the column hydraulic plots tool were used, since an adequate diameter is such for which the column hydraulic plots are correctly generated. This value was found to be 4.5 m.

Within the scope of the rating problem, the absorber was simulated so far as an equilibrium block. Running the simulation solved the performance problem. On the other hand, all the specifications mentioned so far have to be set when building an equilibrium-based model of an absorber. As soon as the absorber converged, the rate-based model was then sought.

Rate-based model setup   Additional details have to be provided if such a model is to be implemented. Aspen Plus® rate-based model relies on the Lewis and Whitman's two-film theory to describe mass transfer phenomena in every single segment in which the column was divided, as elaborated in chapter 2. Accordingly, for a given segment, both the bulk and the film zones must be described. To that purpose, different parameters and options must be set under the RADFRAC model.

Modeling the bulk phase   Regarding the bulk phase, RADFRAC requires the user to specify the flow model in each column segment. Several models are available as *mixed flow* or *VPlug*, among others. While in the *VPlug* model, a combination between the average and the outlet conditions of each segment is assumed, in the *mixed flow* option the bulk phase of each segment is modelled as a CSTR (according to the two-film theory, *cf.* chapter 2). This means that the bulk conditions are equal to the conditions at the segment outlet [61], which implies the column is modelled as a series of CSTRs. Note that a series of n CSTRs is asymptotically equivalent to a plug-flow reactor. Therefore, in light of the desired column representation as a series of CSTRs, the *mixed flow* model was adopted.

Modeling the film phase   Now, moving on to the film phase. Several aspects need to be considered, namely the film resistances, the film discretization and the correlations used to calculate a number of important parameters:

Film resistances recall what was said in chapter 2 about the mass transfer profiles during CO_2 absorption. Both films behave differently (*i.e.*, have different resistances), which justifies a different modelling approach for each one [67]:

- for the gaseous film, the option *consider film* was selected, since the film exists, but no reaction takes place in it (if not convinced, take a look at the mass transfer profiles - chapter 2);

- for the liquid film, the option *discretize film* was considered, because not only reactions take place in the liquid film, but also these reactions are quite fast. Therefore, the film must be discretized, so that mass transfer profiles are adequately described.

Liquid film discretization it was just seen that film discretization is needed for adequate profile description. So, discretising the film means the film is divided into a certain number of intervals or points. The question that now poses is how will the discretization points be arranged along the film. Should the points be placed equidistantly or rather more concentrated around the interface? Think of the reactions happening in the liquid film and what was discussed in chapter 2: the CO_2-MEA reactions occur rapidly in the liquid film, which is why profiles should exhibit high steepness close to the interface [61]. Therefore, more detail (meaning more points) is needed in that zone to generate the profiles. As per Madeddu et al. [61], it is preferable to have few points concentrated at the interface rather than having many equidistant discretization points along the film. *Geometric discretization* option is activated to that purpose. Aspen Plus® requires the user to specify the following parameters to implement film discretization:

i) the *reaction condition factor* (RCF) which weights the bulk *vs.* film conditions to compute the film reaction rates. In particular, consider the case of CO_2 capture with MEA: reactions take place exclusively in the liquid film and are very fast, so reactants will react as soon as they arrive at the film. In other words, reactants will not penetrate deeply into the film ahead of its reaction. Therefore, bulk conditions will be of higher importance on the reaction rates computation rather than film conditions. For this reason, RCF was fixed at 0.9.

ii) the number of discretization points was set to be 5, following Madeddu et al. [61] work.

iii) the *film discretization ratio* (FDR) defines the width of the discretization intervals in the liquid film, which in turn establishes how concentrated are these intervals around the interface. In fact, for values larger than 1, the intervals become smaller moving towards the interface. However, a trade-off between the number of discretization points and the FDR exists as a too large FDR value can lead to numerical problems, owing to the small discretization steps close to the interface. The FDR was fixed at 10, as per Madeddu et al. [61] work.

Rate-based correlations differently from equilibrium-models, a number of characteristic parameters that depend on the packing type must be evaluated in a rate-based model. These are:

- the wetted surface area, which is the area available for gas-liquid mass transfer;
- material and energy transfer coefficients, defined as the diffusion coefficient divided by the film thickness and the thermal conductivity divided by the film thickness, respectively;
- fractional liquid holdup, which quantifies the volume of packing occupied by the liquid in the column.

Aspen Plus® provides several correlations for the computation of these parameters. In table 3.5, the correlations used for estimation of the abovementioned parameters are summarised, as in Madeddu et al. [61] work:

Table 3.5 – Selected correlations for the absorber simulation.

	Correlations
Wetted surface area	Bravo *et al.* [73]
Material transfer coefficients	Bravo *et al.* [73]
Heat transfer coefficients	Chilton and Colburn [74]
Fractional liquid holdup	Bravo *et al.* [75]

3.2.6.3 A design problem - the design criteria

Revisiting the absorber diameter   The problem then turns to that of selecting an adequate column diameter, that fulfills the desired capture rate (*i.e.*, the design constraint). This marks the beginning of the design problem. Keep in mind that the amount of gas to be treated as well as the amount of lean solvent required to fulfill the separation task define the column diameter. Thanks to design tool embedded in the RADFRAC rate-based model, and through the careful inspection of the column hydraulic plots, a column diameter can be easily determined, only requiring the specification of two parameters [61]:

- base flood. For every column design, there is a gas velocity for which the column gets flooded. The base flood parameter corresponds to the maximum allowed percentage of that flooding velocity. In this work, a gas velocity of 78% of the flooding velocity was selected as the base flood;

- base stage (or better, segment). The column diameter must be chosen with reference to the most constrained point in the column, since that will be the point where the gas flow rate is the highest. In theory, this point is neither at the top nor at the bottom of the column, but rather somewhere at the middle of the column, as most of the reactions will take place there. Besides, the CO_2 absorption process is highly exothermic, which means water from solvent will vaporize into the gas phase. Therefore, gas flow rate will increase due to the vaporised water.

3.2.7 Stripper design

As it was seen under chapter 2, the rich solvent consisting mainly of CO_2, MEA and H_2O goes to the stripper, where its regeneration is performed, and usually a combination of techniques are employed to desorb the CO_2. One possible choice could be to flash the CO_2-rich solvent at the stripper inlet, then vaporise it at the reboiler, thus originating a vapor flow rate that allows to strip the CO_2 contained in the rich solvent.

As with any other column, the task of designing a stripper is not an easy one and involves determining the diameter of the column for which a desired degree of separation is attained. In fact, the success of such vapor-liquid separation operation depends on a good design. Madeddu et al. [61] methodology was closely followed when designing the stripper.

3.2.7.1 Stripper configuration

The gas stream exiting at the top of the stripper consists mainly of CO_2 and H_2O. Therefore, depending on the condenser operating temperature, it is expected that only H_2O condense. As of now, there are several possible configurations for the stripper, regarding the column condenser.

A possible configuration could be mixing the condensate with the lean solvent exiting the lean-rich heat exchanger. An alternative would be to reflux the condensate back to stripper. Notwithstanding the fact that reflux would enter at lower temperature than that of the stripper feed, thus leading to a decrease in the temperature at the top of the column, this was the chosen configuration.

3.2.7.2 Stripper operating conditions - design specifications

At the beginning of section 3.2.7, it was stated that, when designing a certain separation task, the designer wants to determine the diameter for which several specifications are satisfied. These specifications may be product specifications or the attained degree of separation. However, not every single piece of information can be blindly specified (as different pieces of information may come into conflict with one another or even contradict each other). This idea is clearly expressed by the *design degrees of freedom* – as stated previously in this chapter.

Assume that stripper feed conditions are known (which is indeed the case), then a column with partial condenser and a reboiler has three degrees of freedom. If one decides to specify the following variables:

- stripper pressure;

- condenser temperature;

- CO_2 flow rate at the stripper overhead.

then the available degrees of freedom are readily exhausted. This set of variables was identified by Madeddu et al. [61] as the most relevant for the stripper design.

Stripper working pressure   In chapter 2, it was seen in that strippers generally operate at pressures higher than the atmospheric. If this were a physical absorption process, lower pressures (generally speaking) would be employed so as to favor desorption. Yet paradoxically, for chemical absorption processes, higher-than-the-atmospheric pressures are set in the stripper. This matter will be subject of greater discussion in chapter 4. In any case, the baseline case stripper will work at a pressure of 2 bara.

Therefore, fixing the stripper pressure within the RADFRAC specifications menu was immediate. However, how could the other design variables - condenser temperature and the CO_2 flow rate exiting at the stripper overhead - be fixed within that same simulation environment? Note that Aspen Plus® does not allow the user to impose the condenser temperature in the RADFRAC menu when a partial condenser with vapor distillate is being employed.

As there is no way to directly specify these variables in the RADFRAC specifications, block design specifications were used to do so. In any simulation, two questions pose when opting for implementing a block design specification:

i) since it is not possible to declare the design variable directly in the RADFRAC specifications, how can it be specified within the block design specification?

ii) and most importantly, on what variables does the design variable depend such that, in the end, the desired specification is attained by their manipulation?

Sometimes the former question boils down to the latter when, given the impossibility of stating the variable of interest explicitly in the block design specification, one must resort to some other variable on which the variable of interest depends in order to specify it. The target value for the specified variable is, computationally speaking, attained through an iterative process that varies another variable (*i.e.*, the manipulated variable).

Condenser operating temperature Not infrequently, strippers employ water-cooled partial condensers. Both streams exiting the partial condenser are at equilibrium. Assume that process cooling water is available at 288.15 K and that it leaves the condenser at 303.15 K. The condenser temperature is set to 303.15 K, which is the temperature at which both streams leaving the condenser will be, since thermal equilibrium is attained. This operating temperature is established considering the available cooling medium and the present condensable species (vapors). *A priori*, at 303.15 K, CO_2 is clearly a non-condensable species. Therefore, as i) the sole condensable species is H_2O and ii) H_2O gets refluxed back only to the stripper, then the condenser operating temperature should influence the stripper reflux ratio to the extent that lower condenser temperatures should mean higher condensate flow rates, and necessarily higher reflux ratios to the stripper.

So, when it comes to the simulation, a block design specification must be imposed in order to assure proper condenser temperature is obtained. In this case, the target condenser temperature can be directly inputted in the block design specification with the reflux ratio being allowed to vary until the target temperature is achieved.

CO_2 flow rate at the stripper overhead Specifying such flow rate is the same as fixing the amount of CO_2 removed in the stripper, which makes this variable a quite important one to specify at a design stage.

Mass balance on CO_2 Look at the fig. 2.12. A steady-state CO_2 global mass balance around the entire capture scheme gives:

$$\{CO_2 \text{ in the flue gas}\} - \{\text{remaining } CO_2 \text{ in the treated gas stream}\} =$$
$$= \{CO_2 \text{ at the condenser overhead}\} \quad [\text{kg/h}] \quad (3.13)$$
$$= \{\text{removed } CO_2 \text{ in the stripper}\}$$

Mass balance (3.13) essentially states that the stripper must be designed in such a way that, at steady-state, the amount of captured CO_2 at the absorber is that removed at the stripper. This, of course, relates with the degree of regeneration, Reg, which is defined as

$$Reg = \frac{\{\text{CO}_2 \text{ } at \text{ } stripper \text{ } inlet\} - \{\text{CO}_2 \text{ } at \text{ } stripper \text{ } outlet\}}{\{\text{CO}_2 \text{ } at \text{ } stripper \text{ } inlet\}} \times 100\% \tag{3.14}$$

Eq. (3.14) is the same as writing $\{$CO$_2$ at the condenser overhead$\} = Reg \{$CO$_2$ at the stripper inlet$\}$. Fixing the extent to which the rich solvent is regenerated greatly affects the absorber performance, as the once-rich solvent is, after regeneration, re-fed to the absorber. Regardless of the stripper being viewed as a standalone equipment or as part of a broader framework[1], the degree of regeneration depends on the stripper performance, which is in turn quantified by operating parameters as the bottoms-to-feed (B/F) ratio, the reflux ratio or the reboiler duty (among others). As such, depending on the set of operating parameters, so will be the amount of CO_2 leaving at the condenser overhead, and thus the degree of regeneration. In fact, as soon as the amount of CO_2 leaving the condenser overhead is determined, the degree of regeneration cannot be set independently. Put differently, for a given set of working parameters, there is a corresponding amount of removed CO_2 at the top of the stripper, which consequently determines the degree of regeneration.

Since the global mass balance determines the CO_2 flow rate leaving at the top of the stripper, the degree of regeneration gets automatically fixed for a given stripper feed[2]. Simply put, by fixing the CO_2 flow rate at the top of the stripper, the amount of removed CO_2 in the stripper is immediately established. Therefore, at this point, neither the degree of regeneration can be specified at the designer's will nor can be, for instance, the bottoms flow rate arbitrarily fixed.

So, the CO_2 flow rate exiting the stripper overhead is to be specified directly under the block design specification, since flow rates are process variables that can be stated effortless and expeditiously under block design specifications. Now, the desired CO_2 flow rate, which is determined by the global mass balance, is, at the same time, ascribable to the stripper operating parameters. In other words, such flow rate is achievable thanks to the manipulation of such service parameters. In that event, it all boils down to find the B/F ratio for which the right amount (or rather, flow rate) of CO_2 is released at the top of the stripper, thereby closing the global mass balance, and consequently ensuring the right degree of regeneration is achieved. Note that the B/F ratio proves to be the best choice as it is a more tangible parameter than the reboiler duty and is easily manipulated by the user in the Aspen Plus® interface. The more rich solvent is sent to reboil – *i.e.*, high B/F ratios –, the better separation is achieved, as more stripping vapor is generated. Subsequently, higher reboiler duties will follow.

3.2.7.3 Simulating the stripper

In order to simulate the stripper, inlet streams data are needed, and the operating conditions must be established as well (considering the design constraints). A kettle-type reboiler and a partial condenser

---

[1]That is, coupled with an absorber, and so integrated in the absorption + desorption process.
[2]Look at eq. (3.14). The degree of regeneration depends unsurprisingly on the flow rate of the stripped CO_2 at the desorber.

were selected. At first, the stripper modeling approach consisted in copying the outlet stream from the absorber to the stripper inlet stream. In a first moment, equilibrium mode was activated to ensure block convergence in agreement to what was done for the absorber.

Column internals   When it comes to the column internals, the following were considered.

Number of stages   It shall be reiterated that no physical stages can be distinguished as this is a packed column. As the stripper height was set to 10 m and 20 segments were assumed, as per [67], the stripper rate-based packed bed was discretized to two segments ("stages") per one meter height.

Stripper packing type and height   As structured packing, Mellapak 250Y™ was once more selected [69, 70], similarly to what was defined for the absorber. Stripper packing height was fixed at 10 m, based on the works of Gardarsdóttir et al. [69].

Stripper diameter   Similarly to the procedure used for the absorber, a diameter was found out by a trial-and-error procedure – a rather cumbersome task –, while resorting to the hydraulic plots tool.

Rate-based model setup   As soon as the stripper converged with the equilibrium-mode activated, the rate-based model option was then selected. Regarding the rate-based model for the stripper, the specifications made for the absorber were the same applied to the stripper. The reader is advised to go back to section 3.2.6.1 for further details.

Revisiting the outlet CO_2 flow rate specification   Let us now address an operational issue regarding the simulation. In a first stage, both the absorber and the stripper were simulated separately. In any circumstance, the right specification of the CO_2 flow rate exiting at the stripper overhead was that the desired flow rate of removed CO_2 equalled the absorbed CO_2 flow rate at the absorber, as mentioned under section 3.2.7.2. This specification was reached, in this first stage, through user manipulation of the B/F ratio. After obtaining reasonable values for the stripper operating parameters, both equipment were connected and the lean-rich heat exchanger was added. At this point, the block design specification was added, and the flowsheet was at a quite preliminary stage. In fact, refer to fig. 3.5, where one can see that mass balance (3.13) does not hold, since the recycle loop does not close. In other words, the lean solvent stream that flows from the lean-rich heat exchanger is not the stream entering the absorber. So, a CO_2 global mass balance must be rather written as:

$$\left\{ \begin{array}{c} CO_2 \text{ in} \\ \texttt{FLUEGAS} \end{array} \right\} + \left\{ \begin{array}{c} CO_2 \text{ in} \\ \texttt{LEANIN} \end{array} \right\} = \left\{ \begin{array}{c} \text{remaining } CO_2 \\ \text{in } \texttt{GASOUT} \end{array} \right\} + \left\{ \begin{array}{c} \text{removed } CO_2 \\ \text{in the stripper} \end{array} \right\} + \left\{ \begin{array}{c} CO_2 \text{ in} \\ \texttt{LO-3} \end{array} \right\} \quad [\text{kg/h}] \quad (3.15)$$

When $\texttt{LEANIN}$ and $\texttt{LO-3}$ coincide, then mass balance (3.15) reduces to mass balance (3.13).

As the flowsheet is at its earliest stage (in the sense that the recycle loop does not close), it is of upmost importance to ensure that mass balance (3.13) is satisfied in order to i) facilitate convergence when

the flowsheet is to be closed and, at the same time, ii) allow (and ease) the conduction of parametric analyses without having the need of closing immediately the loop. This way, the validity of the results is still ensured. So, with a view to assure the global mass balance still gets closed and attain the desired degree of regeneration, the amount of absorbed CO_2 into the amine solvent is calculated, and copied into the target CO_2 mass flow rate leaving at the condenser top (declared in the block design specification), which translates mass balance (3.13). Once more, as this design specification targets the amount of CO_2 exiting the stripper, it directly concerns the degree of separation achieved at the stripper. The B/F ratio is allowed to vary until the targeted amount of removed CO_2 at the stripper is attained (to which a degree of regeneration corresponds).

Revisiting the stripper diameter   Similarly to the absorber, within the scope of the stripper design problem, its diameter was determined using the RADFRAC rate-based design tool. Once more, the diameter was adjusted within a 78% flooding constraint.
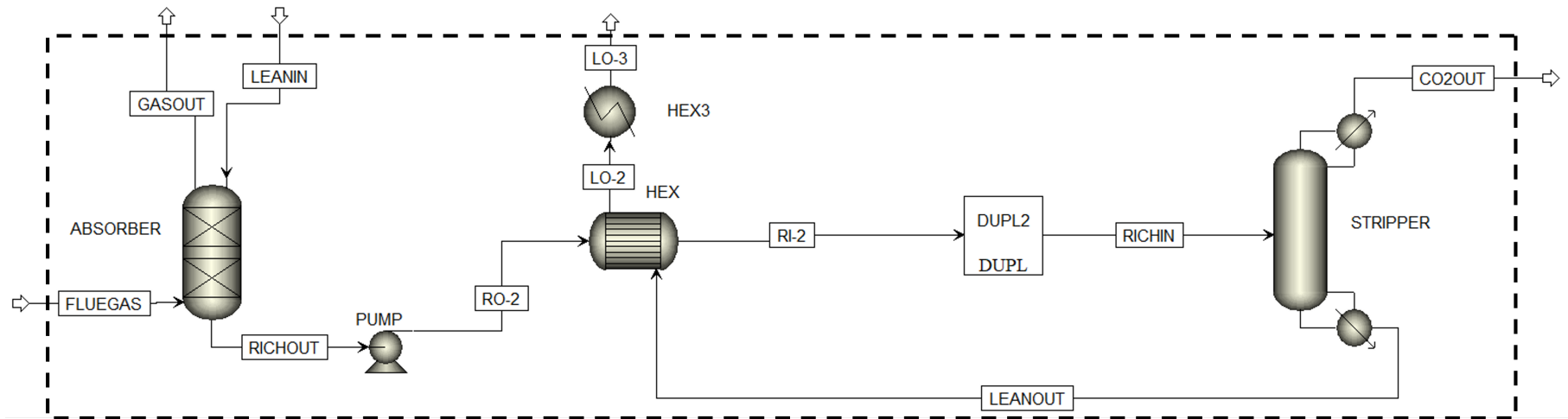
Figure 3.5 – Preliminary process flowsheet for the base case simulation. Note the control volume enclosure for the global mass balance.

3.2.8 Lean-rich heat exchanger design

A shell-and-tube countercurrent heat exchanger was designed to withdraw sensible heat from the hot lean solvent stream coming from the reboiler and supply it to the cold rich solvent stream exiting the absorber. Designing a heat exchanger means determining its area.

This heat exchanger sets the rich solvent temperature to be fed to the stripper. What is more the stripper feed temperature plays a crucial role in the stripper thermal energy requirements. As it was seen previously, high stripper feed temperatures are desirable as thermal energy requirements are minimized. However, achieving high temperatures depends on the lean-rich heat exchanger design, which in turn is constrained by minimum temperature approach. Besides, there are references in the literature to a solvent degradation temperature at 395.15 K [61], meaning that the lean solvent (cold) outlet stream cannot leave the heat exchanger at a temperature greater than 395.15 K.
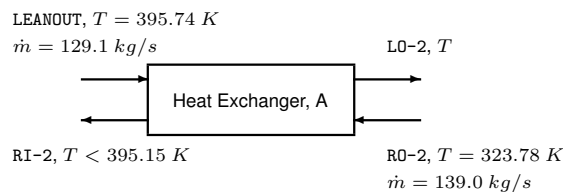
Figure 3.6 – Illustration of the lean-rich heat exchanger for design purposes. Note that LEANOUT is the stream exiting the stripper, while RICHOUT is that leaving the absorber – refer to table 3.1.

In fig. 3.6, the lean-rich heat exchanger is shown, where the hot lean solvent coming from the stripper goes into the shell, while the cold rich solvent flows inside the tubes, since the rich solvent will contain greater amounts of MEA. As per the heat exchanger design heuristics, the most corrosive fluid should flow inside the tubes, in order to facilitate the heat exchanger maintenance [40]. Having these aspects into consideration, the lean-rich heat exchanger was first simulated by means of a HeatX block, using the *shortcut* method. Recall that, at this point, the hot rich stream coming to the absorber is connected to the heat exchanger, but it is not directly connected to the stripper inlet. Only when the lean-rich heat exchanger design was completed was the stream RI-2 leaving from the heat exchanger tubes (see table 3.1) connected to the stripper.

Initial thermal problem data was inputted and the overall heat transfer coefficient, U, defined as 0.85 kW/m^2 K, which is in agreement with the values pointed out by Green and Southard [76] and reported by [67]. In fact, Green and Southard [76] mentions that U is between 0.79 kW/m^2 K and 1.14 kW/m^2 K for MEA aqueous solutions circulating on both sides of a shell-and-tube heat exchanger. No dirt factors were considered, making this is a rather ideal design approach to the heat exchanger. Furthermore, a pressure drop of 0.1 bar was considered in both the hot and the cold sides.

In a given heat exchanger, there will always be a side in which heat transfer is most constrained. To that purpose, a minimum approach temperature, ΔT_{min}, must be defined. As there are many definitions

on this concept, the approach temperature is defined in this work as either:

$$\Delta T_{\min} = \begin{cases} T_{ho} - T_{ci}, \\ \vee \\ T_{hi} - T_{co} \end{cases} \tag{3.16}$$

whichever is the smallest (thus, constricting heat transfer). T_{ho} is hot outlet temperature, T_{ci}, the inlet cold temperature, T_{hi}, hot inlet temperature, and T_{co}, the outlet cold temperature. $\Delta T_{\min}$ was set to 10 K. Greater temperature approaches would mean the cold stream outlet temperature would be lower, which is undesirable.

As this is a countercurrent heat exchanger, the outlet hot stream and the inlet cold stream (or vice versa) must approach each other with a temperature difference of, at least, 10 K. This is a crucial detail to consider when designing a heat exchanger to fulfill a given heat duty, Q. Its area can be determined by the design equation (3.17):

$$Q = UA\Delta T_{LN} \tag{3.17}$$

where Q is the heat duty (kW), U, refers to the overall heat transfer coefficient (kW/m^2 K), A is the heat transfer area (m^2), and ΔT_{LN}, the log-mean temperature difference (K). Given the problem data, simulation is now needed to solve this problem: both the heat exchanger area for such heat duty and the cold stream outlet temperature are to be determined. As for the hot outlet temperature, it is first user-defined as a design specification within the HeatX block, given its importance to the heat exchanger design: the highest possible hot outlet temperature that still satisfied the MEA degradation temperature constraint was inputted. Simulation returned the required area and all outlet temperatures. After taking a close look at the obtained thermal results, the temperature difference between the hot outlet stream and the cold inlet stream demonstrated to be the most constrained side of the heat exchanger. For this reason, a new specification was then considered: the temperature difference between the hot outlet stream and the cold inlet stream, which was set to 10°C (the same as the minimum approach temperature) in order to maximize the heat exchange between both streams. Once more, the required heat transfer area and all outlet temperatures were computed by simulation. Results are shown in table 3.6.

Table 3.6 – Thermal results following the *shortcut* lean-rich heat exchanger design in the baseline case simulation.

	Inlet streams		Outlet streams	
	LEANOUT	RO-2	LO-2	RI-2
Temperature (K)	395.74	323.78	333.78	379.59
Pressure (bar)	2.01	2.90	1.91	2.80
Heat duty (kW)	2.91×10^4			
Overall heat transfer coefficient (kW/m^2.K)	0.85			
Required exchange area (m^2)	3.26×10^3			

Considering the intriguing value for the heat transfer area resulting from this *shortcut* design method,

a more rigorous design was looked for using the Aspen EDR® tool, whose results are summarised in table 3.7, in an effort to explain such results. In effect, the high flow rates being handled in this heat exchanger can partly explain the required area for heat transfer.

Table 3.7 – Design results for the lean-rich heat exchanger in the base case simulation.

Heat duty (kW)	2.91×10^4
Average heat transfer coefficient (kW/m^2.K)	0.861
Required heat transfer area (m^2)	3.35×10^3
Geometry:	
TEMA type	BEM
Exchanger length (m)	5.85
No. of shells:	
Parallel	4
Series	4
Required heat transfer area/shell (m^2)	209
Tubes arrangement	Triangular
Tube material	Carbon steel
Shell material	Carbon steel

3.2.9 Scrubber design

During the absorption operation, some MEA can evaporate from the solvent as absorption reactions are exothermic. A common practise is to install a washing section in the absorber in order to avoid unwanted emissions into the atmosphere and potentially recover the amine (as the MEA solvent cost is quite high, refer to chapter 4). Notwithstanding, in this work, it was chosen to simulate the washing section in an additional equipment – an amine scrubber – for ease of simulation and better analyse that same section [71].

As the absorber and scrubber should be within the same equipment, the structure packing from which the absorber is made is the same of the scrubber. Gardarsdóttir et al. [69] and other authors point out maximum packing heights of 4 m for typical washing sections. Considering Mellapak 250Y™ HETP as being approximately 0.4 m, then the number of equilibrium stages must necessarily be equal to 4/0.4 = 10. Here, the scrubber was simulated as an equilibrium block, following Chung et al. [28] works.
The gas stream at the scrubber outlet is considered to be a clean gas, whose content in MEA must comply with strict legislation that regulates MEA emissions into the atmosphere. In particular, Italian law fixes that value on a MEA concentration equal or below 20 mg/Nm^3.

Washing water flow rate Perhaps the most important data to provide when designing a scrubber is the required washing water flow rate to fulfil the desired degree of separation. In this case, a preliminary simulation has showed that a pure water flow rate of 300 kg/h ensured no MEA was released along with the clean gas. However, Aspen Plus® does not have adequate correlations in its library to generate the

scrubber hydraulic plots for this type of packing and such low flow rates. Consequently, the washing water flow rate was set instead to 1250 kg/h. Such flow rate plainly guarantees that the clean gas is virtually MEA-free. Up to now, it had been considered that fresh water could be continuously fed to the scrubber. However, doing so is both economically unfeasible and unsustainable, which is why some washing water must be recycled.

3.2.9.1 Water wash recycle section

Recycling the washing water entails revising upwards the inlet washing water flow rate due to the recycle effect that allows some MEA to accumulate undesirably within the recycle, which removes dissolving capacity of the washing water (in comparison to pure water). For this reason, a purge should be added to avoid uncontrolled MEA accumulation that stops normal process operation. Moreover, a fresh water make-up must be provided to compensate for the water leaving at the purge, thus closing the mass balance to the water wash section. In chapter 4, a comprehensive discussion on this matter is presented.

Clean gas MEA concentration compliance   In order to ensure that the MEA concentration in the clean gas does not exceed that established by law (*i.e.*, ≤ 20 mg/Nm^3), a flowsheet design specification was implemented. Accordingly, the mass flow rate of the water make-up varied until the desired outlet gas concentration was obtained.

3.2.10   Global mass balance - amine solution make-up

At last, the global mass balance was closed by connecting streams `LO-3`, `SPURGO` and `AMMKUP` with `LEANIN` – please refer to table 3.1. This way the purge stream, which is essentially is a MEA + water stream, is recovered. Besides, an amine make-up (stream `AMMKUP`) is due, since there are amine irrecoverable losses throughout the process. As soon as all the streams were connected, the capture rate flowsheet design specification was deactivated.

Chapter 4

Results and Discussion

If my answers frighten you, then you should cease asking scary questions.

JULES WINNFIELD, *Pulp Fiction*, 1994

At the beginning of this chapter, the problem under analysis is reiterated. Chapter 4 is divided in three parts: in a first part, in order to identify the best operating conditions for the considered amine-based chemical absorption CO_2 capture plant applied to a mini-mill, the influence of some operating parameters on the process performance is studied, building on the base case steady-state simulation of such process. In a second part, the actual conditions in terms of fumes flow rate variability are introduced and studied. At last, an economic evaluation of the process is presented. All obtained results are showcased, followed by a comprehensive discussion.

4.1   A problem wrap-up

Let us start by recapitulating the problem analysed in this work. During a batch operation of an electric arc furnace (EAF), fumes are intermittently exhausted, being thereafter submitted to a post-treatment procedure designed to purify and clean that gaseous stream. The EAF exhaust gas is handled from a solids point of view and CO is eliminated during that process. However, there are still considerable amounts of CO_2 in the off-gas. Therefore, in order to mitigate these polluting CO_2 emissions, a CO_2 capture plant may be placed downstream to the aforementioned handling system. A strategy that can reconcile the capture plant continuous operation with the batch nature of the EAF must be devised.

4.2   Baseline case simulation results

The problem under study and the inputted data were thoroughly explained in chapter 3. It is worth recalling that, in this work, 50 kNm^3/h of untreated gas, consisting of 40%mol in CO_2, were admitted to the CO_2 capture plant. Yet, this is the gas composition immediately after being extracted from the

EAF via the fourth hole and not that usually measured after the exhaust gas is subjected to the cleaning process (and is ready for admission to the absorber). As elucidated in chapter 2, the CO_2 mole fraction in the off-gas dramatically decreases to around 11%mol following the atmospheric air intake. In spite of such inconsistency, the absorber gas feed was preliminarily set to 40%mol in CO_2, a rather conservative approach, but necessary if the most extreme possible situation is to be assessed.

Following what was laid out in chapter 3, the results of the column sizing procedure are shown in table 4.1. It should be noted that safety factors of 25% were included in the column total heights. Please recall some of adopted design criteria in table 4.1.

Table 4.1 – General design criteria used to build the base case simulation and column sizing results.

Design criteria	
Absorber working pressure, P_{abs} (bara)	1
Stripper working pressure, P_{stp} (bara)	2
Column flooding limit (%)	78
Lean cooler discharge temperature (°C)	40
Lean-rich minimum approach temperature, ΔT_{min} (°C)	10
CO_2-rich gas temperature at the stripper condenser outlet (°C)	30
MEA concentration in clean gas (mg/Nm^3)	20

Column sizing results after design	
Absorber packing height, H_{abs} (m)	32.0
Absorber total height (m)	40.0
Absorber diameter (m)	3.97
Scrubber packing height (m)	4.00
Scrubber diameter (m)	2.18
Stripper packing height, H_{stp} (m)	10.0
Stripper total height (m)	12.5
Stripper diameter (m)	3.77

Having all the capture process equipment designed and the base case steady-state simulation running, the capture plant performance was then assessed with tailor-made key performance indicators (KPI). Essentially, these quantify the capture plant performance in terms of the process material needs:

- thermal energy requirements in the reboiler – *TER* – (GJ/t CO_2 removed);

- cooling water consumption in the capture process – *CWC* – (m^3 cooling water/t CO_2 removed);

- lean solvent requirements for the desired absorption rate. That is, the lean solvent flow rate divided by the flow rate of absorbed CO_2 – *SR* – (m^3 solvent/t CO_2 removed).

Note for instance the TER KPI, where a high (reboiler) performance means a low value for the performance indicator, since it is expressed on the basis of an energy consumption rate. All the considered KPIs are reported on the basis of a tonne of CO_2 removed, which helps to perform comparisons between KPIs. These were carefully chosen as they provide a rather important insight in both capital and operating expenditures. On the one hand, both the cooling water consumption rates and the used solvent flow rate determine the size of the equipment (*i.e.*, diameter), which influences greatly the capital costs. On the other, as stated in chapter 2, the reboiler TER is a decisive factor in the plant operating expenditures, given the cost of steam. In fact, the latter is such a pivotal criteria that it was the determining factor when selecting the optimal lean solvent loading, as explained ahead in section 4.4.

The main results of the baseline simulation are summarised in table 4.2, and allow to examine the capture process efficiency in terms of the defined KPIs.

Table 4.2 – Base case simulation results.

	Base case scenario
Capture rate (%)	90
Amine lean solvent loading (mol CO_2/mol MEA)	0.090
Amine rich solvent loading (mol CO_2/mol MEA)	0.532
Reboiler TER (GJ/t CO_2)	5.385
Required solvent flow rate (m^3/t CO_2)	9.94
Required cooling water (m^3/t CO_2)	770.5
at stripper condenser (m^3/t CO_2)	90.31
at lean solvent cooler (m^3/t CO_2)	656.7
at water cooler (m^3/t CO_2)	23.38
at amine scrubber (m^3/t CO_2)	0.114

4.3 Parametric analyses

After the performance of the base case capture plant was determined, parametric analyses were then conducted to identify the best case regarding the plant operating conditions, based on the approach presented by Abu-Zahra et al. [68]. In other words, the most important parameters that affect the capture process were subjected to variations in order to observe their impact on the capture process performance.

It is widely acknowledged that the main parameters affecting the capture process are:

- solvent lean loading (mol CO_2/mol MEA);
- stripper operating pressure;
- capture rate (*i.e.*, amount of removed CO_2);
- MEA concentration in the solvent;
- lean solvent temperature.

Recall that the lean solvent loading can be changed only if the degree of regeneration at the stripper has been altered. This may be achieved through the manipulation of the stripper working parameters (*e.g.*, reboiler duty or the B/F ratio). As for the capture rate, no other capture rate than 90% was considered. Taking the works of Li et al. [60], Abu-Zahra et al. [68], Adu et al. [77] into consideration, no clear benefit was seen in repeating that same analysis. In addition, it was observed that variations of the CO_2 capture rate between 85%, 90% or 95% do not substantially impact the capture plant performance in terms of the benchmark performance indicators to be defined ahead. When it comes to the MEA concentration in the solvent, a 30%wt MEA solution was the only considered, in view of several other investigations which have already studied the influence of the MEA concentration on the capture process. It is worth mentioning that 30%wt MEA solutions are currently the benchmark for what concerns chemical absorption processes. Li et al. [60], Abu-Zahra et al. [68], Adu et al. [77] (which the reader is strongly advised to read) concluded that the thermal energy requirements decrease with increasing MEA concentration in the solvent. However, as MEA concentration increases, corrosion issues are expected to arise, thus increasing capital costs. Regarding the lean solvent temperature, it was specified

as 40°C, having remaining unaltered for the rest of this work.

From all the parameters listed in the preceding lineup, some were varied, others were kept unchanged, and some others were chosen instead for their equally important nature. All in all, the following parameters were subjected to variations:

- solvent lean loading, α_{LEAN} (from 0.09 mol CO_2/mol MEA to 0.29 mol CO_2/mol MEA);

- absorber packing height, H_{abs} (from 8 m to 32 m);

- stripper packing height, H_{stp} (from 6 m to 10 m);

- stripper operating pressure, P_{stp} (from 1 bara to 2 bara).

The effect of the variation of these parameters on the capture process performance was evaluated thanks to the previously defined KPIs in section 4.2.

4.3.1 Effect of the lean loading and absorber packing height on the KPIs

4.3.1.1 TER and SR changes after α_{LEAN} and H_{abs} variations

Building on the baseline case simulation results and relying on some parametric analyses, the best case scenario (*i.e.*, optimal case) was now looked for.
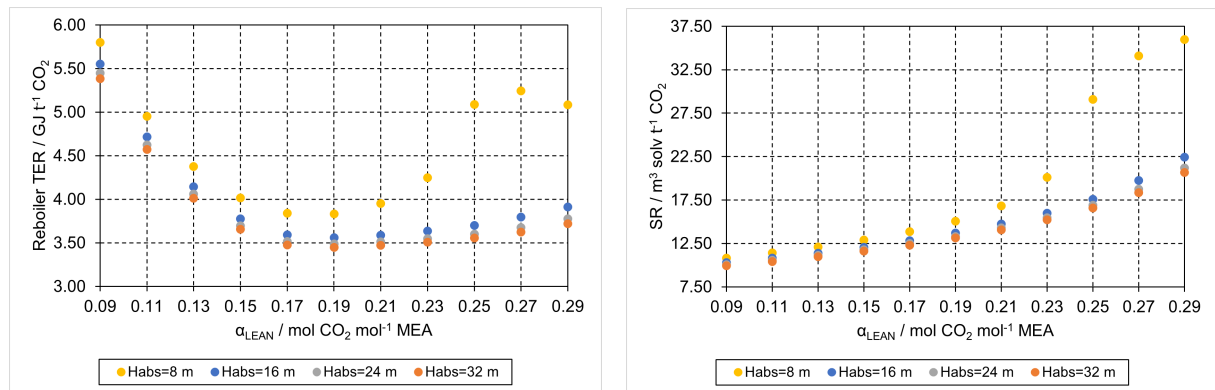
(a) Reboiler thermal energy requirements at various solvent lean loadings (0.09 to 0.29 mol CO_2/mol MEA) for different absorber packing heights, H_{abs}, for a capture rate of 90%.

(b) Volumetric quantity of solvent required per tonne of removed CO_2 at several lean solvent loadings (0.09 to 0.29 mol CO_2/mol MEA) for different absorber packing heights, H_{abs}, for a capture rate of 90%.

Figure 4.1 – Effect of the α_{LEAN} on two of the studied KPIs in order to assess the best α_{LEAN}.

In fig. 4.1, the reboiler thermal energy requirement and the (lean) solvent requirements are plotted against different lean solvent loadings for the absorber packing heights of 8, 16, 24 and 32 m. Considering the capture plant flowsheet, where the once-rich solvent is sent to the absorber after its regeneration, it may be asserted that the degree of regeneration is directly represented by the lean solvent loading. That is, the better regeneration at the stripper, then the smaller lean solvent loading will be [68]. So, the lean solvent loading will, of course, indicate to what extent was the solvent regenerated in the stripper.

According to Abu-Zahra et al. [68], the optimum lean solvent loading can be recognized by spotting the point at which the reboiler TER is the lowest. Thus, the lean solvent loading was varied until the solvent loading for which the reboiler TER is minimal was found out. It is also noteworthy that the thermal energy costs attributable to the reboiler have a decisive role in the operating costs of a chemical absorption capture plant, given the reboiler utility costs. Changes in the abovementioned parameters will reflect on the reboiler energy requirement, having in turn great effects on the operating costs. Therefore, selecting the process operating conditions that lead to the smallest TER brings savings.

When analysing the TER *vs.* α_{LEAN} plot, as fig. 4.1(a), the three components in which the reboiler TER can be decomposed should be kept in mind – *cf.* chapter 2. Changing the degree of regeneration will directly affect the performance of the absorber. Begin by considering a given H_{abs}. On the one hand, for low lean solvent loadings, reboiler TER quickly escalates, due to the abrupt increase in the amount of stripping steam needed to originate such poor solvent composition in CO_2 at the stripper outlet, but, on the other hand, the required solvent flow rates that ensure the 90% capture rate at the absorber are also quite reduced, given the increased solvent absorption capacity, as shown in fig. 4.1(b). However, it is not feasible to regenerate the solvent to that great extent, because high regeneration levels require (and consume) great amounts of stripping vapor. On the other hand, as the lean solvent loadings get higher, the solvent circulation flow rate will have to vary in accordance with these changes in the degree of regeneration, if the CO_2 capture rate is to be maintained. For this reason, reboiler TER is also expected to rise quickly (although not as sharply as it did for low lean solvent loadings) on account of the higher solvent circulation flow rates. In fact, the required solvent flow rate to remove a tonne of CO_2 rises on such grounds, see fig. 4.1(b), where, for H_{abs} = 24 m, the lean solvent consumption increased fourfold within the range of the considered α_{LEAN}. Now, the observed reboiler TER is due to the rich solvent heat up as it enters the stripper. In fact, for high lean solvent loadings, the sensible heat component has the biggest share of the reboiler TER. Therefore, as the TER *vs.* α_{LEAN} curve is flanked by two relative maxima, a minimum TER (saddle) should be expected in between, which indeed shows up, as in fig. 4.1(a). This is consistent with the works reported by Abu-Zahra et al. [68], Soltani et al. [78]. As such, in this work, a lean loading of 0.19 mol CO_2/mol MEA is identified as the optimal lean solvent loading, being also the optimal α_{LEAN} for all the absorber packing heights considered.

Now, take again a constant H_{abs} = 24 m: to α_{LEAN} = 0.09 mol CO_2/mol MEA corresponds a TER equal to 5.45 GJ/t CO_2. As α_{LEAN} moves towards 0.19 mol CO_2/mol MEA – the optimal α_{LEAN} – TER decreases to 3.49 GJ/t CO_2. Then, as α_{LEAN} moves away from 0.19 mol CO_2/mol MEA, it rises again, but at a different rate of change, so that, in the end, for α_{LEAN} = 0.29 mol CO_2/mol MEA, TER equals 3.78 GJ/t CO_2. In fact, compare the TER values between α_{LEAN} = 0.09 and 0.19 mol CO_2/mol MEA (TER decreases 36%) and that of 0.19 and 0.29 mol CO_2/mol MEA (TER increases just 8%).

In addition, higher reboiler TER can be, in general, achieved with smaller absorber packing heights, as fig. 4.1(a) shows. Take, for example, the optimal α_{LEAN} of 0.19, if the base case H_{abs} is reduced in -75% a TER increase of 11% follows. In chapter 2, it was seen that the packing height determines the available length for gas-liquid contact, which in turn may affect the quality of the gas-liquid separation. Whenever the packing height is enlarged, the contact area increases, resulting in increased absorption

capacity. So, it can be inferred that, for a given solvent lean loading, reboiler TER increases as the H_{abs} diminishes.

4.3.1.2 Influence of α_{LEAN} and H_{abs} on the CWC KPI

It should be noted that process water is used in four different equipment:

- at the stripper condenser;

- at the lean cooler after the lean-rich heat exchanger;

- at the MEA scrubber;

- at the washing water cooler.

For this reason, the results exhibited in fig. 4.2 are the outcome of the influence of these four contributions. For all the absorber packing heights evaluated, both the stripper condenser and the lean cooler are the biggest consumers of process water, and together are responsible for about 95% of the total required cooling water. However, lean cooler water requirements themselves account for a greater share (around 86%) than the water demand of the stripper condenser, since, for different lean solvent loadings, the lean cooler process water requirements grow at a markedly higher rate than the condenser water requirements. As a result, the global profile of the cooling water consumption rates *vs.* lean solvent loading follows the behaviour of the lean cooler water usage. Put differently, the lean cooler process water demand is dominant compared with the remaining three components.
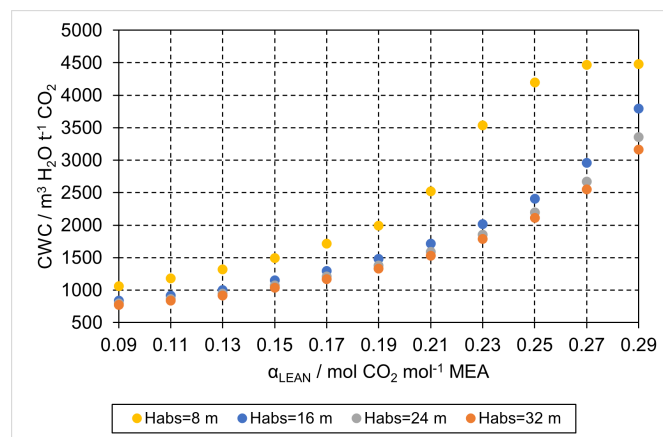
Figure 4.2 – Cooling water consumption rates at various lean solvent loadings (0.09 to 0.29 mol CO_2/mol MEA) for different absorber packing heights, H_{abs}, for a capture rate of 90%.

It was just seen that, for low lean solvent loadings, smaller solvent flow rates are needed to achieve the desired 90% capture rate. As smaller flow rates are to be handled in the lean cooler, positioned just after the lean-rich heat exchanger, the cooler duty reduces, thus diminishing the cooling water consumption. The opposite effect is noticed for high lean solvent loadings, resulting on the observations depicted in fig. 4.2.

At the same time, for low lean solvent loadings, the stripper condenser cooling water requirements naturally spike, which is attributable to the amount of stripping vapor flowing in the column for the stripper

operation. In effect, for increasingly smaller lean loadings, more stripping vapor needs to be generated at the reboiler to achieve such poor compositions in CO_2. As a result, not only do the reboiler TER increase (as was previously seen) but also vapor flows within the column rise, which in turn means that greater mass flow rates will pass through the condenser. Therefore, greater cooling water flow rates are required.

Recall that, for a given absorber packing height, as the lean solvent loading increases, greater solvent flow rates need to be fed to the absorber to keep the design capture rate. For this reason, the liberated heat, that in any case would have been evolved by the exothermic MEA-CO_2 absorption reactions, is more distributed for the solvent high flow rate than it might have been for lower solvent flow rates. This ultimately means that the outlet gas stream leaves the absorber at a smaller temperature, which indeed occurs – see fig. 4.3.
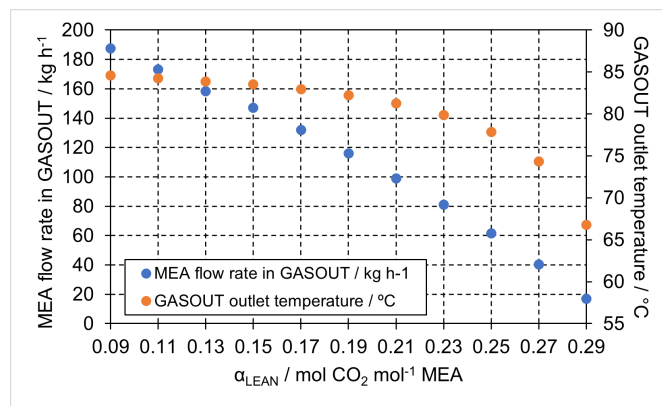
Figure 4.3 – Effect of the lean solvent loading on the MEA evaporation into the gas phase and on the outlet gas temperature.

In that event, the absorber must have been working at a smaller temperature range, with the vapor-liquid equilibrium being displaced to lower temperatures. As a result, less MEA vaporises into the gas phase as the lean solvent loading increases, thus lowering the washing water requirements. In addition, if the washing water requirements are diminished, then smaller flow rates circulate within the washing loop, which in turn reduce the washing cooler duty, as well as the cooler utility requirements.

4.3.2 Effect of the stripper operating pressure on the KPIs

4.3.2.1 Influence of P_{stp} on the TER

Stripper operating conditions play a major role in the success of the desorption task. Thus, the effect of different temperature and pressure conditions on the regeneration efficiency was examined, whose results are shown in fig. 4.4. The kettle-type reboiler operates with low pressure (LP) steam at 144°C (circa 4 bara [79]), coming, for instance, from an utility plant installed at the industrial facility or from a power plant nearby.

High stripper pressures help reduce quite substantially the reboiler TER in about 36%, as shown in fig. 4.4(a). Whenever the reboiler temperature changes, the stripper operating pressure changes

(a) Reboiler TER for different stripper operating pressures.

(b) Process steam consumption rates at the reboiler for different stripper working pressures.
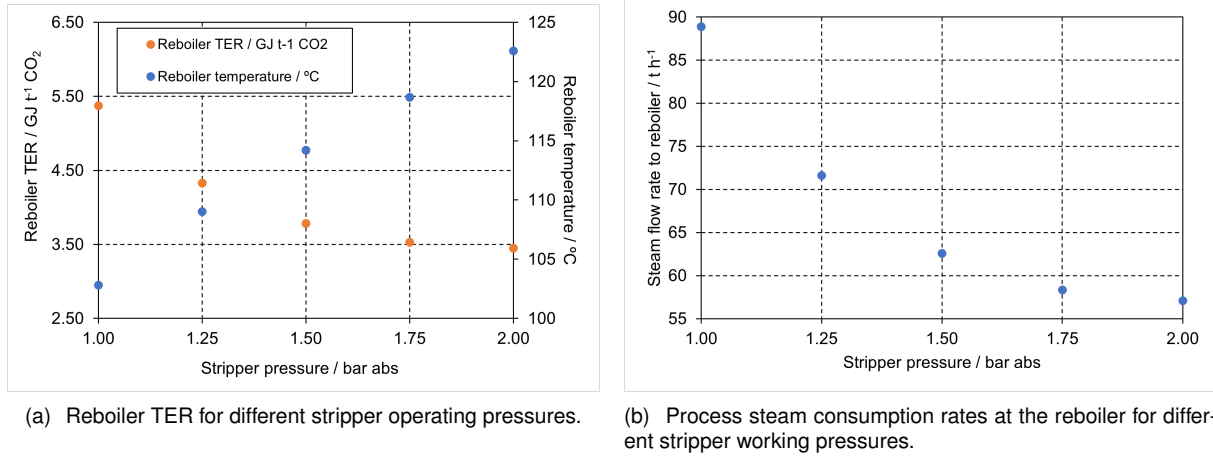
Figure 4.4 – Effects of the stripping working pressure on the reboiler TER and on the steam consumption rates.

accordingly (and vice-versa). Increasing reboiler temperatures decrease the ratio of the water partial pressure to the CO_2 equilibrium partial pressure with the amine solution, p_{H_2O}/p_{CO_2} [57], owing to:

i) the CO_2 vapor pressure, $p_{CO_2}^{sat}(T)$, which increases more rapidly with temperature changes than the H_2O vapor pressure, $p_{H_2O}^{sat}(T)$, according to the Clausius-Clapeyron equation, eq. (4.1). This is due to the fact that the heat of absorption (which is the opposite of the heat of desorption) of CO_2 is almost twice the heat of vaporization of H_2O.

$$\frac{\partial \ln p}{\partial (1/T)} = -\frac{\Delta H}{R} \Leftrightarrow \frac{\partial \ln p}{\partial T} = \frac{\Delta H}{RT^2} \tag{4.1}$$

where R stands for the ideal gas constant (Pa m^3/mol K), p the pressure (Pa), T the temperature (K), and ΔH, a heat of absorption or vaporization (J/mol).

Therefore, at greater-than-the-atmospheric stripper working pressures, the stripper operates at higher temperatures, resulting in a CO_2 vapor pressure increase. As a consequence, so does the driving force for CO_2 stripping, ultimately leading to higher CO_2 mass transfer rates.

Put differently, for a given temperature, an equilibrium CO_2 partial pressure exists, which is to say $p_{CO_2}^* \doteq p_{CO_2}^{sat}(T)$. What drives CO_2 mass transfer in the stripping process is the difference between the CO_2 concentration in the liquid phase and the CO_2 partial pressure in the gas phase. Due to unit inconsistency, the driving force cannot be expressed this way, but rather as the difference between the CO_2 equilibrium partial pressure (that were to be in equilibrium with the CO_2 in the liquid amine solution and would correspond to a given amine concentration in the liquid phase) and the actual CO_2 partial pressure, $(p_{CO_2}^* - p_{CO_2})$. Mass transfer would then cease when pressure equilibrium were to be attained. So, as temperature increases the equilibrium partial pressure shifts accordingly towards greater pressures. This, in turn, enhances the driving force for mass transfer, thus reducing the amount of stripping vapor needed. As a result, the reboiler duty lowers (that is, the reboiler is under less demand);

ii) as the CO_2 stripping reactions are endothermic, benefit with higher temperatures.

Both effects i) and ii) result on a easier CO_2 desorption task;

74

iii) as the reboiler temperature rises, so does $p_{H_2O}^{sat}(T)$ as well. This means that, for a fixed pressure, water boils at a higher temperature, which makes it more difficult for water to evaporate. In fact, at 2 bara, water boiling point is around 121°C [76]. Therefore, elevating the stripper pressure to values greater-than-the-atmospheric suppresses water vaporisation.

Overall, these effects culminate in a lower reboiler TER when P_{stp} is raised. In addition, reboiler duty goes hand in hand with process steam consumption rates. That is, greater specific reboiler duties require greater process LP steam flow rates, as shown in fig. 4.4(b). Steam consumption savings of the order of 36% can be attained when increasing P_{stp} from 1 bara to 2 bara.

4.3.2.2 SR and CWC changes following P_{stp} variations

The influence of the stripper working pressure on the other two defined KPIs is shown in fig. 4.5. It was found that the stripper pressure had no influence or whatsoever on the solvent requirements. This fact comes as no surprise as these are mainly set by the absorber operation. On the other hand, greater stripper working pressures reduce the cooling water requirements. In particular, greater pressures imply cuts of the order of 49% in the amount of cooling water employed in the condenser.
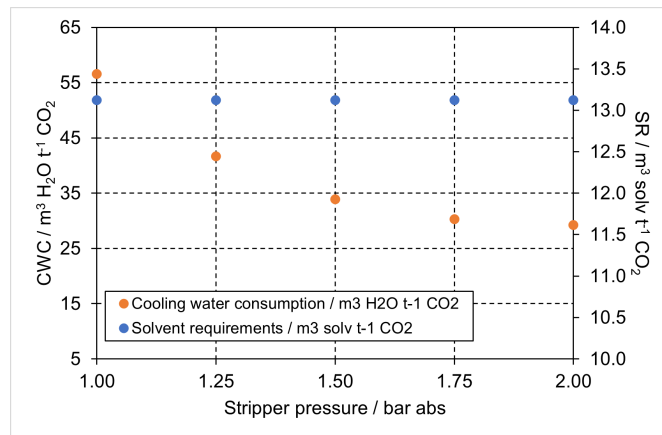
Figure 4.5 – Effect of stripper working pressure on the CW and SR KPIs.

4.3.3 Effect of the stripper packing height on the KPIs

The effect of the stripper packing height on the previously defined KPIs was also investigated, as in table 4.3. From these results, it appeared that the stripper packing height did not greatly influence the capture plant performance, since variations of this parameter in -20% and -40% did not substantially change the TER; as for the other KPIs, solvent requirements remained unchanged as expected, while the cooling water consumption rates increased slightly with the studied variations.

In order to confirm such conclusions, the column temperature and composition profiles were inspected for the aforementioned three cases, which are present in the appendix B. As the profiles did not greatly differ between them, the initial observations were corroborated. In fact, decreasing the stripper packing height in as much as 40% does not translate itself in higher energy requirements at the reboiler.

Table 4.3 – Variation of -20% and -40% in the H_{stp} with respect to the base case H_{stp} and its effect on the defined KPIs. The stripper diameter here indicated is that calculated by the rate-based model design tool.

$H_{stripper}$ (m)	$D_{stripper}$ (m)	TER (GJ/t CO$_2$)	Steam flow rate (t/h)	SR (m^3 solv/t CO$_2$)	CWC (m^3 H$_2$O/t CO$_2$)
6	3.25	3.52	58.2	13.1	33.6
8	3.23	3.46	57.3	13.1	32.7
10	3.22	3.45	57.1	13.1	32.4

4.3.4 Water wash section for MEA emissions compliance

At any vapor-liquid operation of this nature, some absorbent can potentially evaporate to the gas stream while flowing through the absorber. However, MEA emissions into the atmosphere are strictly regulated by law. Therefore, an important part of any chemical absorption capture plant is the water wash section, which is commonly installed within the absorber column. Nonetheless, in this work, the washing system was simulated in a separate, dedicated column. Either way, with such system, MEA can be recovered and recirculated to the absorber, thus diminishing amine losses. Recall the water wash section diagram, purposely shown in fig. 4.6 for the reader's convenience:
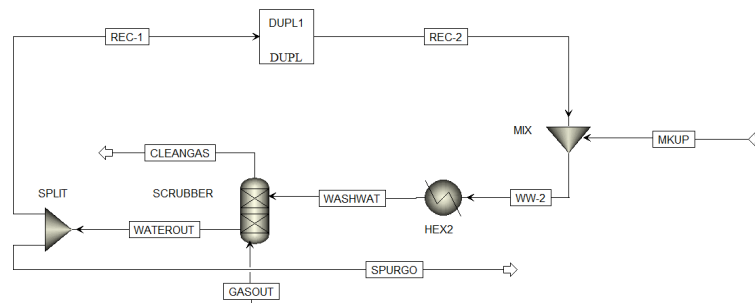
Figure 4.6 – Scheme of the water wash section.

A water mass balance to a control volume enclosing all the washing section essentially states that the water make-up must be such that compensates for the water rejected in the purge stream (at the splitter) and that exiting with the clean gas. However, most of the water in the GASOUT condenses along the scrubber:

$$\{H_2O \text{ in } \texttt{GASOUT}\} + \{H_2O \text{ make-up in } \texttt{MKUP}\} = \{H_2O \text{ in } \texttt{SPURGO}\} + \{H_2O \text{ in } \texttt{CLEANGAS}\} \quad [kg/h] \quad (4.2)$$

Washing water is continuously recycled in a circuit: every time MEA gets dissolved back in the washing water, it loses some absorption capacity. For this reason, some washing water must be bled off to avoid unwanted MEA accumulation that would jeopardize the operation of the washing section. So, a value of the purge fraction, f_{purge}, must be selected within that framework. The appropriate one will be such that process water requirements are the smallest.

Effect of the purge fraction on the make-up water requirement In this respect, the f_{purge} was varied and its influence on the amount of recycled water and on the required make-up were analysed. As this was a closed loop within the flowsheet, a tear stream emerges, which, in this case, was stream REC-2. Results are showcased in table 4.4. Thanks to a flowsheet design specification, the absolutely necessary make-up was determined: its value was that for which the MEA concentration in the outlet gas stream was just below the maximum allowed outlet concentration (20 mg/Nm^3). Greater reductions in the MEA outlet concentration would imply greater water make-up flows, which is undesirable for economic reasons. So, the adequate design value for the purge fraction will be that for which a) MEA concentration in the outlet gas complies with the threshold value, and simultaneously b) the water make-up is the lowest as possible. There is still a third, more operational condition that must be satisfied regarding the minimum admissible liquid and gas flow rates for which Aspen Plus® is able to generate the scrubber hydraulic plots for the used type of structured packing, which was identified as 1000 kg/h H_2O.

Table 4.4 – Influence of the variation of the purge fraction on the water make-up requirements and on the scrubber flows.

f_{purge}	WASHWAT flow rate (t/h)	WATEROUT flow rate (t/h)	H_2O flow rate in REC (t/h)
0.9	2.101	2.097	0.210
0.7	8.682	9.299	2.790
0.5	20.21	21.91	10.96
0.3	40.97	44.64	31.25
0.1	94.61	103.4	93.07

f_{purge}	H2OMKUP flow rate (t/h)	$D_{scrubber}$ (m)	C_{MEA} (mg/Nm^3)
0.9	1.892	2.02	19.998
0.7	5.893	2.18	19.999
0.5	9.251	2.36	19.993
0.3	9.719	2.59	19.994
0.1	1.549	2.95	20.000

As per table 4.4, low f_{purge} imply, as expected, greater material flows in the washing water recycle circuit. However, quite surprisingly, as more material is recirculated (lower f_{purge}) higher make-up flow rates have to be provided until a maximum value is reached for f_{purge} = 0.3. Passed that maximum make-up value, it then decreases abruptly. For all the cases evaluated, the water make-up flow rates are somewhat greater that what would be expected, and thus may be, at first sight, perceived as exaggerated. In effect, Li et al. [71] work, which also focused on the scrubbing section of MEA absorption process, reported a ratio of 43.06 kg of make-up H_2O per kg of MEA removed for a f_{purge} = 0.07, which compares with 13.47 kg of make-up H_2O per kg of MEA removed at this work for an approximately equal f_{purge} = 0.1. In addition, as f_{purge} increases, so does the scrubber diameter in order to effectively handle greater flow rates, as shown in table 4.4.

Lastly, recall that the composition of the flue gas under study has a considerable higher composition

in CO_2 than, for instance, that coming from power plants, whose CO_2 content is generally around 13% [80]. Fundamentally, more heat is expected to evolve as MEA reacts with the CO_2, still ensuring the 90% capture rate. In consequence, more MEA is expected to evaporate into the gas phase, being then necessary to scrub that amount of evaporated MEA at upstream unit operations, which may reinforce the need for these water flows. In fig. 4.7, it is depicted the MEA concentration profile on the vapor phase, which resoundingly demonstrates the importance of the washing section. The MEA concentration in the gas decreases along the scrubber packing height to a practically negligible concentration value.
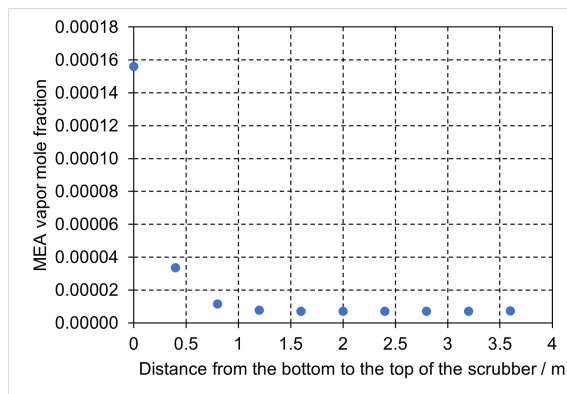
Figure 4.7 – Profile of the vapor composition in MEA along the scrubber.

Table 4.5 – Design results for the water-wash section.

Inlet MEA flow rate (kg/h)	115.9
MEA recovery rate (%)	99.03
Outlet MEA concentration (mg/Nm^3)	20.000

Having these aspects into consideration, the case for which f_{purge} = 0.1 was selected as it guaranteed a smaller make-up requirement.

4.4 The best case scenario

4.4.1 Recognising the best case

It was seen previously that the minimization of the reboiler TER was prioritised over the remaining KPIs, given its contribution on the process economics - the price of steam is much higher than that of process water, *cf.* section 4.6.2. The reboiler TER *vs.* lean solvent loading analysis revealed the α_{LEAN} for which TER was minimal, for that the best case was identified as the one in which α_{LEAN} = 0.19 for an absorber packing height of 32 m. Moreover, it was observed that a lower reboiler TER entails higher solvent requirements. However, SR will increase invariably as the reboiler TER diminishes so as to maintain a constant capture rate. Furthermore, as increasing P_{stp} gives rise to a more efficient regeneration, P_{stp} should be equal to 2 bara in the best case scenario. Regarding the stripper packing height, the highest considered packing height – H_{stp} = 10 m – is selected for the sake of mass transfer efficiency.

For illustrative purposes, temperature and composition profiles of the absorber are presented in appendix A.

4.4.2 Final considerations

Taking these aspects into consideration, both the baseline and the optimal cases may now be compared in terms of the previously defined KPIs. Whether it is for economic (savings) or sustainable reasons, the smaller (as possible) the process requirements (*i.e.*, the required amounts of solvent, process water, and steam) the better. For this reason, the set of operating parameters that lead to such low process requirements must be chosen. For instance, greater reboiler duties imply higher demands for process steam, which is, generally, generated through fossil fuels combustion, thus raising the question of the secondary emissions that, in any case, are not innocuous.

Table 4.6 – Comparison between the base case simulation results and those of the identified best case.

	Scenarios	
	Base case	Best case
Capture rate (%)	90%	
Amine lean solvent loading (mol CO_2/mol MEA)	0.090	0.190
Amine rich solvent loading (mol CO_2/mol MEA)	0.532	0.525
Reboiler TER (GJ/t CO_2)	5.385	3.449
Required solvent flow rate (m^3/t CO_2)	9.94	13.1
Required cooling water (m^3/t CO_2)	770.5	1331
at stripper condenser (m^3/t CO_2)	90.31	48.39
at lean solvent cooler (m^3/t CO_2)	656.7	1272
at water cooler (m^3/t CO_2)	23.38	10.56
at amine scrubber (m^3/t CO_2)	0.114	0.053

Delving into the results shown in table 4.6, it can be observed that the best case outperforms the baseline one only in the reboiler TER, which is undoubtedly the most important factor to consider when selecting the best operating conditions. Its effect on the operating expenditures outweighs the effect of the solvent and cooling water (CW) requirements on the process economics. The reasons for such claim were already made clear previously. In effect, increasing the lean solvent loading from 0.09 to 0.19 achieves a 36% reduction in TER, which is beneficial in terms of energy efficiency. This effect is even more pronounced when lower lean loadings are under study: despite non being exhibited in this work, additional obtained results have shown that raising α_{LEAN} from 0.03 to 0.19 allow astonishing (and quite remarkable) TER reductions of the order of 400% be attained.

Regarding the SR performance criterion, a clear trade-off between lower reboiler TER and higher solvent requirements is identified. In fact, smaller TERs (*i.e.*, poorer regeneration at the stripper) can only be achieved at the expense of higher SRs provided that the capture rate at the absorber is to remain unchanged for both cases.

As for the remaining performance criterion – CWC –, the baseline case scenario globally shows smaller solvent and process water consumption than the best case scenario found. Notwithstanding, for the latter KPI, a careful inspection of the results reveals otherwise. That is, in fact, all but one process water requirements diminish as α_{LEAN} increases, however these reductions are completely overshadowed, since the lean cooler water requirements dominate over the other components to a great extent.

As a consequence, the overall result is that shown in section 4.3.1 - the cooling water requirements grow as the α_{LEAN} increases.

4.5   Final process operation - flexibility analysis

So far, all the simulations conducted assumed that the EAF fumes were admitted to the capture plant at a constant flow rate. The real situation is, however, quite different, as pointed out in chapter 3. So, after the optimal case was identified, a sort of dynamic simulation should be carried to transpose the obtained steady-state results to a discontinuous operation.

The final process operation should be as that depicted in fig. 4.8. Recall that, during an EAF working cycle, there is a portion of time during which the EAF is not operating, which is to say EAF fumes are exhausted in a intermittent manner. Therefore, the proposed CO_2 capture plant must operate in a flexible way, which is one of the major goals of this investigation. The suggested operation mode incentives the full application of this technology at the industrial scale. With a view to enable such flexible operation, the present work recommends the following operation mode for a single working cycle:

- during the time in which the EAF is operating:

    - fumes coming from the EAF cleaning system arrive at the absorber, where CO_2 is absorbed into the MEA-based solvent. The required solvent flow rate that ensures the desired capture rate is provided;

    - the three-way valve directs the newly-rich solvent to the rich solvent tank, and then to the regeneration section.

- during the time in which the EAF is not operating:

    - as there will not be any emissions coming from the EAF, no gas stream containing CO_2 will be passing through the absorber. Nonetheless, the absorber still continues at service in a continuous manner, which is why atmospheric air should be made to pass through the absorber in order to ensure correct operation of the absorption unit.
    This is a rather feasible solution: whether fumes are evolving from the EAF or not, atmospheric air is always admitted to the process right after the EAF fourth gap. In other words, while the EAF is under operation, off-gases evolve from the furnace, go through the fourth hole, and then into the cleaning circuit, where atmospheric air is added to the off-gas at some stage. Off-gas is diluted as a consequence, and CO post-combustion is allowed to happen. After going through the cleaning section, the EAF exhaust gas arrives at the absorber. If, on the other hand, no off-gas evolves from the EAF, then atmospheric air is still admitted to the process and flows into the cleaning circuit and then into the capture plant.
    This means that there will be some variability in the gas flow rates entering the absorber, which in turn poses a problem regarding the equipment size, namely the column diameter. This parameter is most influenced by the amount of fluid (both gas and liquid) being handled

in the equipment. However, this effect may be swiftly minimized with a greater intake of air at the air gap.

– lean solvent flowing through the column will not absorb CO_2, which is why it may be recirculated to the top of the absorber. To that end, the three-way valve now shifts position, opening the solvent recycle loop in the absorber – see fig. 4.8.

During the entire operation cycle, regeneration takes place. Freshly regenerated solvent is directed to the lean solvent tank. During the time no EAF off-gas is being fed to the absorber (*i.e.*, atmospheric air is the fed gas stream), lean solvent is continuously recirculated, and so there is no need to feed more lean solvent than that recirculating. Therefore, freshly regenerated solvent is stored in the lean solvent tank.

4.5.1   Implementation in Aspen Plus®

Both the absorber and the stripper must be disconnected, since the system will not be in steady-state. In that event, after the absorber is simulated, the rich solvent stream compositions are copied into the stripper feed stream. However, what should be the stripper inlet flow rate (`RICHIN`)? Could it be the same as that of the rich solvent leaving the absorber (`RICHOUT`)?
Begin by assuming a cycle of 50 min, in which the EAF:

• operates during 40 min with subsequent emissions;

• remains idle for 10 min due to furnace cleaning works and liquid steel withdrawal.

So, for this reason, both flow rates cannot be equal, because the absorber will only absorb CO_2 for 40 min, thus releasing for 40 min a loaded `RICHOUT`, while the stripper will be able to regenerate for 50 min. In the optimal case steady-state simulation, the required lean mass solvent flow rate to absorb 90% of the CO_2 contained in the flue gas was roughly equal to 8.08×10^3 kg/min. This flow rate amounts to 3.23×10^5 kg of lean solvent entering in the absorber during the 40 min in which the absorber will be actually absorbing CO_2. For the remaining 10 min, 8.08×10^4 kg of lean solvent will be recirculated to the top of absorber, as no CO_2 has been absorbed.
Now, focus solely on the 40 min of operation: those 3.23×10^5 kg of lean solvent will absorb 90% of the CO_2 in the flue gas, and, after absorption, will be directed to the rich solvent tank, before going to the stripper for regeneration. Steady-state simulation revealed that `RICHOUT` mass flow rate is 8.34×10^3 kg/min. In 40 min, 3.34×10^5 kg of rich solvent will be generated and directed to the lean solvent tank, and then to the stripper. This amount of rich solvent will be handled by the stripper in a different time scale. In other words, as the stripper operates for 50 min this amount of rich solvent needs to be distributed (or better, divided) for this time. As a result, `RICHIN` mass flow rate should be equal to $3.34 \times 10^5/50 = \underline{6.67 \times 10^3 \text{ kg/min} = 4 \times 10^2 \text{ t/h}}$.

4.5.2   Final results

Before moving on to the engineering economic evaluation, a brief overview of the streams involved in the process under the flexible mode – the one proposed for implementation in mini-mills – is shown in table 4.7.
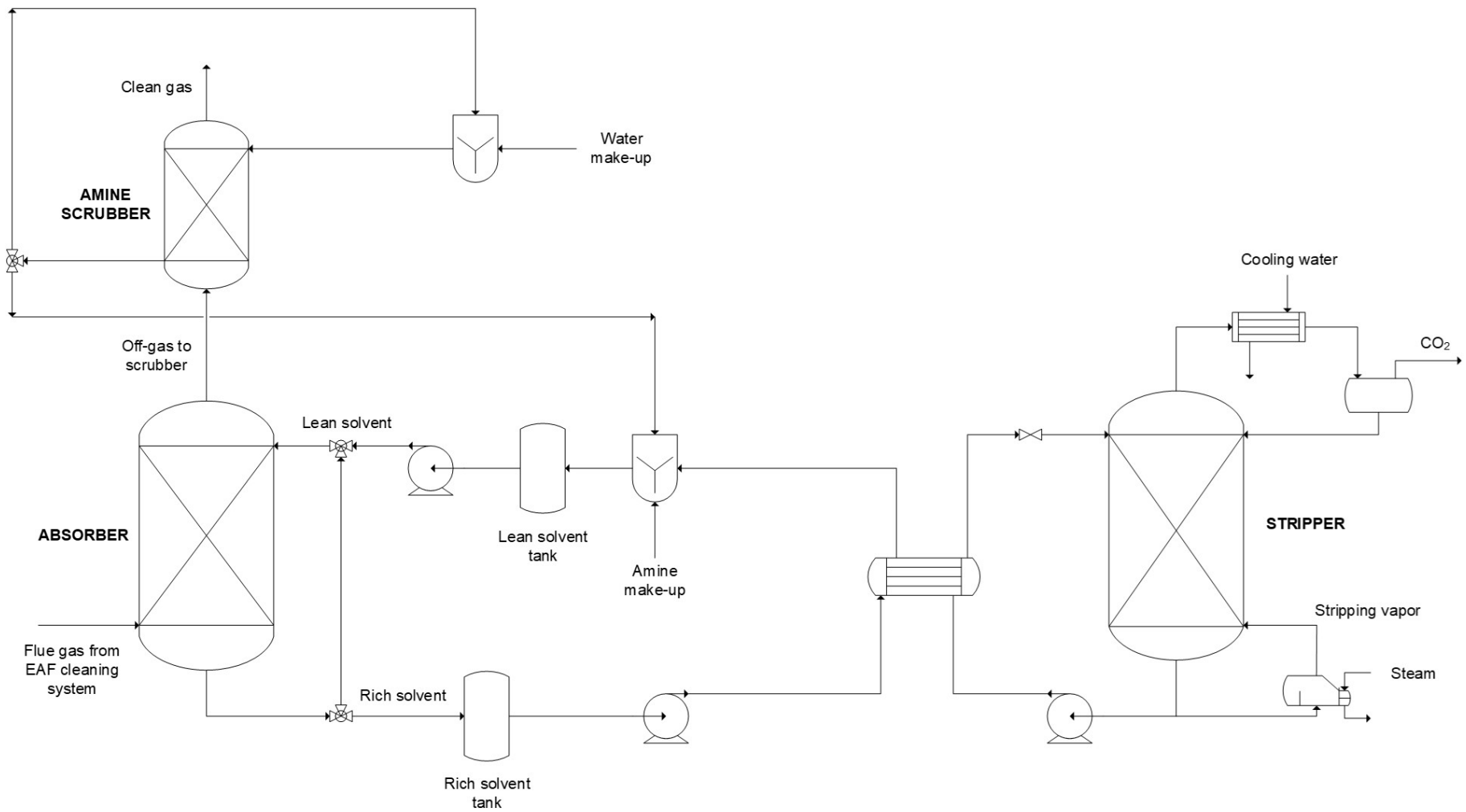
Figure 4.8 – Final flowsheet for the simulated process under flexible operation.

Table 4.7 – Overview of the process streams in the final flowsheet for the flexible mode operation.

Stream	Molar flow rate (kmol/h)	Mass flow rate (t/h)	Temperature (°C)	Molar vapor fraction	Molar compositions				
					CO_2	MEA	H_2O	N_2	O_2
Vapor phase									
FLUEGAS	2230	76.78	48.0	1.00	0.40	0.00	0.01	0.56	0.03
CO2OUT	821.7	35.69	30.0	1.00	9.78×10^{-1}	1.82×10^{-10}	2.15×10^{-2}	5.98×10^{-4}	5.89×10^{-5}
GASOUT	2516	61.13	82.2	1.00	3.54×10^{-2}	7.54×10^{-4}	4.41×10^{-1}	4.96×10^{-1}	2.66×10^{-2}
CLEANGAS	2033	52.34	69.7	1.00	0.04	0.00	0.31	0.61	0.03
Liquid phase									
LEANIN	2.005×10^4	484.7	40.0	0.00	0.02	0.12	0.86	0.00	0.00
RICHOUT	1.896×10^4	500.3	51.1	0.00	6.23×10^{-2}	1.19×10^{-1}	8.19×10^{-1}	3.04×10^{-5}	2.99×10^{-6}
RICHIN	1.527×10^4	400.3	108	0.01	6.23×10^{-2}	1.19×10^{-1}	8.19×10^{-1}	3.04×10^{-5}	2.99×10^{-6}
LEANOUT	1.515×10^4	364.6	124	0.00	0.01	0.13	0.86	0.00	0.00
WASHWAT	5199	94.61	25.0	0.00	9.74×10^{-4}	3.25×10^{-3}	9.96×10^{-1}	4.42×10^{-6}	4.07×10^{-7}
WATEROUT	5681	103.4	78.3	0.00	9.90×10^{-4}	3.30×10^{-3}	9.96×10^{-1}	4.49×10^{-6}	4.14×10^{-7}
REC	5113	93.07	78.3	0.00	9.90×10^{-4}	3.30×10^{-3}	9.96×10^{-1}	4.49×10^{-6}	4.14×10^{-7}
SPURGO	568.1	10.34	78.3	0.00	9.90×10^{-4}	3.30×10^{-3}	9.96×10^{-1}	4.49×10^{-6}	4.14×10^{-7}
MKUP	85.99	1.549	25.0	0.00	0	0	1	0	0
AMMKUP	538.8	9.707	25.0	0.00	0.00	3.47×10^{-5}	1.00	0.00	0.00

4.6 Project economic evaluation - analysis of cost estimation

At last, an economic evaluation of this project was entirely carried out resorting to the Aspen Process Economic Analyser® (APEA), based on USD for the first quarter of 2018.

Every chemical process project involves estimating both the investment costs and the production costs to assess its inherent feasibility. In particular, for a CO_2 capture plant project, one must have a clear definition on what is done with the final product, that is: the question of whether is this a carbon capture and storage (CCS) or a carbon capture and utilisation (CCU) project must be answered, as it will influence cost estimation:

- if a CCU project is aimed at, then the removed CO_2 must serve some other purpose. In other words, CO_2 must be used as feedstock for another process, for instance selling CO_2 to an urea production facility → **scenario I**;

- if, on the other hand, a CCS project is on the table, then the removed CO_2 is to be compressed and stored into a geological formation (a classic example of CCS) via a compression train → **scenario II**.

To contemplate the aforementioned alternatives, these two scenarios were investigated. The main assumptions for this economic evaluation are summarized in table 4.8.

Table 4.8 – Economic evaluation assumptions.

Present value	USD 2022
Plant operating period	8000 h/year [81, 82]
Economic life of project	30 years [83]
Interest rate	8% [81, 83, 84]
Tax rate	40%
Salvage value	20% of capital costs [82]
Depreciation method	Straight-line method
Cost of CO_2 ETS certificate	93.42$/t CO_2eq [85]
Carbon tax	25.40$/t CO_2eq [86]
Working capital percentage	5% of total capital investment
Labour cost	20$/operator/h
Supervisor cost	35$/operator/h
Operating charges	25% of operating labor
Plant overhead cost	50% of operating labor and maintenance
General and Administrative expenses	8% of total direct production costs
Project capital escalation	5%
Raw material escalation	3.5%
Utilities escalation	3%
Operating and Maintenance labor escalation	3%

4.6.1 Capital investment (capital costs)

Large amounts of money have to available before a given chemical plant can be put into operation. That is, capital must be available to:

i) arrange the manufacturing and other plant facilities, that is the so-called *fixed-capital investment*, which is required for:

- purchasing (*equipment costs*) and installing (*installed costs*) all the equipment, including control and piping between equipment;
- obtaining land and service facilities.

ii) guarantee the required funds to pay expenses involved in the plant operation before product sales become available, the so-called *working capital*.

4.6.1.1 Fixed-capital investment (FCI)

Equipment cost Recall that all prices returned by APEA referred to mid-2018. As prices change considerably with time (due to changes in economic conditions), these prices must be updated to be representative of today's conditions.

Cost indexes To that purpose, one resorts to cost indexes. Chemical Engineering Plant Cost Index (CEPCI) for July 2022 was equal to 829.8, while CEPCI for 2018 was 603.1 [87]. Prices are then updated using eq. (4.3):

$$P_{2022} = P_{2018} \frac{I_{2022}}{I_{2018}} \tag{4.3}$$

A side note on scenario I Scenario I is the simplest in terms of equipment purchase. All necessary equipment to keep the capture plant running is that shown in fig. 4.8.

A side note on scenario II Scenario II requires more equipment than scenario I: CO_2 must be compressed after removal at the stripper, being then transported through pipelines (either onshore or offshore) or ships, and later stored in a geological site – as a saline aquifer. For this scenario, it will only be considered the compression train costs, and not the costs associated with CO_2 transport and storage. In any case, as a side note, a benchmark value for CO_2 transport and storage cost may be around 10\$/ton CO_2[1]. However, Smith et al. [88] stressed that these costs are subject to quite some regional variability, since:

- CO_2 transport costs vary with the transport method (*i.e.*, by offshore or onshore pipeline or by ship), the quantity of CO_2 transported, the transport distance, which in turn depend on the geography and geology settings;

---

[1]The ton unit refers to the Imperial - IP - unit system.

- on the other hand, CO_2 storage costs also depend on the amount of CO_2 stored and on geologic characteristics of the formations on which CO_2 is to be stored.

Therefore, these costs may be realistically placed between 4-45$/ton CO_2 [2]. Typical pressure values for gas transport on pipeline are around 15 MPa, a greater pressure than the critical pressure of CO_2 – $P_c(CO_2)$ = 7.38 MPa [76]. So, the stripper overhead gas mixture must be compressed from the atmospheric pressure to 15 MPa [89], while passing the CO_2 critical pressure. At atmospheric pressure, CO_2 is a gas, but its behaviour changes as the critical pressure is attained and surpassed (*i.e.*, supercritical CO_2). Furthermore, these compression subsystems typically comprise other process equipment than compressors [69, 89, 90]:

- water-based coolers are installed in the compression line as compression inevitably heats up the gas mixture;

- knock-out (flash) drums are also installed to recover the water that condenses as the gas mixture is compressed. The condensed water alongside with the CO_2 flow might have corroded the downstream pipeline. In this case, knock-out drums are not required, since it was assumed, as an approximation, that a pure CO_2 stream exits the stripper (which is then sent to the compression line).

In accordance with Mostafa et al. [91] work, a train of 4 compressors, *i.e.* $N_{train} = 4$, with an intercooler in between each compressor was chosen. In addition, the last stage was a pumping stage. It was considered an isentropic efficiency of 80% for all the compressors, and a mechanical efficiency of 80% for the pump. Suction temperature at each compressor was set at 20°C.

Table 4.9 – Considered data for the compression and pumping train design and results [91].

	Stage	η	Inlet pressure (bar)	Outlet pressure (bar)	Compression ratio (CR)	Net work (kW)
Compressor	1	0.8	2	4.45		607,96
	2	0.8	4.45	11.66		710.75
	3	0.8	11.66	30.54	2.43	679.40
	4	0.8	30.54	70		503.76
Pump	5	0.8	70	150	–	126.99

In fig. 4.9, the distribution of the equipment costs are shown for both scenarios. On the one hand, it can be observed that, for scenario I, the packed columns (absorber + scrubber + stripper) are responsible for 65% of all equipment costs. The balance is almost divided between the mixers and required heat exchangers. On the other hand, for scenario II, the compressors and packed columns together account for 78% of the equipment costs, while the heat exchangers are responsible for just 13% of those costs.

---

[2]See footnote 1.

(a) Scenario I.   (b) Scenario II.
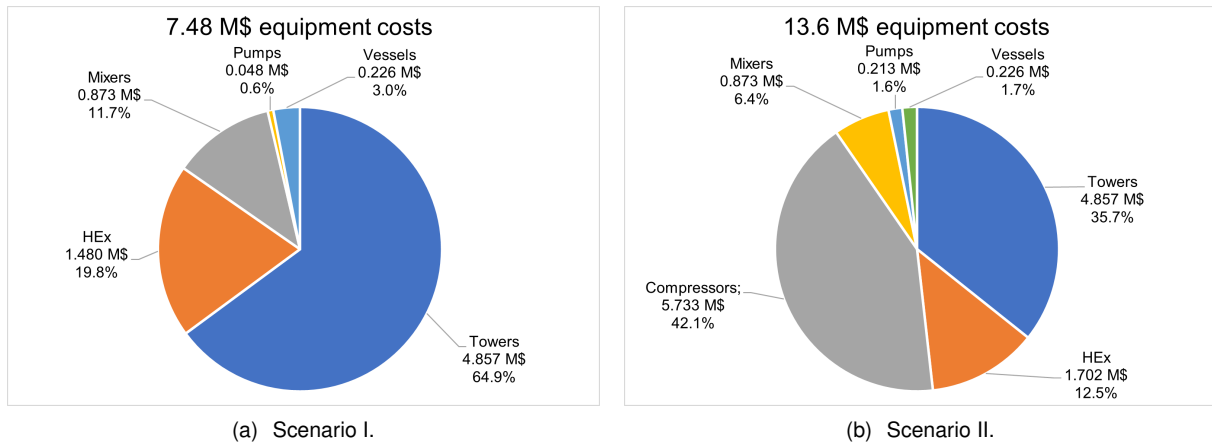
Figure 4.9 – Distribution of the purchase costs (from APEA) of the equipment needed in each of the considered scenarios.

4.6.1.2 Total capital investment (TCI)

The total capital investment (TCI) is the sum of the fixed-capital investment (FCI) and the working capital (WC), $TCI = FCI + WC$. All components of the capital investment, which were estimated by APEA, are summarised in table 4.10.

Table 4.10 – Breakdown of the capital investment items.

Capital costs	Cost (M$)	
	Scenario I	Scenario II
Direct costs		
Purchased	7.485	13.60
Installation	0.172	0.247
Piping	1.995	2.819
Civil	0.405	0.529
Steel	0.320	0.359
Instrumentation	1.674	2.453
Electrical	1.563	3.093
Insulation	0.476	0.571
Paint	0.122	0.173
Others	7.204	10.60
Total direct costs	**21.42**	**34.44**
Indirect costs		
Design, Eng, Procurement costs	3.594	5.121
G&A overheads	0.541	0.904
Contract fee	0.860	1.252
Contingencies	4.148	6.737

Total indirect costs	**9.143**	**14.01**
FCI = Direct + Indirect	**30.56**	**48.46**
Working capital	1.528	2.423
TCI = FCI + WC	**32.09**	**50.88**
Salvage value	6.417	10.18

4.6.2 Production costs

The cost of producing the product is generally divided into two groups: *manufacturing costs* and *general expenses*. *Manufacturing costs* are the so-called *operating costs*, which are of the upmost importance.

4.6.2.1 Manufacturing costs

All expenses connected with the manufacturing operation fall into this category. It is widely acknowledged that manufacturing expenses can be grouped into the following categories: variable (or direct) production costs (DPC), fixed charges and plant overhead costs.

Direct production costs   All costs directly related with the production stage come under this category. As such, these costs vary with production rates. Examples of such expenditures are those for raw materials, operating labor and supervision, catalysts, among others.

Raw materials   Regarding the raw materials employed, only MEA is to be considered, as the process water is accounted under the process utilities.

Table 4.11 – Prices of the raw materials [82].

MEA solvent	1.44$/kg

MEA is to be acquired at the beginning of the project. Smaller MEA make-up is then added.

Plant utilities   Whenever process streams are not available for heat exchange with other process streams, one must resort to utilities:

- **cooling water**. Assuming mild spring conditions, process water may be available at 15°C (a rather optimistic assumption). After the usual water treatment, it is then directed to the different heat exchange equipment, where its outlet temperature will vary depending on heat duties involved. That is:

  - at the stripper condenser and at the lean cooler, water may leave at 30°C;
  - while on the cooler of the water wash circuit, it may only leave at 20°C.

- **LP steam**. Low pressure steam to be fed to the stripper reboiler was considered to be at 144°C;

- **electricity**, which is needed to power the installed pumps along the process.

Table 4.12 – Utilities specific costs considered [61].

Process (cooling) water	0.082$/t
Low pressure steam	13$/t
Electricity	0.1$/kWh

Table 4.13 – Utilization and costs for the utilities considered in **scenario I**.

	Usage (t/h)	Duty (kW)	Total cost (M$/y)
Cooling water			
Stripper condenser	1358	23653	0.891
Lean cooler	452.2	7876.0	0.297
Water make-up at MEA scrubber	1.543	–	1.11×10^{-3}
Washing water cooler	987.5	5737.1	0.648
Low pressure steam			
Stripper reboiler	78.29	46449	8.14
Electricity			
Pumps	–	41.760	0.033

Table 4.14 – Utilization and costs for the utilities considered in **scenario II**.

	Usage (t/h)	Duty (kW)	Total cost (M$/y)
Cooling water			
Stripper condenser	1358	23653	0.891
Lean cooler	452.2	7876.0	0.297
Water make-up at MEA scrubber	1.543	–	1.11×10^{-3}
Washing water cooler	987.5	5737.1	0.648
Coolers at compression line	278.6	4890.2	0.183
Low pressure steam			
Stripper reboiler	78.29	46449	8.14
Electricity			
Pumps	–	181.82	0.145
Compressors	–	2621.1	2.10

Fixed charges   These expenses refer to costs that virtually do not change with the amount of production and essentially have to do with the financing arrangement and the capital investment. Among these, only depreciation is noteworthy, as follows.

Depreciation   Any physical facility deteriorates with time, while equipment become obsolescent with time and their usefulness decreases, which is why all assets have a certain lifetime (*i.e.*, a service

life). To put it another way, assets *depreciate* as time goes by. An investment in any depreciable asset is not registered at the time of payment in a single entry of the corporate books (that is, registered as a one-time expense); instead, capital investments are registered in a fractional manner along a given period of time. In other words, the investment cost is distributed along time, with a fraction of the invested capital being charged as an operating expense every year. Originally, these expenses – which go also by the name of *depreciation* – were charged during the service life of the property. However, nowadays the period over which depreciation is charged is called *recovery period* as established by tax authorities. This time period has little relationship with the asset lifetime [92] in that it does not reflect the actual working life of an asset (*e.g.*, an equipment), but states the period over which depreciation is allowed. So, a deduction for depreciation is charged as a manufacturing expense during the recovery period for every asset, even though it does not correspond to an actual payment. This would theoretically mean that there would be more expenses, hence reduced profit before tax (PBT/EBT), ultimately meaning less taxes[3]. Therefore, tax-payers manage to save money during the time assets depreciate that can be later used to reinvest in newer assets. In any case, even if this money were not to be reinvested in newer assets, this "artifact" is simply the acknowledgement by tax codes that investors recover the original investment through depreciation [92]. Recall that in order to have an operable production plant, equipment, buildings and others must be bought, which require a significant initial investment (that is often shared with other investors or by contracting a loan). It is therefore reasonable to think that this investment must be paid back to the investor, or put differently the invested principal must be recovered by the investor.

Depreciation calculation methods   There are several ways of calculating depreciation. As this matter is beyond the scope of this work, it is only noteworthy to say that the *straight-line method* was the only considered. In this method, (depreciable) property value is decreases linearly with time over the recovery period [92].

4.6.2.2 General expenses

Under the general expenses, fall the administrative, distribution and marketing and research and development costs, which are generally called general and administrative (G&A) costs. These costs are associated with management and administrative-level activities. In this work, these will be estimated as being equal to 8% of the subtotal operating costs, as in table 4.8.

4.6.3 Total cost evaluation

Ultimately, the total costs of any plant will be the sum of both the capital costs and the production costs, that can be approximated to the operating costs. The latter are always specified per a time basis, while capital costs correspond to a single expenditure of money [93]. Recall that in order to i) ensure unit consistency; ii) account for the time value of money, either capital costs must be *annualized* or operating

---

[3]For this reason, recovery periods are strictly established by law, since this accounting "artifact" influences the amount of taxes paid by companies.

Table 4.15 – Breakdown of the product costs into the manufacturing (or operating or production) costs and general expenses, estimated by APEA. DPC stands for the direct production costs.

Product cost		Cost (M$/y)	
		Scenario I	Scenario II
Manufacturing costs			
Direct PC	Raw materials	11.18	11.18
	Utilities	10.01	12.40
	Operating labour	0.480	0.960
	Operating supervision	0.280	0.280
	Maintenance cost	0.462	0.588
	Operating supplies and laboratory charge	0.190	0.310
Other	Plant overhead cost	0.611	0.914
Subtotal manufacturing costs		**23.22**	**26.63**
Fixed charges	Depreciation	0.521	0.846
Total manufacturing costs		**23.74**	**27.48**
General expenses			
	G&A cost	1.877	2.152
Total general expenses		1.877	2.152
Total product cost		**25.61**	**29.64**

costs have to be *capitalized* so that all costs are referred to the same time base. In this work, capital costs will be annualized. That is,

$$TAC = ACC + OC \tag{4.4}$$

where TAC designates the total annual cost, ACC the annualized investment (or capital) costs and OC the operating costs.

Capital costs annualization   In order to annualize the investment costs, one may hypothesise that the capital to be invested is borrowed from a bank. In this way, the capital investment is replaced by annual bank payments, which not only will repay the loan but also the interest on the loan. Therefore, capital investment is now in the same units as the operating costs [93, 94]. A way to do so is through the concept of depreciation, as the bank annual payments need to recover the FCI. Note that, of all TCI, only the working capital cannot be depreciated. If straight-line depreciation is considered, then $AFCI = FCI/n$, where $AFCI$ is the annualized fixed-capital investment, FCI stands for the fixed-capital investment and n the expected project life. If, on the other hand, the time value of money is to be accounted, then a capital recovery factor (CRF) must be used, as in eq. (4.5) [94]. Here, FCI was converted into a series of constant payments for every year of project life, that is $AFCI$ is an *annuity* (non-linear depreciation):

$$TAC = AFCI + OC = FCI \underbrace{\frac{(1+i)^n \, i}{(1+i)^n - 1}}_{CRF} + OC \tag{4.5}$$

where TAC stands for total annual costs, OC for operating expenditures, and i, the discount rate. So, capital costs are depreciated over the economic life of project with a 8% discount rate as per table 4.8. The capital recovery factor allows to determine the amount of each future annuity to pay for a given present value, provided that the interest rate is known as well as the number of payments (for each project year). Dividing the TAC by the amount of captured CO_2 allows to determine the cost of CO_2 removal.

Table 4.16 – Total plant costs for the considered scenarios.

CRF = 8.9%	Scenario I	Scenario II
Annualized capital costs (M$/y)	2.714	4.304
Operating costs (M$/y)	25.61	29.64
Total plant costs - TAC (M$/y)	**28.33**	**33.94**

In CCUS projects, CO_2 is just removed for the raising environmental concerns, and not for the project attractiveness in terms of the oncoming benefits of the product sales. In fact, for the first scenario, where CO_2 is sold to an urea production facility, CO_2 is a cheap commodity in that project revenues will not cover even the operating expenses; while, in scenario II, no specific revenues can be identified. In any case, for this type of projects, only the total plant costs can be analysed and no profitability analysis can be carried out. That being said, it is certainly of interest to compare the cost of CO_2 removal with the prices of the carbon taxes and/or other regulations in place, as will be explained in section 4.6.5, to have an idea of the feasibility of such a project.

Product sales (revenues) for scenario I As of today, there are few prices for bulk CO_2 as these are typically agreed in private negotiations. However, typical values range from 3-15/ton [4] of bulk gaseous CO_2 [95].

4.6.4 Cost of CO_2 removal

More precisely, the CO_2 capture cost can be calculated as per eq. (4.6) [29]:

$$CO_2 \ capture \ cost = \frac{COHRC_{w/ \ cap} - COHRC_{w/o \ cap}}{CO_2 \ captured} \tag{4.6}$$

After the raw liquid steel is produced from the EAF, further upstream processing is carried out from which the different final products are withdrawn. Among these, there is the hot rolled coil (HRC). In eq. (4.6), which is an adaptation of that used in the power industry sector, COHRC refers the cost of hot rolled coil (HRC). COHRC is, in fact, the result of both capital and operating costs from both plants involved in the process. That is, the iron and steel production plant and the CO_2 capture plant. In this work, it was assumed that the iron and steel production plant is being retrofitted to consider the CO_2 capture plant, as generally is the case. Therefore, both the capital expenditures (CAPEX) and the operating

---

[4]See footnote 1.

expenditures (OPEX) of the main process (*i.e.*, the iron and steel one) remain unchanged. In that event, eq. (4.6) reduces to eq. (4.7):

$$\text{CO}_2 \ capture \ cost = \frac{CAPEX_{cap \ plant} + OPEX_{cap \ plant}}{\text{CO}_2 \ captured} = \frac{TAC_{cap \ plant}}{\text{CO}_2 \ captured} \qquad (4.7)$$

In any case, recall that the cost of CO_2 capture depends on what is done with the removed CO_2. In table 4.17, the total plant costs for the considered scenarios, the amount of CO_2 avoided, and the corresponding CO_2 capture costs are summarised.

Table 4.17 – CO_2 capture costs *vs.* the total plant costs for both scenarios.

	Scenario I	Scenario II
Total plant costs - TAC (M\$/y)	28.33	33.94
CO_2 avoided (Mt CO_2/y)	0.310	0.310
Cost of CO_2 removal (\$/t CO_2)	**91.39**	**109.5**

In order to provide the big picture, all components of the previous cost estimation were now considered on the basis of the annually removed CO_2, being then broken down in three groups - annual capital expenditures, fixed and variable operating and maintenance costs (O&M), as shown in fig. 4.10. Displaying costs in this way is usually performed in works of CCUS applied to power plants, and was borrowed to this research work for the insight it provides. Note that the fixed O&M costs include operating labour and general and administrative cost. Depreciation is also included under this category. On the other hand, the variable O&M costs include the consumables (*i.e.*, raw materials) costs, the utilities costs and plant overhead costs [82, 96].

For both scenarios, it can be observed that the highest capture cost corresponds to the variable O&M expenses that represent over 70% of the overall CO_2 capture cost. Together the O&M costs express 90% and 87% of the capture cost for scenarios I and II, respectively. In addition, some interesting conclusions can be made:

- the cost for raw material replenishment (MEA make-up) and the steam cost, which remain naturally unaltered in both scenarios, account together for 68% and 57% of the CO_2 capture cost for scenarios I and II, respectively. The great contribution of the steam cost to the overall capture cost reinforces the need for giving priority to the minimization of the reboiler TER when designing the carbon capture plant;

- annual CAPEX increases 59% from scenario I to scenario II given the need of more equipment in the latter (for the compression train). In the same manner, the cost of the electricity (variable O&M) rises from scenario I to scenario II, in virtue of the compressors/pump installed at the compression line.
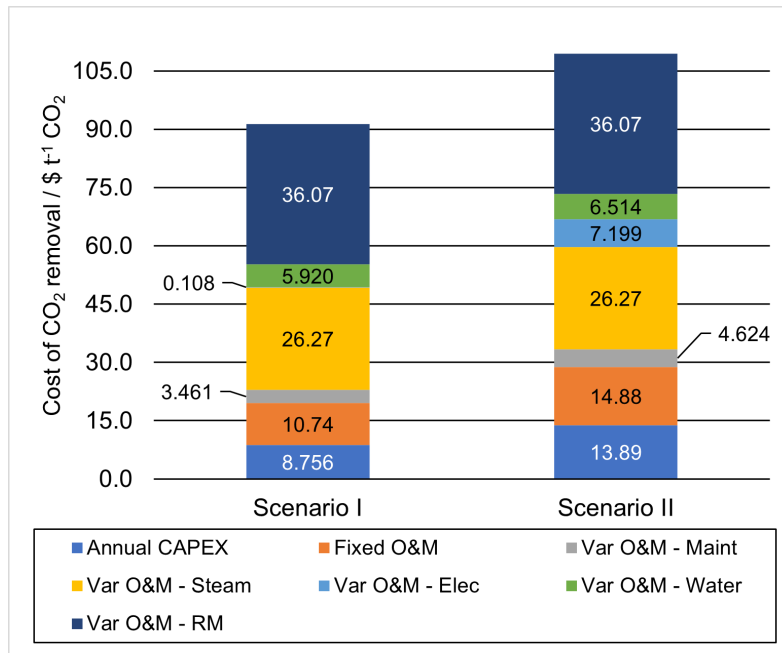
Figure 4.10 – Breakdown of the CO_2 capture cost per tonne of CO_2 captured for the considered scenarios. *Maint.* stands for maintenance, *Elec.* for electricity, *RM* for raw materials (consumables).

4.6.5 Carbon tax and ETS permits

Given the awareness of the climate change due to GHG emissions, governments have started to institute environmental regulations, namely:

- on the one hand, the *carbon taxes* under which a price for each tonne of emitted GHG is set [97]. For example, as of April 1st, 2022, carbon tax in Portugal is around 23.88€/t CO_2eq [86], which is equivalent to 25.40$/t CO_2eq at the currency rate as of December 9th, 2022;

- on the other hand, the *emissions trading system* (ETS), which is based on the so-called "cap and trade" principle [98]. That is, GHGs emissions for the installations covered by the ETS are *capped*. Emissions allowances (or permits) can be given to the installations, but installations can also buy emissions allowances, so that, in the end, the total emissions of an installation are fully covered by the allowances. If not, heavy fines are applied to the non-compliant installations. In addition, the imposed limit on the emissions is not fixed over time, but rather decreases over time, so that total emissions are reduced, hence mitigating climate change.

  Permits can also be *traded* with other installations that are short of allowances to cover their emissions. As of December 9th, 2022, a ETS permit costs 87.84€/t CO_2eq [85], which is equivalent to 93.42$/t CO_2eq at the present currency rate.

For instance, Italy has joined the ETS but does not have a carbon tax in force, while Portugal has implemented both [97]. So, it is quite interesting to compare the CO_2 capture cost with the current carbon tax, since if it were not for the raising environmental concerns, CO_2 would not be removed, as CO_2 capture projects are not economically attractive in the sense that high costs are usually involved – see table 4.18.

Table 4.18 – Comparison between the cost of CO_2 removal and the carbon tax and ETS permits in force.

	Scenario I	Scenario II
Carbon tax ($/t CO_2eq)	25.40	
Cost of ETS certificate ($/t CO_2eq)	93.42	
Cost of CO_2 removal ($/t CO_2)	91.39	109.5

4.6.6 Final considerations

As mentioned previously, amine-based chemical absorption technologies are considered highly-mature, with a vast portfolio of industrial applications. For this reason, this technology is currently labelled as TRL 9. This fact explains why this carbon capture, storage and utilisation (CCUS) technology was selected over the existing others and may incentive its application to capture the specific CO_2 emissions coming from mini-mills.

The analysis of the results arising from the economic evaluation reveals that scenario I is less expensive than scenario II, considering from the outset the additional equipment needed in the compression line - see fig. 4.10. It should be also noted that the cost estimation for scenario II was not comprehensive of the transport or storage costs, which would certainly increase expenses (*i.e.*, both capital and operating costs) even further. What is more scenario I promotes circular economy, since the sub-products of an industry are the raw materials of another one.

On the other hand, it is difficult to establish a solid comparison between the attained CO_2 capture costs with others obtained for other mini-mill plants (under the same circumstances), as to the author's best knowledge little or none cost estimation reports for the application of carbon capture to mini-mills have been described in the literature. Nonetheless, Wiley et al. [72] reported a value of 250A$/t CO_2 avoided at 2011, which translates to 342A$/t CO_2 avoided, considering Australia's current inflation rate. This in turn corresponds to 239$/t CO_2 avoided at the currency rate of December 2022, 23rd. The estimation made by Wiley et al. [72] considered a CCS scenario and, strictly speaking, cannot be compared with the obtained value in this work, given the different units. However, for lack of better reported values, it will suffice to say that both estimates are of the same order of magnitude.

On the one hand, looking at the capture costs for both scenarios, and confronting them with the carbon tax in Portugal, it would seem from the profitability point of view that implementing a CO_2 capture system would not be feasible, as the current Portuguese carbon tax is substantially smaller than the cost of removal for both scenarios. However, different countries enforce more or less tighter environment policies, ultimately meaning that there is quite some variability on these charges, depending on the plant location. In fact, if this plant were to be installed in Sweden, it would be subject to a stricter carbon tax - *cf.* 25.40$/t CO_2 in Portugal *vs.* 100€/t CO_2 in Sweden (which is equivalent to 124.61$/t CO_2, as per the currency rate of December 2022, 23rd). In consequence, this local variability on the carbon tax enforcement hinders more uniform and stricter control on CO_2 emissions, which is why a satisfactory comparison between the obtained CO_2 capture costs and the carbon tax cannot be performed and cannot be used as a decision criterion for the implementation of such carbon capture plant.

On the other hand, regarding the ETS permits, the results from table 4.18 would suggest that it would be economically favourable to pay just for enough allowances such that the uncovered emissions by the free allowances are then covered, rather than investing in a CO_2 capture project. As of now, some of the total CO_2 emitted per *annum* will be covered by allocated free allowances, while the remaining emissions are covered through paid allowances. However, it is important to not keep out of sight that, according to [98], ETS free allowances will decrease over time, until a situation of all emitted CO_2 is to be charged (*i.e.,* ceases the allocation of free allowances). In that event, considering the obtained CO_2 removal costs in this work and the ETS permits cost, the choice for implementing such solution is clear as the capture costs for both scenarios and the current ETS costs are quite competitive with each other. Moreover, the costs for these permits will increase foreseeably over time, which encourages even further the application of the present technological solution to a mini-mill. So, although, at first sight, it did not seem practicable to go for a project of such nature, the fact that the ETS policy is getting harsher as time goes by and as many governments acknowledge the urgency of this problem, demonstrates how companies are necessarily forced to reduce CO_2 emissions in the long term, with CO_2 capture playing a role within that scope.

Therefore, scenario I is proposed for supplementary analysis, as it shows a slightly lower capture cost than that of scenario II.

Chapter 5

Conclusions and future work

In light of the growing greenhouse gases emissions by the industrial sector to which the iron and steel industry belongs, this dissertation auspiciously proposed the application of CO_2 capture via chemical absorption to a mini-mill plant, even if at a conceptual stage. That is to say the point for adopting such conceptual solution was successfully made. To the author's best knowledge, there are no references in the literature to an Aspen Plus® simulation of a chemical absorption plant installed in the electric arc furnace (EAF) exhaust gas system.

Carbon capture is widely acknowledged as being the sole alternative capable of curbing CO_2 emissions from this industrial sector. Currently, there are many technological solutions for carbon capture, such as: adsorption techniques (as the Ca looping cycle), absorption (physical or chemical) or even membranes. However, carbon capture via chemical absorption with amine-based solvents is currently classified with TRL 9, which makes the case for chemical absorption.

The rate-based model developed, due to its rigor, can be used as a guide for CO_2 absorption processes using MEA solvent. Furthermore, this work aimed at finding the best working conditions for the operation of the carbon capture system applied to a mini-mill. From all the studied parameters, it was identified the particular and critical role of the lean solvent loading, α_{LEAN}, on the design of a absorption + stripper unit. Besides the lean solvent loading, which was varied between 0.09 mol CO_2/mol MEA and 0.29 mol CO_2/mol MEA, the following parameters were also changed: absorber packing height (8 m $< H_{\text{abs}} <$ 32 m), stripper operating pressure (1 bara $< P_{\text{stp}} <$ 2 bara), stripper packing height (6 m $< H_{\text{stp}} <$ 10 m). The effect of their variation on the process performance was assessed by means of key performance indicators (KPI).

Most importantly, given the tremendous amounts of energy usually involved in solvent regeneration, reducing the reboiler thermal energy requirements (TER) were a key priority. For this reason, the case in which the reboiler TER were minimal was considered to be the best one, thereby fixing both the lean solvent loading and the absorber packing height. In fact, compared to the baseline case, TER reductions

of 36% were achieved when α_{LEAN} was increased from 0.09 to 0.19, while, at the same time, it was found that, for a fixed lean solvent loading, smaller absorber packing heights led to higher reboiler TER, *e.g.* for α_{LEAN} = 0.19 and for H_{abs} = 32 m, TER = 3.45 GJ/t CO_2; while, for the same α_{LEAN} and H_{abs} = 8 m, TER = 3.83 GJ/t CO_2.

Furthermore, thanks to the remaining parametric analyses, the optimal case could be completely outlined. Some other main findings were:

- reducing the stripper operating pressure from 2 bara to 1 bara entails TER increases of 55%, ultimately leading to an increase of order of 56% in the steam consumption rate. In other words, increasing the stripper operating pressure would give rise to a more efficient regeneration;

- the stripper operating pressure does not influence substantially the remaining performance criteria;

- the stripper packing height does not have any effect on the defined KPIs.

In summary, the optimal operating conditions were α_{LEAN} = 0.19, H_{abs} = 32 m, H_{stp} = 10 m and P_{stp} = 2 bara, which resulted in a TER of 3.45 GJ/t of removed CO_2. As MEA emissions into the atmosphere are strictly regulated, a washing section had to be designed. Due to the flue gas CO_2 concentration, a higher temperature range along the absorber was noticed, which thereafter influenced the amount of vaporized MEA. This, in turn, revealed to be a crucial detail for the scrubber design, which is also dependent on the specification of the water purge fraction. Interesting results were obtained, and a f_p = 0.1 was selected, corresponding to a water make-up flow rate of 1.55 t/h.

Only after the steady-state best operating conditions were identified could the flexible operating mode be laid out, which exploited the dedicated air gap for CO post-combustion: inasmuch as fumes are being exhausted from the EAF, the absorber operates; when the EAF remains idle, only atmospheric air is to be admitted to the absorber. The flexible operation mode was one of the main deliverables of this dissertation, being in fact the point that enables its industrial application. In addition, the stripper feed flow rate, which was the major process variable to determine at that stage, was identified as 400 t/h. In fact, the obtained results in the flexible mode simulation ascribed for the feasibility of such solution.

Lastly, an economic evaluation of this project was carried out, in which both a carbon capture and storage (CCS) and a carbon capture and utilisation (CCU) scenarios were considered. Capital costs for the CCS scenario (32.09 M$) were higher than those for the CCU scenario (50.88 M$), owing to the compression train. In regard to the operating costs, the steam and raw material costs combined account for 68% and 57% of the operating costs belonging to scenarios I and II, respectively.

Globally speaking, the CO_2 capture total cost for the CCU scenario was smaller than that for the CCS scenario – 91.39 $/t CO_2 captured *vs.* 109.5 $/t CO_2 captured, respectively. For this reason, the CCU scenario (scenario I) is recommended for further analysis. In any case, the obtained values if compared with the cost of the ETS certificates (whose price will predictably increase over time) compel decision-makers regarding the implementation of this solution at mini-mill plants, as these are quite close among themselves. Ultimately, this solution will contribute to a healthier planet Earth.

In the near future, the most immediate point to develop would be a further analysis of scenario I, considering this time a flue gas consisting of 11%mol CO_2. In effect, this would correspond to the actual

process conditions. Nonetheless, in this work, an absorber gas feed with 40%mol CO_2 was considered as part of a conservative approach to this problem. It is expected that process solvent requirements would lower substantially for these newer feed conditions. Furthermore, additional studies regarding the utilisation of other types of solvents may well be carried out, especially considering that state-of-the-art, greener solvents are being developed as part of a rather intense field of investigation. In fact, a more eco-friendly solvent would enhance even more the sustainability of the process. On the other hand, other process configurations such as the absorber intercooler or the rich-split process could also be simulated in Aspen Plus® to examine their benefits on the studied process. These alternative configurations have already been studied in other applications with much promising results.

References

[1] National Aeronautics and Space Administration. Global Climate Change, Vital Signs of the Planet. `https://climate.nasa.gov`. [Online; accessed 5 April 2022].

[2] M. Bailera, P. Lisbona, B. Peña, and L. M. Romeo. A review on CO_2 mitigation in the Iron and Steel industry through Power-to-X processes. *Journal of CO_2 Utilization*, 46:101456, 2021. ISSN 2212-9820. doi: https://doi.org/10.1016/j.jcou.2021.101456.

[3] M. Draxler et al. Greensteel for Europe: Technology assessment and roadmapping. `https://ec.europa.eu/clima/eu-action/climate-strategies-targets/2050-long-term-strategy_en`, March 2021. [Online; accessed 21 April 2022].

[4] IEA. Global CO_2 emissions by sector. `https://www.iea.org/data-and-statistics/charts/global-co2-emissions-by-sector-2018`, 2018. [Online; accessed 07 April 2022].

[5] IEA. Tracking Industry 2020. `https://www.iea.org/reports/tracking-industry-2020`, 2020. [Online; accessed 07 April 2022].

[6] J. Kim, B. K. Sovacool, M. Bazilian, S. Griffiths, J. Lee, M. Yang, and J. Lee. Decarbonizing the iron and steel industry: A systematic review of sociotechnical systems, technological innovations, and policy options. *Energy Research & Social Science*, 89:102565, 2022.

[7] *Industrial Transformation 2050—Pathways to Net-Zero Emissions from EU Heavy Industry*. Material Economics, 2019.

[8] W. D. Callister Jr. and D. G. Rethwisch. *Fundamentals of materials science and engineering: an integrated approach*. John Wiley & Sons, 2020.

[9] Worldsteel Association. Steel Facts. `https://worldsteel.org/about-steel/steel-facts/`, 2022. [Online; accessed 10 April 2022].

[10] EUROFER. European Steel in figures 2022 - data covering 2021. `https://www.eurofer.eu/publications/brochures-booklets-and-factsheets/european-steel-in-figures-2022/`, 2022. [Online; accessed 07 August 2022].

[11] *Steeling demand: mobilising buyers to bring net-zero steel to market before 2030*. Material Economics and Energy Transitions Commission, July 2021.

[12] Á. A. Ramírez-Santos, C. Castel, and E. Favre. A review of gas separation technologies within emission reduction programs in the iron and steel sector: Current application and development perspectives. *Separation and Purification Technology*, 194:425–442, 2018.

[13] Worldsteel Association. World Steel in Figures 2019. `http://www.worldsteel.org`, 2019. [Online; accessed 10 April 2022].

[14] Z. Fan and S. J. Friedmann. Low-carbon production of iron and steel: Technology options, economic assessment, and policy. *Joule*, 5(4):829–862, 2021.

[15] H. Raupenstrauch, K. Doschek-Held, J. Rieger, and W. Reiter. Recodust—an efficient way of processing steel mill dusts. *Journal of Sustainable Metallurgy*, 5(3):310–318, 2019.

[16] R. S. Treptow and L. Jean. The iron blast furnace: A study in chemical thermodynamics. *Journal of Chemical Education*, 75(1):43, 1998.

[17] A. Carpenter. CO_2 abatement in the iron and steel industry. `https://usea.org/sites/default/files/012012_CO2%20abatement%20in%20the%20iron%20and%20steel%20industry_ccc193.pdf`, 2012. [Online; accessed 5 April 2022].

[18] K. De Ras, R. Van de Vijver, V. V. Galvita, G. B. Marin, and K. M. Van Geem. Carbon capture and utilization in the steel industry: challenges and opportunities for chemical engineering. *Current Opinion in Chemical Engineering*, 26:81–87, 2019.

[19] A. Arasto, E. Tsupari, J. Kärki, E. Pisilä, and L. Sorsamäki. Post-combustion capture of CO_2 at an integrated steel mill–Part I: Technical concept analysis. *International Journal of Greenhouse Gas Control*, 16:271–277, 2013.

[20] The new generation of direct technology and steelmaking integration. `https://www.energiron.com/wp-content/uploads/2019/05/ENERGIRON-DR-Technology-Overview.pdf`, 2012. [Online; accessed 10 April 2022].

[21] B. Ellis and W. Bao. Pathways to decarbonisation episode two: steelmaking technology. `https://www.bhp.com/media-and-insights/prospects/2020/11/pathways-to-decarbonisation-episode-two-steelmaking-technology/`, 2020. [Online; accessed 21 April 2022].

[22] *Carbon-free steel production: cost reduction options and usage of existing gas infrastructure*. European Union Parliament, April 2019.

[23] M. A. Quader, S. Ahmed, R. A. R. Ghazilla, S. Ahmed, and M. Dahari. A comprehensive review on energy efficient co2 breakthrough technologies for sustainable green iron and steel manufacturing. *Renewable and Sustainable Energy Reviews*, 50:594–614, 2015.

[24] A.-V. Luca and L. Petrescu. Membrane technology applied to steel production: Investigation based on process modelling and environmental tools. *Journal of Cleaner Production*, 294:126256, 2021.

[25] C.-C. Cormos. Evaluation of reactive absorption and adsorption systems for post-combustion CO_2 capture applied to iron and steel industry. *Applied Thermal Engineering*, 105:56–64, 2016.

[26] X. Zhang, K. Jiao, J. Zhang, and Z. Guo. A review on low carbon emissions projects of steel industry in the world. *Journal of Cleaner Production*, 306:127259, 2021.

[27] IEA. Iron and steel. `https://www.iea.org/reports/iron-and-steel/`, 2021. [Online; accessed 07 August 2022].

[28] W. Chung, K. Roh, and J. H. Lee. Design and evaluation of CO_2 capture plants for the steel-making industry by means of amine scrubbing and membrane separation. *International Journal of Greenhouse Gas Control*, 74:259–270, 2018.

[29] S. Yun, M.-G. Jang, and J.-K. Kim. Techno-economic assessment and comparison of absorption and membrane CO_2 capture processes for iron and steel industry. *Energy*, 229:120778, 2021.

[30] A. J. Pimm, T. T. Cockerill, and W. F. Gale. Energy system requirements of fossil-free steelmaking using hydrogen direct reduction. *Journal of Cleaner Production*, 312:127665, 2021.

[31] M. Karbowniczek. *Electric Arc Furnace Steelmaking*. CRC Press, 2021.

[32] T. Hay, V.-V. Visuri, M. Aula, and T. Echterhof. A review of mathematical process models for the electric arc furnace process. *Steel Research International*, 92(3):22, 2021.

[33] M. E. Fabiani. *Recupero energetico dagli off-gas dei forni elettrici ad arco tradizionali. Applicazione di un procedimento innovativo con materiali a cambiamento di fase [Energy recovery from conventional electric arc furnaces off-gas. Innovative applications with phase change materials.]*. PhD thesis, Università degli Studi di Udine, 2012. URL `https://core.ac.uk/download/pdf/158819635.pdf`.

[34] M. Kirschen, V. Velikorodov, H. Pfeifer, R. Kühn, S. Lenz, J. Loh, and K. Schaefers. Off-gas measurements at the EAF primary dedusting system. *EEC*, 2005.

[35] S. U. Nimbalkar, A. Thekdi, J. R. Keiser, and J. M. Storey. Preliminary results from electric arc furnace off-gas enthalpy modeling. Technical report, Oak Ridge National Lab.(ORNL), Oak Ridge, TN (United States), 2015.

[36] F. Trivellato and L. Labiscsak. The post-combustion chamber of steelmaking plants: Role of ambient air in reactant exhaust fumes. *Applied Mathematical Modelling*, 39(1):19–35, 2015.

[37] P. Cavaliere and A. Silvello. *Ironmaking and steelmaking processes*. Springer, 2016.

[38] United States Environmental Protection Agency. Learn about dioxin. `https://www.epa.gov/dioxin/learn-about-dioxin`. [Online; accessed 15 August 2022].

[39] O. Sorg. Ahr signalling and dioxin toxicity. *Toxicology letters*, 230(2):225–233, 2014.

[40] R. Smith. *Chemical process: design and integration*. John Wiley & Sons, 2nd edition, 2016.

[41] P. Argenta and M. Bianchi Ferri. The EAF technology evolution and the Consteel® system. *La metallurgia italiana*, 1:2005, 2005.

[42] F. Memoli and M. B. Ferri. New track record for Consteel due to new environment-friendly features. *Metallurgical Plant and Technology International*, 30(5):58, 2007.

[43] F. Memoli, A. Grasselli, and C. Giavani. Consteel© EAF and conventional EAF: a comparison in maintenance practices. *La Metallurgia Italiana*, 2010.

[44] D. Kearns, H. Liu, and C. Consoli. Technology readiness and costs of CCS. Technical report, Global CCS Institute, March 2021.

[45] J. Holtbrügge, A. K. Kunze, A. Niesbach, P. Schmidt, R. Schulz, D. Sudhoff, and M. Skiborowski. *Reactive and membrane-assisted separations*. Walter de Gruyter GmbH, 2016.

[46] J. Seader, E. J. Henley, and D. K. Roper. *Separation process principles: with applications using process simulators*. John Wiley & Sons, 4th edition, 2016.

[47] P. C. Wankat. *Separation process engineering*. Pearson Education, 3rd edition, 2006.

[48] H. Bosch and A. B. De Haan. *Industrial Separation Processes*. Walter de Gruyter GmbH, 2013.

[49] Ö. Yildirim, A. A. Kiss, N. Hüser, K. Leßmann, and E. Y. Kenig. Reactive absorption in chemical process industry: A review on current activities. *Chemical engineering journal*, 213:371–391, 2012.

[50] R. Turton, R. C. Bailie, W. B. Whiting, and J. A. Shaeiwitz. *Analysis, synthesis and design of chemical processes*. Pearson Education, 3rd edition, 2008.

[51] R. Ravi, R. Vinu, and S. N. Gummadi. *Coulson and Richardson's Chemical Engineering: Volume 3A: Chemical and Biochemical Reactors and Reaction Engineering*. Butterworth-Heinemann, 2017.

[52] C. G. Hill. *Introduction to chemical engineering kinetics and reactor design*. John Wiley & Sons, 1st edition, 1977.

[53] E. L. Cussler. *Diffusion: mass transfer in fluid systems*. Cambridge University Press, 3rd edition, 2009.

[54] P. Muchan, C. Saiwan, J. Narku-Tetteh, R. Idem, T. Supap, and P. Tontiwachwuthikul. Screening tests of aqueous alkanolamine solutions based on primary, secondary, and tertiary structure for blended aqueous amine solution selection in post combustion CO_2 capture. *Chemical Engineering Science*, 170:574–582, 2017.

[55] F. Bougie and M. C. Iliuta. Sterically hindered amine-based absorbents for the removal of CO_2 from gas streams. *Journal of Chemical & Engineering Data*, 57(3):635–669, 2012.

[56] I. M. Bernhardsen and H. K. Knuutila. A review of potential amine solvents for CO_2 absorption process: Absorption capacity, cyclic capacity and pKa. *International Journal of Greenhouse Gas Control*, 61:27–48, 2017.

[57] S. S. Warudkar, K. R. Cox, M. S. Wong, and G. J. Hirasaki. Influence of stripper operating parameters on the performance of amine absorption systems for post-combustion carbon capture: Part I. High pressure strippers. *International Journal of Greenhouse Gas Control*, 16:342–350, 2013.

[58] P. Feron, editor. *Absorption-based post-combustion capture of carbon dioxide*. Woodhead Publishing, 2016.

[59] H. F. Svendsen, E. T. Hessen, and T. Mejdell. Carbon dioxide capture by absorption, challenges and possibilities. *Chemical Engineering Journal*, 171(3):718–724, 2011.

[60] K. Li, A. Cousins, H. Yu, P. Feron, M. Tade, W. Luo, and J. Chen. Systematic study of aqueous monoethanolamine-based CO_2 capture process: model development and process improvement. *Energy Science & Engineering*, 4(1):23–39, 2016.

[61] C. Madeddu, M. Errico, and R. Baratti. *CO_2 Capture by Reactive Absorption-Stripping: Modeling, Analysis and Design*. Springer, 2018.

[62] M. Errico, C. Madeddu, D. Pinna, and R. Baratti. Model calibration for the carbon dioxide-amine absorption system. *Applied Energy*, 183:958–968, 2016.

[63] Aspen Technology Inc. *Aspen Plus V11 Help pages*. Burlington (USA), 2019.

[64] N. Asprion. Nonequilibrium rate-based simulation of reactive systems: simulation model, heat transfer, and influence of film discretization. *Industrial & engineering chemistry research*, 45(6): 2054–2069, 2006.

[65] L. E. Øi. Comparison of Aspen HYSYS and Aspen Plus simulation of CO_2 absorption into MEA from atmospheric gas. *Energy Procedia*, 23:360–369, 2012.

[66] L. E. Øi. *Removal of CO_2 from exhaust gas*. PhD thesis, Telemark University College, 2012.

[67] Aspen Technology Inc. *Rate-based model of the CO_2 capture process by MEA using Aspen Plus*. Burlington (USA), 2014.

[68] M. R. Abu-Zahra, L. H. Schneiders, J. P. Niederer, P. H. Feron, and G. F. Versteeg. CO_2 capture from power plants: Part I. A parametric study of the technical performance based on monoethanolamine. *International Journal of Greenhouse gas control*, 1(1):37–46, 2007.

[69] S. Ó. Gardarsdóttir, F. Normann, R. Skagestad, and F. Johnsson. Investment costs and CO_2 reduction potential of carbon capture from industrial plants–A Swedish case study. *International Journal of Greenhouse Gas Control*, 76:111–124, 2018.

[70] M. Sundqvist, M. Biermann, F. Normann, M. Larsson, and L. Nilsson. Evaluation of low and high level integration options for carbon capture at an integrated iron and steel mill. *International Journal of Greenhouse Gas Control*, 77:27–36, 2018.

[71] B.-H. Li, N. Zhang, and R. Smith. Simulation and analysis of CO_2 capture process with aqueous monoethanolamine solution. *Applied Energy*, 161:707–717, 2016.

[72] D. E. Wiley, M. T. Ho, and A. Bustamante. Assessment of opportunities for CO_2 capture at iron and steel mills: an Australian perspective. *Energy Procedia*, 4:2654–2661, 2011.

[73] J. L. Bravo, J. A. Rocha, and J. Fair. Mass transfer in gauze packings. *Hydrocarbon processing (International ed.)*, 64(1):91–95, 1985.

[74] T. H. Chilton and A. P. Colburn. Mass transfer (absorption) coefficients prediction from data on heat transfer and fluid friction. *Industrial & engineering chemistry*, 26(11):1183–1187, 1934.

[75] J. Bravo, J. Rocha, and J. Fair. A comprehensive model in the performance of columns containing structured packings, distillation and absorption, institution of chemical engineers symposium series 128. *Inst Chem Eng*, 1:PA48–A507, 1992.

[76] D. W. Green and M. Z. Southard. *Perry's Chemical Engineers' handbook*. McGraw-Hill Education, 2019.

[77] E. Adu, Y. Zhang, D. Liu, and P. Tontiwachwuthikul. Parametric process design and economic analysis of post-combustion CO_2 capture and compression for coal-and natural gas-fired power plants. *Energies*, 13(10):2519, 2020.

[78] S. M. Soltani, P. S. Fennell, and N. Mac Dowell. A parametric study of CO_2 capture from gas-fired power plants using monoethanolamine (MEA). *International Journal of Greenhouse Gas Control*, 63:321–328, 2017.

[79] E. J. G. de Azevedo. *Termodinâmica aplicada*. Escolar Editora, 4th edition, 2018.

[80] C. Song, W. Pan, S. T. Srimat, J. Zheng, Y. Li, Y.-H. Wang, B.-Q. Xu, and Q.-M. Zhu. Tri-reforming of Methane over Ni Catalysts for CO_2 Conversion to Syngas With Desired H_2/CO Ratios Using Flue Gas of Power Plants Without CO_2 Separation. In S.-E. Park, J.-S. Chang, and K.-W. Lee, editors, *Carbon Dioxide Utilization for Global Sustainability*, volume 153 of *Studies in Surface Science and Catalysis*, pages 315–322. Elsevier, 2004.

[81] Y. Qiao, W. Liu, R. Guo, S. Sun, S. Zhang, J. J. Bailey, M. Fang, and C. Wu. Techno-economic analysis of integrated carbon capture and utilisation compared with carbon capture and utilisation with syngas production. *Fuel*, 332:125972, 2023.

[82] S. N. Hassan, P. L. Douglas, and E. Croiset. Techno-economic study of CO_2 capture from an existing cement plant using MEA scrubbing. *International journal of green energy*, 4(2):197–220, 2007.

[83] K. Li, W. Leigh, P. Feron, H. Yu, and M. Tade. Systematic study of aqueous monoethanolamine (MEA)-based CO_2 capture process: Techno-economic assessment of the MEA process and its improvements. *Applied Energy*, 165:648–659, 2016.

[84] M.-O. Schach, R. Schneider, H. Schramm, and J.-U. Repke. Techno-economic analysis of post-combustion processes for the capture of carbon dioxide from power plant flue gas. *Industrial & Engineering Chemistry Research*, 49(5):2363–2370, 2010.

[85] European Union carbon permits costs. `https://tradingeconomics.com/commodity/carbon`. Accessed on: 10-12-2022.

[86] S. Bray. Carbon taxes in Europe. `https://taxfoundation.org/carbon-taxes-in-europe-2022/`. Accessed on: 22-11-2022.

[87] Chemical Engineering Plant Cost Index values from 2001 to present. `https://www.toweringskills.com/financial-analysis/cost-indices/`. Accessed on: 30-11-2022.

[88] E. Smith, J. Morris, H. Kheshgi, G. Teletzke, H. Herzog, and S. Paltsev. The cost of CO_2 transport and storage in global integrated assessment modeling. *International Journal of Greenhouse Gas Control*, 109:103367, 2021.

[89] D. L. McCollum and J. M. Ogden. Techno-economic models for carbon dioxide compression, transport, and storage & correlations for estimating carbon dioxide density and viscosity. `https://escholarship.org/uc/item/1zg00532`, 2006.

[90] X. Luo, M. Wang, E. Oko, and C. Okezue. Simulation-based techno-economic evaluation for optimal design of CO_2 transport pipeline network. *Applied Energy*, 132:610–620, 2014.

[91] M. Mostafa, C. Varela, M. B. Franke, and E. Zondervan. Dynamic modeling and control of a simulated carbon capture process for sustainable Power-to-X. *Applied Sciences*, 11(20):9574, 2021.

[92] M. S. Peters, K. D. Timmerhaus, R. E. West, et al. *Plant design and economics for chemical engineers*. McGraw-Hill Education, 2003.

[93] J. M. Douglas. *Conceptual design of chemical processes*. McGraw-Hill New York, 1988.

[94] D. Papavassiliou. Economic design criteria. `https://coecs.ou.edu/Dimitrios.V.Papavassiliou/che4253/econ-lec.pdf`. Accessed on: 11-12-2022.

[95] A. Varone. The CO_2 Economy – The Transformation of Carbon Dioxide from a Liability to an Asset. `https://www.iass-potsdam.de/en/blog/2016/07/co2-economy-transformation-carbon-dioxide-liability-asset`. Accessed on: 17-11-2022.

[96] E. S. Rubin. Understanding the pitfalls of CCS cost estimates. *International Journal of Greenhouse Gas Control*, 10:181–190, 2012.

[97] Carbon tax basics. `https://www.c2es.org/content/carbon-tax-basics/`. Accessed on: 22-11-2022.

[98] EU Emissions Trading System (EU ETS). `https://climate.ec.europa.eu/eu-action/eu-emissions-trading-system-eu-ets_en`. Accessed on: 22-11-2022.

Appendix A

Absorber design

In the following appendix, an outline of the absorber design is given and some additional information on the absorber performance for the identified best case is provided.

A.1 Outline of the absorber design

The absorber design procedure consisted on sizing the column (*i.e.*, determining the diameter) for which a desired performance is attained, while carefully bearing in mind the column profiles. This last condition is of the upmost importance to assure the designed column is feasible from the hydrodynamics point of view.

In addition, the number of segments on which the axial domain of the column is discretized is another point to give particular attention, in order to obtain correct and consistent numerical solutions of the model. In this study, the benchmark number of 20 segments was chosen in accordance with the Chung et al. [28] work.

A.2 Absorber temperature and composition profiles

The absorber profiles for the case in which α_{LEAN} = 0.19 are shown in fig. A.1.
Regarding fig. A.1(a), the following observations can be made:

- the temperature range along the column is higher than that usually observed in other cases (*cf.* [71]). This fact can be ascribed to the CO_2 composition in the flue gas;

- no plateau is observed in the absorber temperature profile. Had it been observed, it would have indicated the presence of isothermal zones, which are undesirable as they denote the absence of reaction;

- there is a zone at the top of the column where a sudden temperature raise is spotted. This is the so-called *temperature bulge*, which is due to the heat transfer phenomena taking place in the
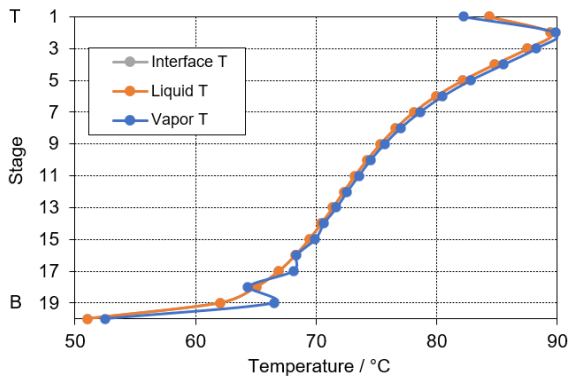
(a) Temperature profile.
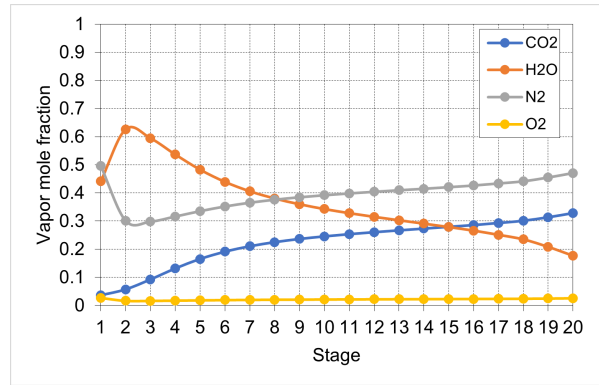
(b) Vapor composition profile.

Figure A.1 – Absorber profiles for the identified best case, α_{LEAN} = 0.19. Note that T stands for the top and B for the bottom of the column.

column, namely the exothermic MEA-CO_2 reactions and water vaporization or condensation. In the temperature bulge zone, reaction activity should be more intense, otherwise temperature would not have spiked.

Looking at the vapor composition profile (*cf.* fig. A.1(b)), as flue gas flows through the packing, it gets poorer in CO_2, while, at the same time, water from the solvent evaporates into the gas phase.

Appendix B

Stripper profiles

In this appendix, further information on the stripper profiles is given, as mentioned in section 4.3.3.

B.1 Effect of the stripper packing height on the composition profiles

We now turn to the stripper composition profiles, as shown in fig. B.1. Recall that stages are numbered from the top to the bottom.
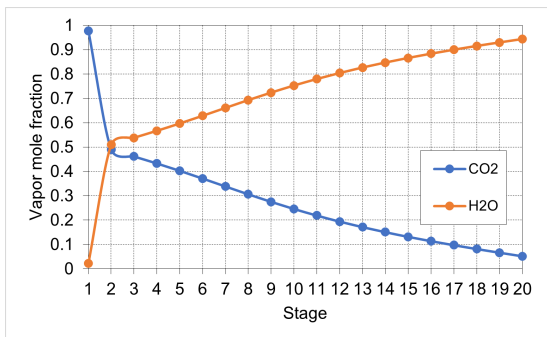
(a) CO_2 and H_2O vapor composition profiles along the column for the **stripper packing height of 6 m**.
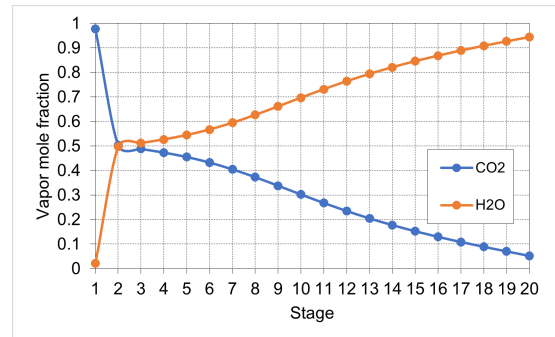
(b) CO_2 and H_2O vapor composition profiles along the column for the **stripper packing height of 8 m**.
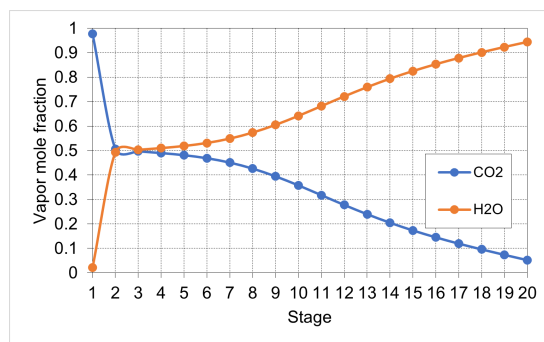
(c) CO_2 and H_2O vapor composition profiles along the column for the **stripper packing height of 10 m**.

Figure B.1 – Vapor composition profiles for the stripper packing heights of 6, 8 and 10 m.

As expected, regardless of the stripper packing height, the vapor enriches progressively in CO_2 towards the top of the column as CO_2 is stripped from the liquid solvent. At the same time, water from the stripping steam condenses, which is why the water vapor composition increases towards the bottom of the column. Let us now focus on the CO_2 vapor composition profiles for all the considered stripper packing heights, depicted in fig. B.2.
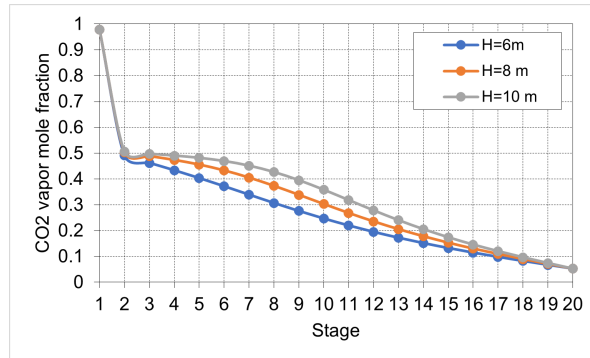
Figure B.2 – CO_2 vapor composition along the stripper column for the packing heights of 6, 8 and 10 m.

One knows *a priori* that higher packing heights allow greater contact lengths, and consequently greater degree of separation. However, this is not the case, as the removed CO_2 is the same for each of the considered heights on the grounds that the lean solvent loading remains unchanged (and equal to the optimal one, *cf.* identified in chapter 4). So, for each stripper packing height, the stripping working parameters will change so as to guarantee the amount of removed CO_2. For this reason, the reboiler duty, for instance, will be slightly greater for lower packing heights than for higher ones. Generally speaking, this result shows that the stripper packing height does not play a crucial role in the reboiler TER. On the other hand, the CO_2 vapor composition profile for $H_{stripper}$ = 6 m shows a more steeper behaviour than $H_{stripper}$ = 10 m due to the shorter contact length, which requires the vapor composition to fall more quickly in order to comply with the fixed amount of stripped CO_2.

B.2   Effect of the stripper packing height on the temperature profiles

In fig. B.3, profiles for the vapor temperatures along the column for all the considered stripper packing heights are shown. Stages 1 and 20 correspond to the condenser and the reboiler, respectively. Both are equilibrium-stages.

The following observations can be made: i) predictably, vapor temperature increases from top to the bottom of the column as it is closer to the reboiler; ii) smaller packing heights imply a higher range of vapor temperatures. In fig. B.4, profiles for the liquid, vapor and interface temperatures along the stripper height are shown.
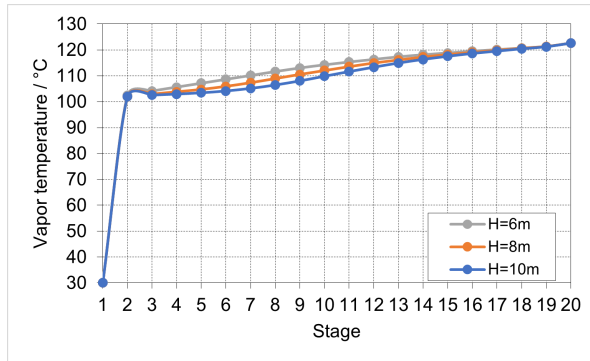
Figure B.3 – Vapor temperature profiles along the stripper column for the packing heights of 6, 8 and 10 m.
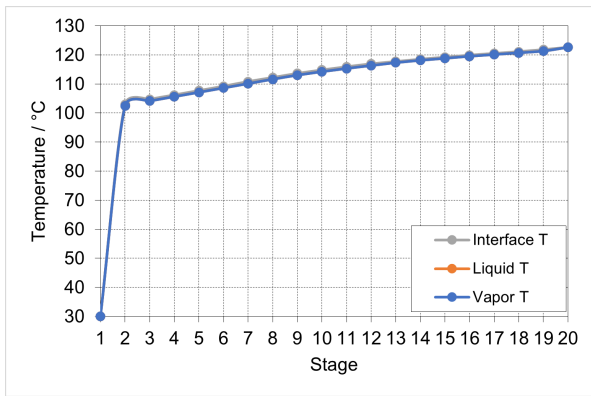
(a) Liquid, vapor and interface temperature profiles for **stripper packing height of 6 m**.
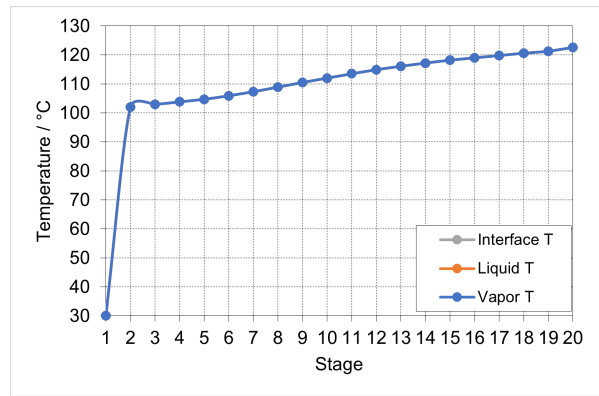
(b) Liquid, vapor and interface temperature profiles for **stripper packing height of 8 m**.
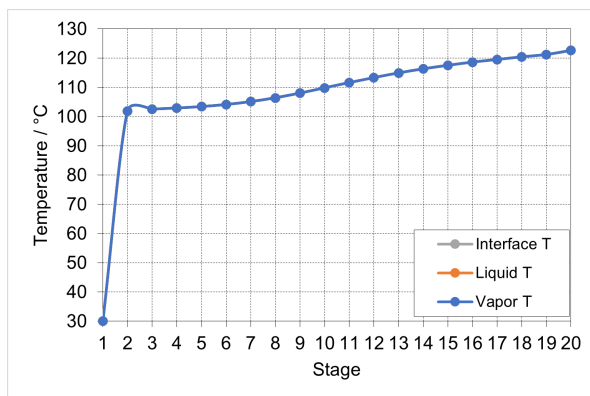
(c) Liquid, vapor and interface temperature profiles for **stripper packing height of 10 m**.

Figure B.4 – Stripper temperature profiles for the packing heights of 6, 8 and 10 m.